Control Strategy for Hydrocarbon Emissions in Turbocharged Direct Injection Spark Ignition Engines During Cold-Start
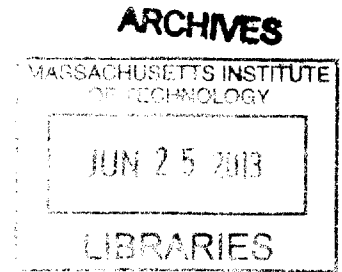
by

Kevin David Cedrone

B.A.Sc., Honours Mechanical Engineering
University of Waterloo (2008)
S.M., Mechanical Engineering
Massachusetts Institute of Technology (2010)

Submitted to the Department of Mechanical Engineering
in partial fulfillment of the requirements for the degree of

Doctor of Philosophy in Mechanical Engineering

at the

MASSACHUSETTS INSTITUTE OF TECHNOLOGY

June 2013
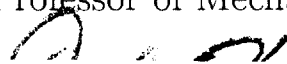
Author . . . . / . . . .
Department of Mechanical Engineering
March 18, 2013

Certified by . . . . ' . . . .
Wai K. Cheng
Professor of Mechanical Engineering
Thesis Supervisor

Accepted by . . . .
David Hardt, Professor of Mechanical Engineering
Chairman, Department Committee on Graduate Theses

Control Strategy for Hydrocarbon Emissions in Turbocharged Direct Injection Spark Ignition Engines During Cold-Start

by

Kevin David Cedrone

Submitted to the Department of Mechanical Engineering
on March 18, 2013, in partial fulfillment of the
requirements for the degree of
Doctor of Philosophy in Mechanical Engineering

Abstract

Gasoline consumption and pollutant emissions from transportation are costly and have serious, demonstrated environmental and health impacts. Downsized, turbocharged direct-injection spark ignition (DISI) gasoline engines consume less fuel and achieve superior performance compared with conventional port fuel injected spark ignition (PFI-SI) engines. Although more efficient, turbocharged DISI engines have new emissions challenges during cold start. DISI fuel injection delivers more liquid fuel into the combustion chamber, increasing the emissions of unburned hydrocarbons. The turbocharger slows down activation (warm-up) of the catalytic exhaust after-treatment system. The objective of this research is to find a control strategy that:

1. Accelerates warm-up of the catalyst, and
2. Maintains low emissions of unburned hydrocarbons (UBHCs) during the catalyst warm-up process.

This research includes a broad experimental survey of engine behaviour and emission response for a modern turbocharged DISI engine. The study focuses on the idle period during cold-start for which DISI engine emissions are worst.

Engine experiments and simulations show that late and slow combustion lead to high exhaust gas temperatures and mass flow rate for fast warm-up. However, late and slow combustion increase the risk of partial-burn misfire. At the misfire limit for each parameter, the following conclusions are drawn:

1. Late ignition timing is the most effective way to increase exhaust enthalpy flow rate for fast catalyst warm-up.
2. By creating a favourable spatial fuel-air mixture stratification, split fuel injection can simultaneously retard and stabilize combustion to improve emissions and prevent partial-burn misfire.

3. Excessive trapped residuals from long valve overlap limit the potential for valve timing to reduce cold-start emissions.

4. Despite their more challenging evaporation characteristics, fuel blends with high ethanol content showed reasonable emissions behaviour and greater tolerance to late combustion than neat gasoline.

5. Higher exhaust back-pressure leads to high exhaust temperature during the exhaust stroke, leading to significantly more post-flame oxidation.

6. Post-flame oxidation in the combustion chamber and exhaust system play a critical role in decreasing the quantity of catalyst-in emissions due to hydrocarbons that escape primary (flame) combustion.

A cold start strategy combining late ignition, 15% excess air, and high exhaust back-pressure yielded the lowest cumulative hydrocarbon emissions during cold start.

Thesis Supervisor: Wai K. Cheng
Title: Professor of Mechanical Engineering

Acknowledgements

This page intentionally left blank

CONTENTS

LIST OF FIGURES

This page intentionally left blank

LIST OF TABLES

This page intentionally left blank

Symbols

Symbol	Units	Description
η_{comb}	—	Combustion efficiency, fraction of fuel that fully combusts
$\eta_{i,g}$	—	Indicated gross fuel conversion efficiency; ratio of indicated gross work to fuel energy
η_v	—	Volumetric efficiency
λ	—	Air-fuel equivalence ratio $(1/\Phi)$
Φ	—	Fuel-air equivalence ratio $(1/\lambda)$
AF_{st}	—	Stoichiometric air-fuel ratio
m_a	kg	Air mass
m_f	kg	Fuel mass

Abbreviations

Abbrev.	Description
ABDC	After bottom dead centre
AFR	Air fuel ratio
ATDC	After top dead centre
BBDC	Before bottom dead centre

BD1090	Burn duration in crank angles between 10% and 90% of total heat release
BTDC	Before top dead centre
CA50	Crank angle at 50% of total heat release
CAD	Crank angle degree
CC	Catalytic Converter
CCV	Cycle to cycle variability
CO	Carbon monoxide
CO2	Carbon dioxide
COV	Coefficient of Variation (stddev/mean)
EVC	Exhaust Valve Closing
EVO	Exhaust Valve Opening
Exh	Exhaust
FTP	(EPA) Federal Test Procedure
GIMEP	Gross Indicated Mean Effective Pressure
HC	Hydrocarbon
HR1090	See BD1090
Ign	Ignition, or spark
Inj	Injection; namely fuel
Int	Intake
IVC	Intake Valve Closing
IVO	Intake Valve Opening
LNV	Lowest Normalized Value (min/mean)
MBT	Maximum Brake Torque
NEDC	New European Drive Cycle
NIMEP	Net Indicated Mean Effective Pressure
NO_x	Oxides of nitrogen including NO and NO_2
NVH	Noise Vibrations and Harshness
NVO	Negative Valve Overlap
OVI	Open valve injection

PGM	Platinum Group Metal
PIMEP	Pumping Indicated Mean Effective Pressure
PMEP	See PIMEP
RGF	Residual Gas Fraction
SOI	Start of Injection
SAI	Secondary Air Injection
UBHC	Unburned Hydrocarbon
VO	Valve Overlap
VVT	Variable Valve timing
WOT	Wide Open Throttle

This thesis adopts nomenclature from Heywood[1]. This DISI engine cutaway diagram is annotated with some important terms. Note the piston ring crevice, which is an important source of hydrocarbon emissions. The exhaust manifold, turbocharger turbine and catalyst (not shown) are downstream from the exhaust port in that order. Original image credit: [2].
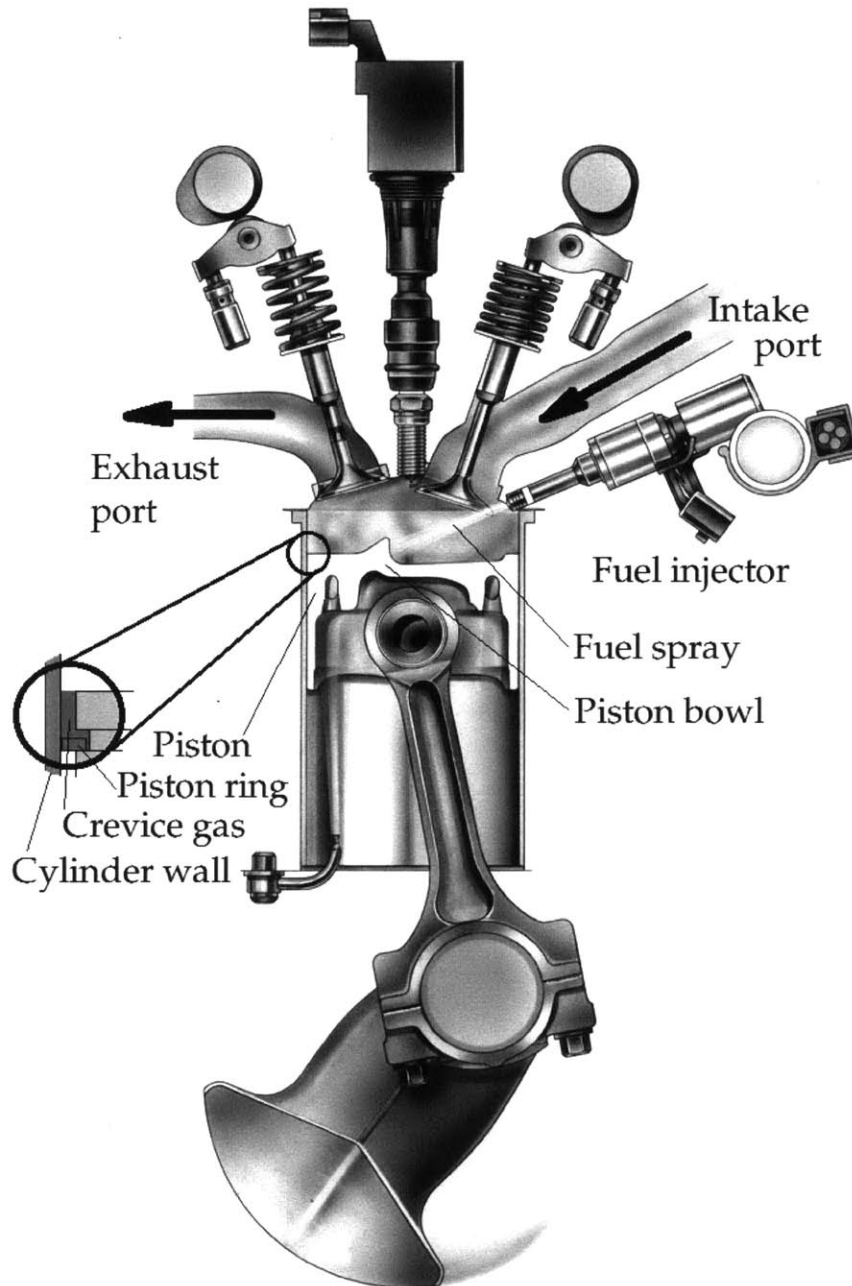
CHAPTER 1 _____

INTRODUCTION

O VER the past 40 years increasingly stringent emissions regulations have reduced vehicle emissions considerably through advances in vehicle emission control technology. Air quality in urban areas has improved in spite of increasing total vehicle miles travelled. The most significant progress was made by emissions technologies aimed at fully warmed-up engine conditions. For example, fuel injection for precise fuel metering and catalytic converters. Catalytic converters are perhaps the most significant of all emissions control technologies. Three way catalysts promote the simultaneous oxidation of unburned hydrocarbon species, oxidation of carbon monoxide and the reduction of oxides of nitrogen found in engine-out exhaust gases.[1, 3]

A typical automotive three-way catalyst can reduce harmful emissions by orders of magnitude. These catalysts are most effective when the engine is operating with a air-fuel mixture close to stoichiometric and when the internal catalyst surface temperature is above approximately 250°C. Below this temperature catalytic converters are virtually inactive. [4] Consequently, in order to meet the most recent and strictest emissions regulations, engine operating strategies focus on a "cold start strategy" to rapidly heat the catalyst (i.e. shorten the period of time in which it is inactive), while simultaneously reducing engine-out emissions during the catalyst warm-up process,

also known as catalyst light-off. This two-pronged approach is shown schematically in Figure 1-1.
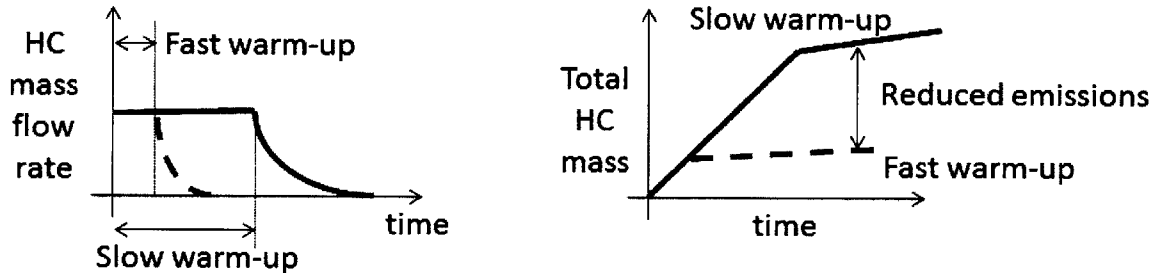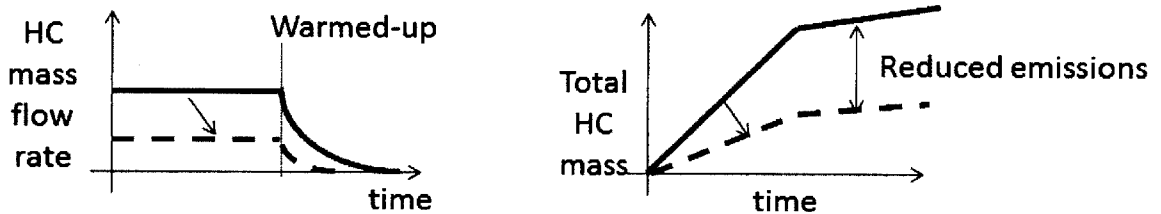
Figure 1-1: Emissions regulations are based on cumulative emissions. Cumulative emissions are reduced by faster warm-up (top) or lower emissions rate during warm-up reduce (bottom).

Concomitant with stricter emissions regulations, fuel economy requirements have increased. In particular, recent and ongoing increases to U.S. Federal fuel economy standards motivates interest in new vehicle technologies to reduce fuel consumption. Lightweight vehicles, hybrid-electric powertrains and advanced engine technology can reduce fuel consumption. One particular type of advanced engine, the downsized spark-ignition engines with turbochargers and direct injection can offer equivalent power with substantial reduction in fuel consumption compared with conventional engines. [5] Such engines can be used in all vehicles be they lightweight, hybrid or conventional powertrains. However, downsized turbocharged DISI engines have renewed emissions challenges, particularly during cold start. [6] The emissions degradation comes from the presence of the turbocharger and the use of direct fuel injection (as opposed to port fuel injection), the very engine features that permit higher efficiency.

This creates a trade-off scenario, with superior efficiency (lower fuel consumption) balanced by inferior emissions.

1.1 Research Objective

This study was initiated to survey engine control strategies for a modern small displacement turbocharged direct injection spark ignition engine and a variety of fuel blends appropriate for an engine of this type. The objectives of this work are to quantify trends in engine-out (catalyst-in) emissions and improve catalyst light-off performance by minimizing cumulative emissions of unburned hydrocarbons during cold-start.

This research can facilitate continued development of fuel-efficient engines, and provide a framework for engine developers working on other cold-start emissions issues such as particulate matter emissions. Furthermore, as fuel economy standards continue to rise, the present research will find application with hybrid vehicles and small, lightweight vehicles whose engines will eventually migrate to downsized turbocharged direct injection architectures.

This research focuses on engine operating strategies to improve catalyst warm-up using technology already common on turbocharged direct injection engines. The advantage is that operating strategies, once developed, are less expensive for manufacturers to deploy and do not need repair or replacement. This improves the likelihood that they will remain effective over the vehicle's life.

1.2 Background

1.2.1 History of Emissions Regulations

Gasoline and diesel internal combustion engines in vehicles are a major source of air pollution in urban areas. There are four main types of regulated engine emissions:

- Particulate matter (PM),

- Carbon monoxide (CO),

- Unburned (or partially burned) hydrocarbon (HC) compounds, and

- Oxides of nitrogen (NO_x). For gasoline engines NO_x is primarily nitric oxide (NO), with a small amount of nitrogen dioxide, NO_2.

These emissions have well known health effects. Particulate matter can be a respiratory irritant and contributes as a greenhouse gas. CO is toxic to humans. HC and NO_x undergo photochemical reactions with sunlight to produce smog and ozone.[3, 4]

Emissions performance standards and relevant drive cycles for evaluating them are specified by government agencies and vary by jurisdiction (e.g. U.S., Europe, Japan).In general the performance standards limit the cumulative quantity of each class of emissions produced by the vehicle over a prescribed drive test cycle.

The first vehicle-out emissions standards in the United States were contained in the 1970 Clean Air Act. The Clean Air Act controlled emissions of CO, hydrocarbons known as volatile organic compounds (VOCs) and NO_x. Starting in 1975, new pollutant limits went into effect limiting cars and light-duty trucks to emit CO at a rate less than 15.0 g/mile, HC less than 1.5 g/mile and NO_x less than 3.1 g/mile based on a Federal Test Procedure (FTP) to simulate average driving conditions. Emissions from these prescribed tests are collected and measured by a constant volume sampling system.

Current emissions standards for vehicles in the United States are complex and differ depending on vehicle type and use. A relevant excerpt of emissions standards for light-duty vehicles not including trucks is presented in Figure 1-2. For the prescribed EPA test cycle, the vehicle's emissions must be within the boundaries to satisfy the emission rating (e.g. TLEV) and satisfy the CO limit in the legend. Regarding emissions regulations, the conclusion for DISI engines is that the technology that improves their fuel efficiency degrades their emissions performance.
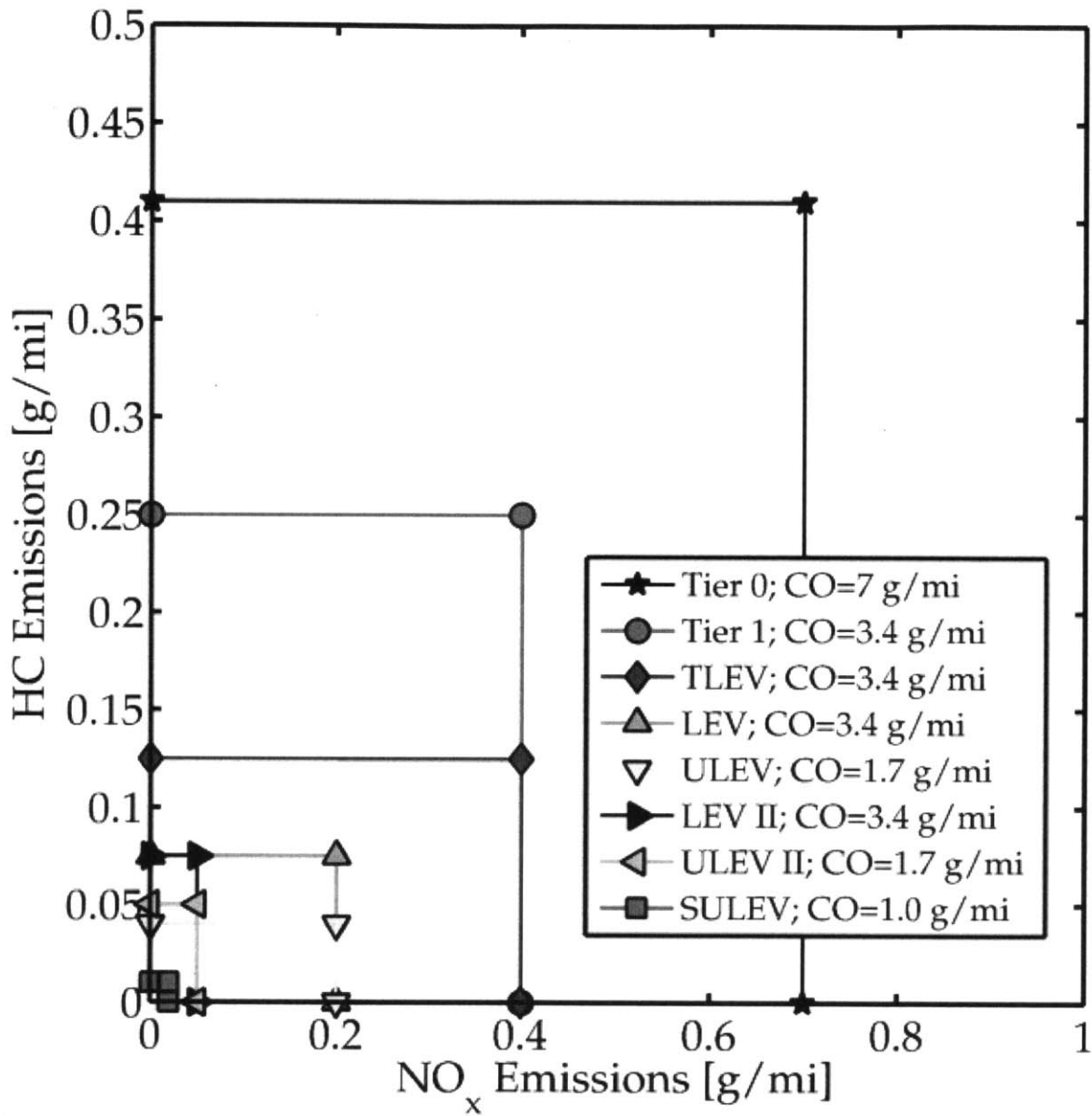
Figure 1-2: For reference, a typical fuel economy of 28 miles per gallon translates to an average fuel consumption rate of 100 grams per mile. The allowable rate of emissions of non-methane organic gas (NMOG) and formaldehyde is approximately 700 times smaller than the fuel consumption rate. This indicates the importance of a well-calibrated emissions control strategy and the strictness of current emissions standards.

1.2.2 Cold-start issues for DISI

Cold start can be roughly defined as vehicle operation after an extended period of non-use. A more precise legal definition describes a period of room temperature soak that vehicles must undergo prior to a prescribed test protocol such as the U.S. Federal Test Procedure (FTP). Currently, the majority of the total cumulative HC and CO emissions during the FTP-75 test are produced during the initial 25 seconds of engine operation before the catalytic converter reaches operating temperature.

Smaller turbocharged direct injection spark ignition engines, used for better fuel economy, introduce new emissions issues that degrade emissions behaviour during cold start by slowing down catalyst light-off and complicate emissions control. The three main cold start emissions issues for DISI engines are:

1) DI fuel injection delivers more liquid fuel to surfaces in the combustion chamber than PFI. In PFI operation, fuel is injected in the intake port upstream of the combustion chamber. Fuel evaporates with heat intake port and valve surfaces and a mixture of air and fuel vapour is inducted into the combustion chamber. In DI operation, fuel is injected directly into the combustion chamber. Some of the liquid fuel will not evaporate. This fuel may be stored on piston surfaces, in the cylinder-wall oil film or combustion chamber crevices. A portion will survive subsequent combustion events unburned or partially burned and be exhausted from the engine. Then, since the catalytic converter is ineffective during cold start, the unburned fuel contributes to engine-out emissions. Figure 1-3 show DI and PFI fuel sprays.

To guarantee that enough fuel evaporates in the intake port to form a combustible air-fuel mixture in the combustion chamber, PFI systems require significant enrichment of the first few cycles. DI fuel systems require far less enrichment because DI fuel injection controls the amount of fuel that enters the combustion chamber better than PFI. However, evaporation of the fuel that enters the combustion chamber is not guaranteed for DI fuel systems. Therefore the cold-start issue is mainly the uncertainty around fuel evaporation and mixing.

There is a related issue for fuels with ethanol content, which have operational syn-
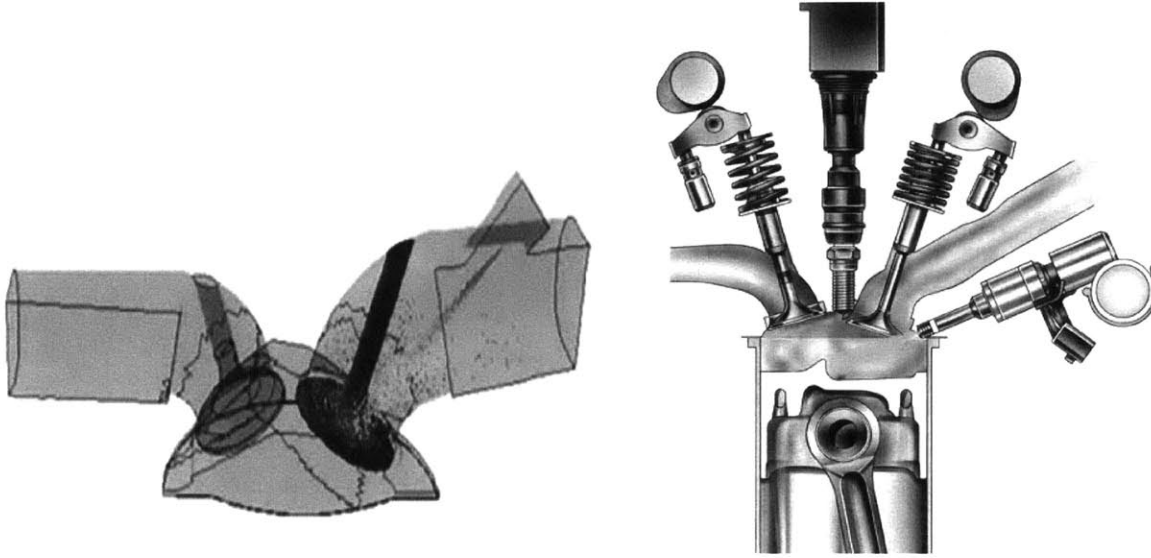
Figure 1-3: Typical PFI fuel spray targets the back surface of the intake valve (left). Liquid fuel evaporates before it is inducted into the combustion chamber. The DI fuel spray (right) contains liquid fuel droplets, which may not evaporate before combustion.

ergies with small, highly boosted direct injection engines. The evaporative properties of ethanol contribute to higher efficiency and autoignition prevention at high load. In addition to its higher heat of vaporization compared to gasoline, ethanol also has lower calorific value. Therefore, compared with gasoline the ethanol-fuelled engine will have a greater quantity of fuel injected, and the fuel may evaporate more slowly, both of which may exacerbate DISI emissions issues.[7]

2) For most engines and catalyst types, the addition of a turbocharger shifts the catalytic converter further down-stream, away from the engine. The high ratio of surface area to volume and relatively large thermal mass of the turbine rotor and shroud absorb thermal energy during warm-up, which delays warm-up of the catalyst that is downstream from them. This delay also reduces the effectiveness of secondary air injection (SAI), which is currently one of the most effective cold start hydrocarbon control techniques. More detail on this limitation is presented in the next chapter.

3) In order to mitigate autoignition (knock), turbocharged engines are designed with lower compression ratios than comparable naturally aspirated engines. The temperature of fuel-air mixture in the combustion chamber is lower at the start of

combustion for an engine with a lower compression ratio. Low temperature at the start of combustion can cause high cycle to cycle variability and/or partial-burn misfire which are undesirable. Combustion robustness is better at high temperature. Many of the strategies used to accelerate catalyst warm-up are limited by cycle-to-cycle variation. Hence, lower compression ratio limits can have an adverse effect on catalyst warm-up.

1.2.3 Engine start-up

The start-up process of an internal combustion engine has five parts:

1. Acceleration from stand still to the cranking speed.
2. Motoring at the cranking speed.
3. Acceleration upon firing in any one cylinder.
4. Acceleration due to firing in the rest of the cylinders. One or more cylinder(s) may misfire causing instantaneous deceleration, but the engine has to accelerate to speed, for a successful start.
5. Deceleration from the peak starting speed to the steady idling speed.

Although a significant portion of emissions occur during cranking and speed flare, the focus of the present work is the fast-idle phase of the start-up procedure because the fast-idle phase is extended duration for DISI turbocharged engines. Moreover, the fast-idle phase is more general whose findings are easier to apply to other engines. In contrast, the cranking and speed flare can depend heavily on the specific engine and details of engine termination from prior periods of operation. The steady idle portion starts around t=4[s] in Figure 1-4

1.3 Research Methodology

The focus of this research is engine operating strategies. The conclusions on engine physics are more widely applicable than those based on engines with unique or exotic equipment. Another reason to focus on engine operating strategies is once they

26
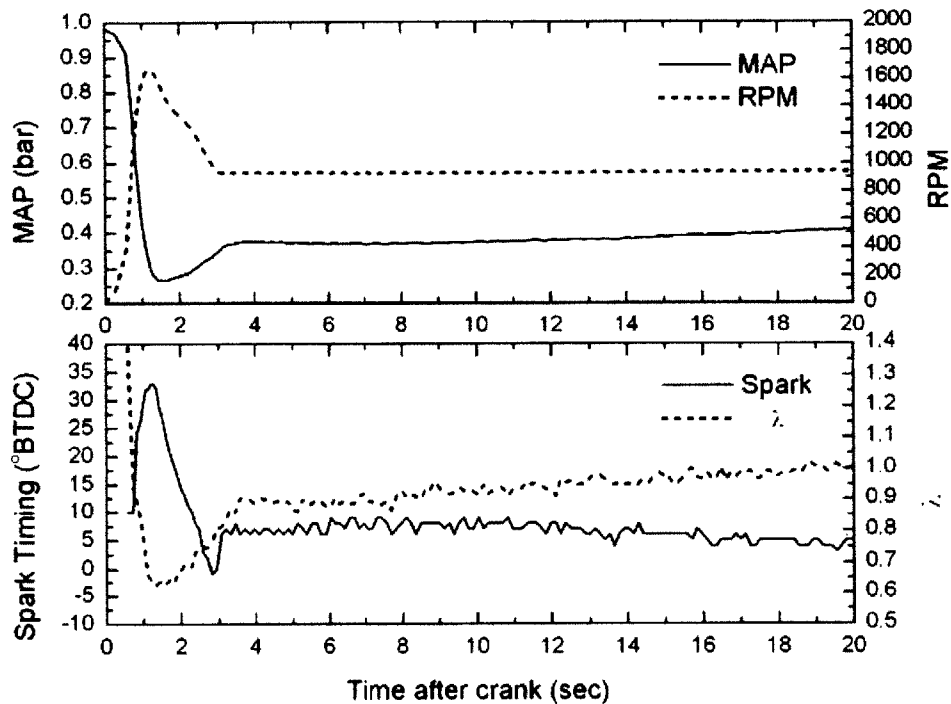
Figure 1-4: The cold idle period is most applicable to other engines and significantly extended by the delay to catalyst warm-up caused by the turbine. Image credit:[8]

are developed, operating strategies can be widely and cheaply disseminated, which bolsters the probability that they will be deployed in emerging markets.

The research is carried out in two broad areas, modelling and experiments.

Modelling

An experimentally-validated 1-D numerical model of the experimental engine is used to estimate the response of engine exhaust thermal enthalpy flow rate to key engine operating parameters. It is also used to probe details of engine operation that are difficult or impractical to measure experimentally. For example, intake and exhaust gas exchange details such as residual gas fraction and intake valve back flow.

A 1-D thermal model of the exhaust components between the engine and the catalyst is used to simulate the temperature profile that occurs while the catalytic converter is warming up.

A 1-D kinetic model of a catalytic converter based on an experimentally charac-

terized catalysts from the literature is used to process experimental engine-out data to simulate catalyst light-off. A detailed chemical kinetics model of the catalyst is used instead of empirically based gross efficiency to allow broader conclusions that are not dependent on manufacturer-specific catalyst formulations, nor on the effects of catalyst ageing.

The experimental exhaust data and computational catalyst model are combined to quantify engine operating strategy impact on light-off, cumulative emissions and strategy limitations.

Experiments

Engine experiments are run at conditions that represent the idle portion of engine start-up. Temperature of fuel, air, coolant and oil are controlled to replicate cold-start.

Engine cold-start operating strategies center on the following engine operating parameters listed below, and explained in greater detail in the next chapter.

- Ignition timing
- Equivalence ratio
- Fuel injection schedule
- Valve timing
- Exhaust back pressure
- Waste-gate bypass
- Fuel ethanol content

Each of the preceding experimental parameters is varied. For a given experiment, the exhaust mass flow rate, temperature and composition is measured. Other engine diagnostics such as cylinder pressure and manifold pressures and temperatures are recorded also.

CHAPTER 2

HYDROCARBON EMISSIONS DURING COLD START

THE objective of engine control during cold-start is to minimize cumulative emissions of hydrocarbons from the vehicle. Cumulative hydrocarbons are minimized by accelerating warm-up of the catalytic converter and minimizing engine-out emissions during the warm-up period when the catalytic converter is inactive. The goal of minimal cold-start emissions is based on regulatory limits on vehicle emissions and emissions testing methods, and an understanding that once the catalytic converter has reached its operating temperature it eliminates virtually all engine-out emissions. This chapter explains why engines emit unburned hydrocarbons, how to control emissions during engine cold-start, reviews existing cold-start literature and predicts engine behaviour in response to engine controls. This chapter is divided in five parts:

1. Description of source of engine hydrocarbon emissions.

2. Explanation of desired engine behaviour during cold-start.

3. Connection of desired cold-start engine behaviour with engine operating parameters to achieve them.

4. Review of existing literature on engine cold-start.

5. Prediction of DISI cold-start engine response to engine parameters.

29

2.1 Hydrocarbon sources

Most of the hydrocarbon fuel in the engine is consumed by turbulent flame propagation initiated by the spark plug. Hydrocarbons which are not consumed (i.e. completely oxidized) during primary combustion contribute to engine-out hydrocarbon emissions. This section describes the major mechanisms through which hydrocarbons can escape complete combustion.

Cheng et al. perform a highly regarded, quantitative and comprehensive investigation of the hydrocarbon pathways in an engine.[9]. They identify the following sources of engine-out hydrocarbon emissions.

- Misfire or partial burn: when combustion is too slow, starts too late or has its flame front extinguished by excessive local strain rate.

- Engine crevices and absorption/desorption from oil films, combustion deposits: As in-cylinder gas pressure rises, some unburnt mixture is stored in crevices (confined spaces too small for flame penetration) and oil films. When in-cylinder gas pressure falls during expansion and exhaust strokes, the stored mixture exits into the combustion chamber. Burnt gas temperature may be too low for full oxidation of crevices gases during the time available.

- Poor mixture preparation: Poor mixing of fuel with air may result in local rich zones and local lean zones, some of which do not oxidize rapidly enough due to paucity of fuel or oxygen.

- During DI engine warm-up when the high pressure fuel pump has not reached its operating pressure, the DI injectors operate at low pressure and produce large fuel droplets. To compensate for slow and/or incomplete evaporation of large droplets, the mixture is enriched (globally rich of stoichiometric) to guarantee enough fuel can vaporize to form a combustible mixture in the gas phase. This type of enrichment is also common in early stages of PFI engine warm-up to compensate for slow evaporation from cold intake port surfaces.

- Short-circuiting of unburned mixture from the intake into the exhaust port during valve overlap. PFI and DI engines differ significantly in terms of short-

circuiting. PFI engines induct air-fuel mixture into the combustion chamber, some of which may short-circuit during the valve overlap period when the intake and exhaust valves are open simultaneously. In contrast, DI engines induct air only, and DI fuel injection occurs after the exhaust valve is already fully closed. Therefore air only, and no fuel can short-circuit into the exhaust system during valve overlap for DI engines.

Fuel hydrocarbons escape oxidation during the primary combustion event through the preceding mechanisms. Research for warmed up engine suggests that around 92 percent of fuel is oxidized during flame propagation and approximately half of the remaining 8 percent will be oxidized in the burnt gas mixture after being expelled from crevices or desorbed from oil films. Of the remaining 4 percent, 50-80 percent will be oxidized in the exhaust port.[9–13] Thus 1-2 percent of the original fuel makes it to inlet of the catalytic converter.

During cold-start, mixture preparation is poorer (slower evaporation) and cold combustion chamber crevices host a greater mass of unburned mixture at higher density. A greater mass of unburned mixture in the crevice is likely to contribute to greater catalyst-in emissions.

On balance, it is probable that in direct injection engines, a greater fraction of fuel will escape flame-front combustion during cold start and contribute to engine-out emissions.

Engine designs and operating strategies to promote effective mixing and minimize crevice volume can improve but not eliminate hydrocarbon emissions. Engines on their own do not meet vehicle emissions standards. Vehicles rely on catalytic converters to consume (i.e. oxidize) engine-out hydrocarbon emissions to satisfy vehicle-out emissions standards. The catalytic converter is effective when warm, so the goals of engine hydrocarbon control must be to warm the catalyst quickly and minimize emissions during the warm-up process. The next section describes engine operating conditions that achieve low engine-out hydrocarbon concentration and fast catalyst warm-up.

2.2   Desirable characteristics during cold-start

This section describes how the engine should operate to accelerate catalyst warm-up and limit emissions during the warm-up period.

The catalyst warm up characteristics are primarily a function of the exhaust gas enthalpy flow. That is, exhaust mass flow rate and exhaust gas temperature. Higher flow rates and higher temperature exhaust gas warm the catalyst more quickly. Higher mass flow rates reduce transit time of exhaust gas from the engine to the catalyst. The reduced residence time overpowers higher convection coefficients (from the higher mass flow rate), and the net result is a higher exhaust gas temperature at the catalyst inlet. Higher exhaust gas temperature in the catalyst at any mass flow rate will cause heat transfer within the catalyst to increase.

However, for a given concentration of engine-out emissions, a higher exhaust mass flow rate equates to a higher emission rate. Put another way, a higher emissions concentration can be tolerated if it occurs for a shorter warm-up period, and a slower warm-up process may be tolerated if the engine-out emissions are low. Therefore, cold-start strategy must strike a balance between high exhaust thermal enthalpy and low engine-out emissions.

2.2.1   High mass flow

Catalyst warm-up is a convective heating process. Higher exhaust gas mass flow rate accelerates the rate of heat transfer from the exhaust gas to the catalyst substrate. The fast idle portion of cold-start occurs at a constant engine speed and engine output (i.e. engine load). To understand how exhaust gas mass flow connects with engine load it is helpful to remind the reader of the definitions of gross, pumping and net mean effective pressure. In what follows, "indicated" means measured by cylinder pressure data as opposed to "brake", which means measured by engine dynamometer.

- **Gross Indicated Mean Effective Pressure (GIMEP)** is gross engine work output per cycle divided by displacement volume. ($GIMEP = W_{i,g}/V_D$).

32

- Pumping work is a sort of "overhead" work done by the engine during gas exchange to pump burned gases out during the exhaust stroke, and pump fresh unburned gases in during the intake stroke. **Pumping Indicated Mean Effective Pressure (PIMEP)** is pumping work per cycle divided by displacement volume. ($PIMEP = W_p/V_D$)

- **Net Indicated Mean Effective Pressure (NIMEP)** is the difference between GIMEP and PIMEP ($NIMEP = GIMEP - PIMEP$)

For a given engine, neglecting losses from friction and accessories, constant engine load means constant Net Indicated Mean Effective Pressure (NIMEP). Equation 2.1 combines the definition of gross, net and pumping indicated mean effective pressures in a useful heuristic for understanding how fuel flow rate, and by consequence exhaust gas mass flow, rate can be increased at constant NIMEP and engine speed.

$$GIMEP - PIMEP = NIMEP = const.$$
$$\left(\frac{(m_f \cdot \eta_{comb}) \cdot Q_{LHV} \cdot \eta_{i,g}}{V_D} \right) - (p_e - p_i) = NIMEP = const. \tag{2.1}$$

V_D is the engine displacement volume, m_f is the mass of fuel injected, η_{comb} is the combustion efficiency or combustion completeness, Q_{LHV} is the lower heating value of the fuel and $\eta_{i,g}$ is the indicated gross fuel conversion efficiency (gross indicated work per cycle divided by fuel energy input, defined in greater detail later), p_e is the exhaust pressure, and p_i is the intake pressure.

At steady state, the mass flow rate of exhaust gas is the sum of the mass flow rate of air and the mass flow rate of fuel. For a given stoichiometry, the mass flow rate of air is proportional to the mass flow rate of fuel. Therefore, an increase in the mass flow rate of fuel will increase the mass flow rate of exhaust gas, but the increase to fuel mass flow rate must be counterbalanced by a concurrent reduction to $\eta_{i,g}$ to maintain the same engine output load (NIMEP). Also, an increase in pumping work will increase the amount of fuel required for constant load.

The fuel mass and combustion efficiency terms ($m_f \cdot \eta_{comb}$) are grouped with parentheses to reinforce the necessity of complete combustion. Injecting a greater

33

fuel mass increases exhaust mass flow rate, which is desirable. However, fuel that is injected but does not react directly increases engine emissions. Hence, the objective is to increase the mass of fuel which reacts while reducing the fuel conversion efficiency to maintain constant engine output. The next question is how to reduce indicated gross fuel conversion efficiency.

Lower gross conversion efficiency

The indicated gross fuel conversion efficiency is the ratio of gross indicated work per cycle to the input fuel energy, for internal combustion engines the latter is usually based on the fuel's lower heating value.

Gross indicated fuel conversion efficiency is lower for late combustion, long combustion duration or excessive heat transfer losses from gases in the combustion chamber. The reason that late combustion results in lower fuel conversion efficiency is explained with an analogy to the ideal Otto cycle. The indicated gross efficiency of the ideal Otto cycle is shown in Equation 2.2

$$\eta_{Otto,ideal} = 1 - \frac{1}{r_c^{\gamma-1}} \tag{2.2}$$

For constant volume combustion heat release, late combustion occurs with a lower effective expansion ratio. Hence from ideal cycle theory, one expects lower conversion efficiency.

Real combustion occurs over a finite duration, not instantaneously at constant volume, so heat release takes place incrementally. In effect, each increment experiencing its own effective compression and expansion ratio, all less than the ideal geometric compression ratio. The gradual heat release leads to lower peak pressures and less work extraction during the expansion stroke.

Real combustion cycles also have irreversibility in chemical reacting mixtures, heat transfer losses to combustion chamber surfaces, crevice effects and blowby of combustion gases past the piston rings which further degrade efficiency.

The useful insight for cold-start strategy is that late, slow combustion will have the

desired low fuel conversion efficiency. *(N.B.: The author generally finds it abhorrent to purposely advocate and design strategies to achieve low fuel conversion efficiency. In the context of emissions control, it is a grudging sacrifice.)*

Increase pumping work

Cold start conditions can be approximated by constant NIMEP. An increase to pumping work (PIMEP) necessitates a concomitant increase to GIMEP to maintain constant NIMEP. Ordinarily engineers strive to reduce pumping work, but the (temporary) objective during cold start is to accelerate catalyst warm-up with higher enthalpy flow rate, that is with higher mass flow rate and temperature of exhaust gases.

2.2.2   High exhaust gas temperature

High temperature exhaust increases the rate of convective heat transfer from exhaust gases to the catalyst. With available oxygen, exhaust temperatures above 750°C facilitate post-flame and post-cylinder oxidation of gas phase engine-out unburned hydrocarbons before they reach the catalyst.

Reduce gross conversion efficiency

Aside from increased mass flow rate of exhaust gas, the added benefit of low fuel conversion efficiency is the rise in exhaust gas temperature that accompanies late combustion. For late combustion, less of the thermal energy from combustion heat release is extracted from the cylinder gases as work by the piston. The remaining internal energy remains in the gas as thermal energy. Hence late and/or slow combustion which degrade indicated gross fuel conversion efficiency increases the temperature and mass flow rate of exhaust gases.

Preheat mixture

For cold-start behaviour there are two practical benefits to pre-heating the mixture. One is that higher temperatures enhance chemical reactivity, which may improve combustion stability and reduce cycle-to-cycle variability and prevent partial-burn misfire. The second advantage is that hotter initial charge temperatures result in proportionally higher exhaust gas temperatures. There is also a moderate pumping work penalty to high initial mixture temperatures, which as explained above for cold start is a moderate pumping work benefit.

Reduce thermal losses

Since the objective is to accelerate the warm-up process of the catalytic converter, it is desirable to reduce the amount of exhaust gas thermal energy lost to the walls of the exhaust system between the engine and the catalyst. This is a strong function of engine and component design, but there are at least two practical operational variables that can reduce heat transfer.

2.2.3   Low emissions

Apart from accelerating catalyst warm-up, an integral part of cold-start emissions control is to minimize the mass flow rate of controlled emissions while waiting for light-off.

Reduce mass flow

Low mass flow rate of exhaust decreases the cumulative emissions. However, this is at odds with the goal of accelerating catalyst warm-up.

Reduce emissions concentration

Low concentration of emissions reduces cumulative emissions. Low concentration is achieved through complete combustion in-cylinder and greater post-flame and post-cylinder oxidation of hydrocarbons that escape primary flame combustion.

Post-flame oxidation

Primary flame combustion ends when the flame arrives at the boundary of the combustion chamber. Post-flame oxidation refers to the oxidation of unburned mixture from oil films and combustion chamber crevices that re-enter the combustion chamber after flame combustion during the expansion stroke and exhaust stroke. Oxidation occurs when unburned mixture mixes with high temperature burned gases. The basic idea is that high combustion chamber gas temperature late in the expansion stroke and during the exhaust stroke will promote continued oxidation of hydrocarbons that escape primary combustion. Post-flame oxidation can continue after gases leave the combustion chamber (i.e. in the exhaust port or exhaust manifold). This post-flame oxidation is called post-cylinder oxidation.

Avoid partial-burn misfire

Engine misfire can cause significant emissions during the warm up period, so it is important to avoid engine misfire. Misfire is an imprecise term that generally implies incomplete combustion, a cycle whose gross work falls well below the mean value for that operating condition. Misfire is thought to occur when combustion fails to complete because it starts late, proceeds too slowly or is quenched by excessive localized flame strain. The cause may be systematic such as excessively late ignition timing or stochastic such as localized eddies that inhibit early flame development. The term partial-burn misfire is preferred because it emphasizes the undesirable emissions impact of incomplete combustion.

Partial-burn misfire is undesirable because it causes torque fluctuations, harsh engine operation and unwanted engine vibration. Partial-burn misfire is also undesirable because incomplete combustion may cause a full charge of fuel and air to leave the cylinder completely unburned. This would be devastating for emissions performance. A typical vehicle can emit a cumulative total of less than about 300 mg of unburned hydrocarbons during the first 30 seconds or 12,000 cycles (for a 4-cylinder engine) of the FTP-75 test. A typical automotive engine at low load during cold-start, burns

37

around 10-20 mg of fuel per cylinder per cycle. This means the fuel delivered to each cylinder, each cycle contains 3-7% of the total allowable emissions. Counting the hydrocarbons that escape combustion (e.g. due to crevices, oil films, etc.), there is practically no remaining "emissions budget" for any totally-incomplete combustion due to partial-burn misfire.

It is possible that a partially burned mixture could continue to oxidize while en route to the catalyst due to post-flame and post-cylinder oxidation, but the danger of misfire is clear. Engine operation during cold-start must be robust.

To summarize, hydrocarbon emissions during cold start are minimized when:

- Fuel and air are well-mixed or preheated for complete evaporation and complete combustion,
- The engine has a high flow rate of exhaust gas for rapid catalyst warm-up,
- Exhaust gas is at high temperature for rapid catalyst warm-up and post-flame oxidation of hydrocarbons, and
- Combustion is stable to avoid partial-burn misfire.

The next section describes the available engine operating variables and how those variables contribute to the desired characteristics.

2.3 Engine operating parameters

In the past, the freedom to change engines operating parameters during operation was limited. Parameters like valve timing were set to a single "static" value found to be workable compromise at all speeds and loads. Because cold-start is a limited portion of the engine operating range, valve timing was set for other conditions. Now modern computer-controlled engines permit realtime optimization of engine parameters for each condition of operation. Therefore it is time to re-examine how engine parameters can be used to accelerate catalyst warm-up and limit engine-out emissions during warm-up.

2.3.1   Ignition Timing (Spark timing)

Spark initiates combustion and therefore controls the timing of combustion heat release. There is an optimal ignition timing called maximum brake torque (MBT) timing, which optimizes heat release and work extraction. MBT ignition timing has maximum indicated gross fuel conversion efficiency $(eta_{i,g})$, minimum fuel consumption and low exhaust gas mass flow rate.

Ignition timing earlier than MBT suffers greater heat transfer and dissociation losses and hence low conversion efficiency$(\eta_{i,g})$ and low exhaust gas temperature which hinder warm-up. Ignition timing later than MBT also has low conversion efficiency $(\eta_{i,g})$ and high gas temperature in the expansion and exhaust stroke for fast catalyst warm-up and post-flame oxidation. The relationship between late ignition, post-flame oxidation and cycle-to-cycle variability is now discussed.

Figure 2-1 plots cylinder pressure for two consecutive engine cycles with some engine events labelled. During a typical cold-start engine cycle, beginning with the intake valve closing (IVC) the mixture is compressed during the piston upstroke. For ignition timing after top dead center, which is typical for cold start, the mixture expands during the piston downstroke. The spark plug is activated, which creates a nucleus of plasma and radicals on the spark plug electrodes. The plasma ball grows into a flame kernel and eventually a turbulent flame expands outward from the spark plug to consume the fuel-air mixture in-cylinder. As the flame front propagates, the flame-front heats and compresses the unburned mixture. At the same time, piston motion during expansion extracts work and cools the charge. The prevailing changes in temperature and pressure due to piston motion are unfavourable for combustion with substantially retarded spark timing. Piston motion during the expansion stroke reduces pressure and temperature and could quench the reaction if the rate of heat release does not overwhelm the rate of work extraction. The rate of heat release depends on the engine operating conditions, mixture properties, turbulence and other variables.

A typical fast idle engine speed during cold start is 1200 RPM. For a 4-stroke

39
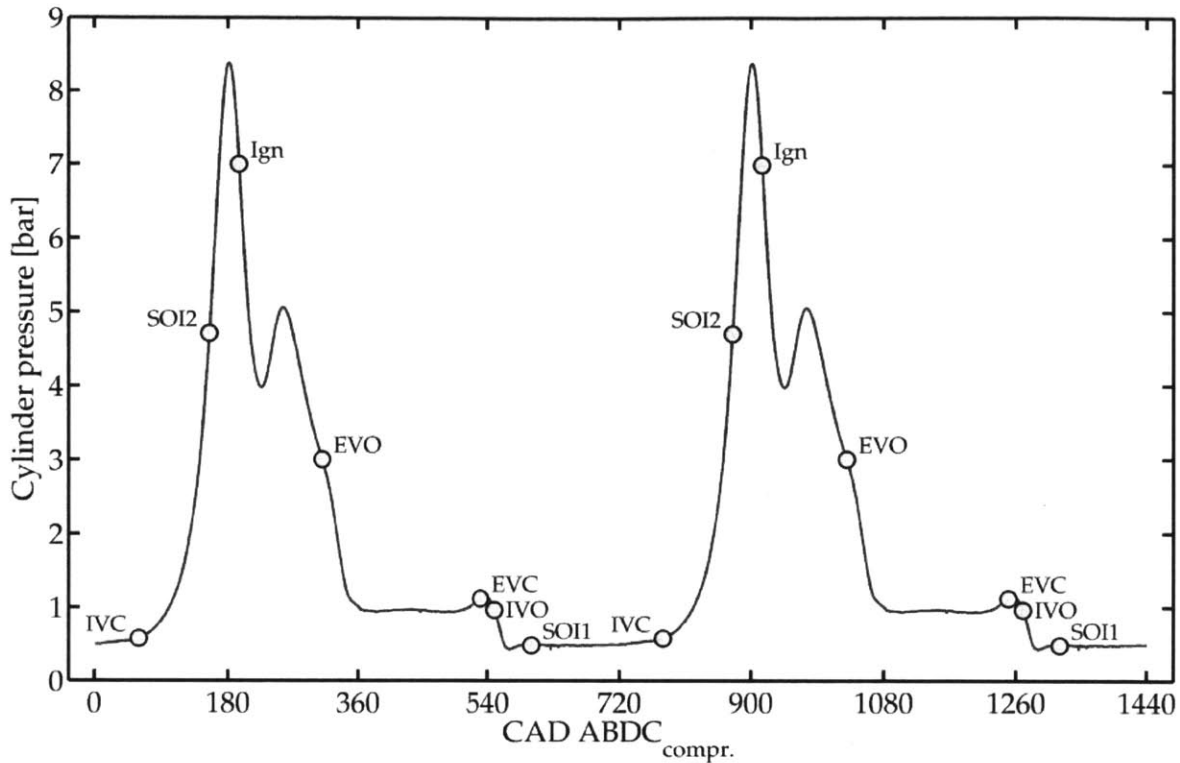
Figure 2-1: Ignition occurs approximately 15 CAD ATDC when piston downstroke is already causing cylinder pressure to fall. Maximum pressure is due to motoring/compression, not combustion.

gasoline engine 1200 RPM is 10 cycles per second or a cycle period of 100ms. That implies that each stroke lasts approximately 25 ms, which is therefore the time scale of post-flame oxidation in the exhaust stroke. Additional time is available for oxidation in the port and runner, but the temperature and hence reaction rate are lower there.

For the oxidation to occur in the time available, the mixture must have sufficient fuel and oxygen at a high enough temperature. For unburned mixture that leaves the piston crevices during expansion and exhaust, the mixture is usually close enough to stoichiometric that oxygen and fuel concentrations are satisfactory. The unburned mixture temperature, which is close to temperature of the cylinder wall, is much lower than the burned gas temperature. Therefore, for effective post-flame oxidation of crevice gases, the unburned mixture temperature in the expansion and exhaust stroke must be high. Research suggests at temperatures above approximately 1500 K, hydrocarbon oxidation is rapid and diffusion-limited. [14]

40

Figure 2-2 visually explains the mechanism of retarded ignition timing as a cold-start strategy. In other words, late combustion has lower mechanical efficiency. Thus
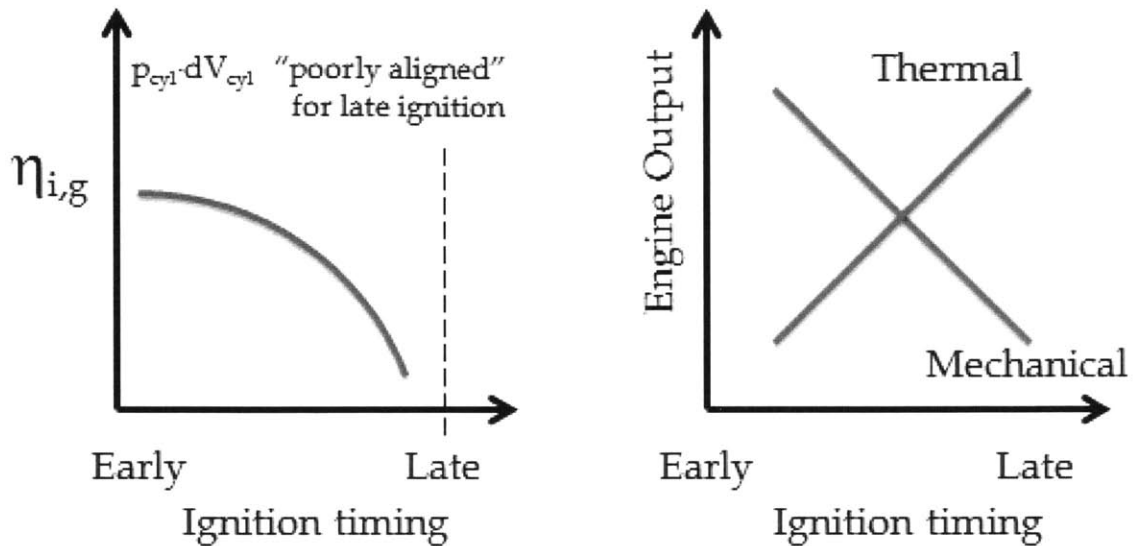
Figure 2-2: When combustion is late, the piston extracts less work from in-cylinder gas therefore more thermal energy remains in the gas.

for constant output torque at lower conversion efficiency due to late ignition, more fuel must be burned. The net result is both higher mass flow of exhaust gases *and* higher exhaust gas temperature. The latter point is important for emissions. When burned gases are at higher temperature, they cause more post-flame oxidation of the unburned mixture from oil films and crevices gases. This relationship is shown schematically in Figure 2-3. At constant output torque, later ignition produces higher temperature exhaust gas and requires a higher consumption rate of air and fuel. The overall mass flow rate of unburned hydrocarbons may decrease, increase or remain the same.

1. Decrease: The increase in exhaust flow rate is offset by a lower concentration of exhaust hydrocarbons due to post-flame oxidation in cylinder, exhaust port and runner.

2. Increase: The increase in exhaust flow rate is greater than the decrease in exhaust hydrocarbon concentration.
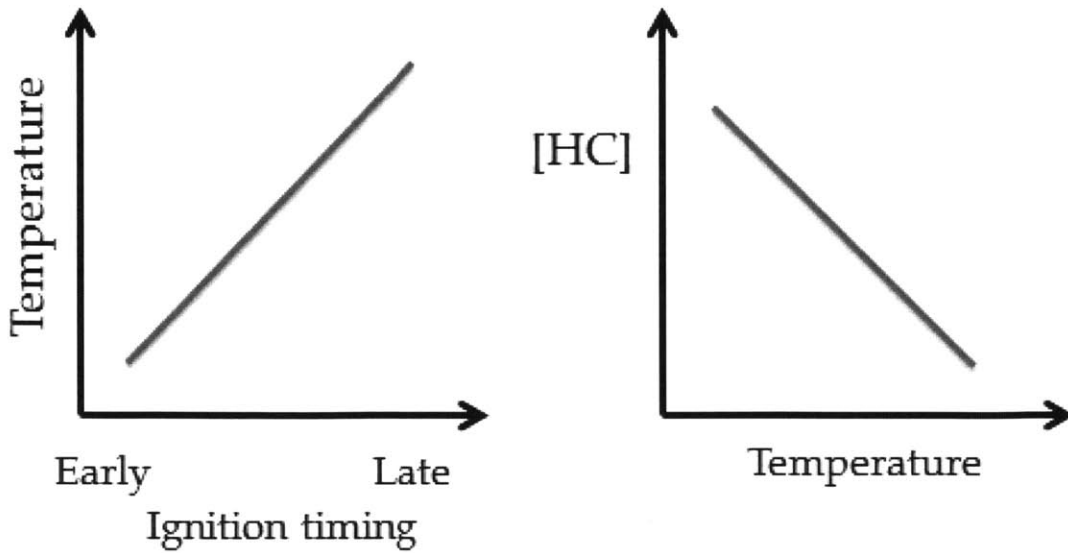
Figure 2-3: High exhaust temperature decreases engine-out hydrocarbon concentration. High exhaust gas temperature facilitates post-flame oxidation of hydrocarbons that would otherwise escape.

3. No change: The increase in exhaust flow rate is exactly balanced by the decrease in exhaust hydrocarbon concentration.

The uncertain outcome of the trade-off between increased mass flow rate and lower hydrocarbon concentration is summarized in Figure 2-4. In most cases overall mass flow rate of hydrocarbons will decrease but it is difficult to predict which scenario will occur in a real engine. The temperature-pressure history of the reacting gas mixture are coupled with the heat release rate and piston kinematics. This is a motivating factor for performing engine experiments. Late ignition has been studied but DI engines have significantly different mixture formation processes that determine emissions behaviour.

If later ignition increases the flow rate of exhaust but decreases the overall mass flow rate of hydrocarbons, late ignition is a win-win strategy. It simultaneously increases thermal enthalpy flow to the catalyst to accelerate light-off and decreases exhaust mass flow rate of hydrocarbons. This suggests there are questions regarding the use of late ignition timing: what is the limitation on arbitrarily late ignition timing?

For later ignition,
need more fuel for
const. output

m_{fuel}

$m_{exh} \sim m_{fuel} + m_{air}$

Early   Late

Ignition timing

$m_{HC} \sim m_{exh}{}^*[HC]$

m_{HC}

?

?

For late ignition, mass
flow rate goes up,
concentration goes down.
What is the next effect?

Early   Late

Ignition timing
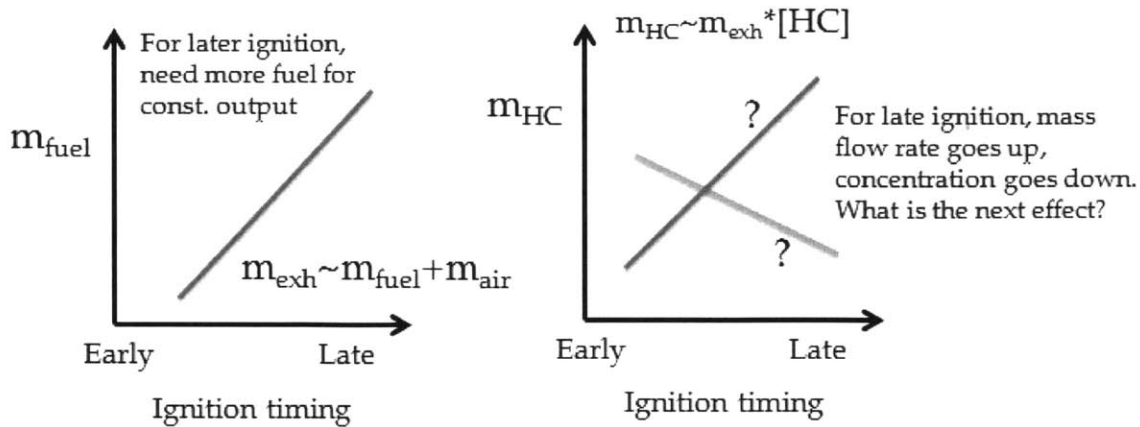
Figure 2-4: For constant engine output, late ignition results in a higher mass flow
rate of exhaust gases at higher temperature. High exhaust gas temperature results
in lower exhaust gas hydrocarbon concentration. It is unknown whether late ignition
leads to a net decrease in mass flow of hydrocarbons.

The combustion chamber environment in which flame propagates following late
ignition is unfavourable. Conventional ignition timing occurs before the piston reaches
top dead center. Ignoring autoignition, for best fuel conversion efficiency, ignition
timing is set such that 50% of fuel mass has burned when the piston is 7-10 CAD past
top dead center. In this configuration, combustion starts while the piston is still rising.
Therefore heat release, compression from flame propagation and piston compression
all increase the temperature and pressure during combustion, which increase the
oxidation reaction rate.

In contrast, cold-start ignition timing is usually after top dead center, much later
than conventional ignition timing. In this configuration, when combustion starts the
piston expansion is already cooling the reacting gas mixture. This degrades rather
than enhances the reaction rate. Hence combustion starts later *and* proceeds more
slowly. Also, late ignition time means more time has elapsed since the intake valve
closed, causing greater dissipation of in-cylinder charge motion and turbulence which
are important mechanisms for flame enhancement. One disadvantage is that cycle-
to-cycle variation increases because longer elapsed time from intake valve closure to
ignition allows flow structures to evolve stochastically, different in each cycle.

To summarize, instability limits late combustion. Late combustion is prone to

failure by partial burning or by high cycle to cycle variation. This applies not only to late combustion caused by late ignition, but also to combustion that is slow or delayed by other means such as mixture stratification, air dilution or high residual content.

The stability constraint on how late one may make combustion then limits the amount of post- flame oxidation one can expect in the combustion chamber.

2.3.2 Air-fuel equivalence ratio

Air-fuel equivalence ratio controls flow rate of chemical enthalpy in the exhaust gases. Lean mixtures (excess air) promote complete combustion and as with ideal Otto cycle higher fuel conversion efficiency. However, dilute fuel-air mixtures from excessively lean mixtures suffer high cycle-to-cycle variability.

Rich mixtures (excess fuel) promote stability at the cost of higher emissions. The emissions from rich combustion can be lowered, sometimes virtually to zero with secondary air injection if it results in successful post-cylinder oxidation. Rich mixtures also reduce in-cylinder temperatures due to evaporative cooling and reduce the specific heat ratio of the fuel-air mixture during the compression stroke.

Residual gases from rich combustion contain significant quantities of carbon monoxide, hydrogen and unburned or partially oxidized hydrocarbons. These residuals may enhance reactivity during subsequent cycles.

2.3.3 Valve timing

Valve timing plays an important role in mixture preparation mainly through exhaust and processes and interactions during gas exchange. This and many contemporary turbocharged direct injection engines feature a fixed-duration variable phase valve timing system. For this engine, intake cam timing can be advanced from a default de-energized position and exhaust cam timing can be retarded from its default de-energized position. The effects of variable valve timing are complex because the fixed duration mean that advancing one valve event, such as intake valve closing (IVC)

44

necessarily changes the companion intake valve opening (IVO) event. In the case of advancing intake cams and retarding exhaust cams, any valve timing change will increase the valve overlap period and therefore increase trapped residual gas fraction, in addition to whatever other physical effects such a valve timing change would have in isolation.

Variable valve timing has potential to improve cold start hydrocarbon emissions by increasing exhaust temperatures and reducing hydrocarbon emissions. Valve timing influences exhaust gas temperatures via intake port heating of fresh air by back flow of residuals to the intake port. Early IVC increase the effective compression ratio to increase peak gas temperatures. Early EVO decreases the effective expansion ratio. Residual gas fraction significantly retards combustion phasing and lengthens combustion duration which decrease indicated gross fuel conversion efficiency.

Valve timing influences hydrocarbon emissions mainly by increasing the amount of crevice gases, which contain unburned or partially oxidized mixture of air and fuel, that are re-breathed into the combustion chamber during valve overlap. The last crevice gases to escape during the exhaust stroke may have an outsize contribution to engine-out emissions of unburned hydrocarbons.. These particular gases experience the least amount of post-flame oxidation since they are exposed to the lowest temperature burned gas with the shortest duration of time.

2.3.4 Exhaust back-pressure

Exhaust pressure restrictions improve cold-start performance by both faster catalyst warm-up and lower concentration of unburned hydrocarbons. The first mechanism is simple, higher back pressure increases PIMEP, which necessitates a greater flow of fuel and air to maintain constant NIMEP during cold-start. The second mechanism is that higher exhaust pressure reduces gas temperature drop at the end of the blowdown process. Higher temperatures in the exhaust process enhance post-flame oxidation of unburned hydrocarbons. This may not be obvious at first sight, so a more detailed explanation of the exhaust process follows.

When the exhaust valve opens the in-cylinder mixture is brought into flow com-

munication with the exhaust manifold environment. The details of gas exchange of the exhaust process are complicated, but the temperature and pressure of gases in the combustion chamber decrease during the exhaust process. This reduces the rate and extent of oxidation reactions taking place. Heywood, Stone, and Taylor describe the exhaust process in great detail in their respective books. [1, 15, 16]

The exhaust process may be divided in two processes, blowdown when the pressure in cylinder rapidly equilibrates with the pressure in the exhaust manifold, then bulk displacement flow when the piston evacuates the cylinder of remaining gases.

Initial exhaust gas flow is choked due to the pressure ratio between the combustion chamber (upstream) and the exhaust system (downstream). The choked flow portion of blowdown is rapid so combustion chamber volume is approximately constant during the blowdown process. At constant volume, with the choked mass flow rate of exhaust independent of downstream pressure, the temperature of the gases in the combustion chamber is independent of the exhaust manifold pressure. However, with a higher exhaust pressure the blowdown period is shorter. That is, the combustion chamber reaches a sufficiently low pressure that flow across the exhaust valve is no longer choked. So the temperature drop during the entire blowdown process is lower. Thus the temperature of the exhaust gas in the displacement process is higher.

Another way to understand the effect of exhaust pressure is to consider the gas that remains in the combustion chamber during blowdown as expanding isentropically. In-cylinder gas pressure gradients are equilibrated quickly so the expansion process is quasi-static. The pressure drop at the exhaust valve acts as a mechanical matching element so the expansion is reversible. The expansion process is fast enough that negligible heat transfer occurs from the gas to the walls of the combustion chamber.

Neglecting heat transfer, the flow of gases through the exhaust valve after the kinetic energy is dissipated may be considered isenthalpic, which for an ideal gas is isothermal. In fact there is usually substantial heat transfer from the exhaust gas to the exhaust valve and port. Hence the gas within the cylinder may be modeled as undergoing an isentropic expansion from the cylinder pressure to the prevailing pressure in the exhaust manifold during the outflow process.

46

2.3.5 Waste-gate bypass

The turbocharger has a boost control and load-limiting feature known as a waste-gate. The waste-gate is a bypass valve that allows exhaust gases to take a shortcut from the exhaust manifold directly to the catalyst inlet without passing through the turbine. Such a shortcut path would decrease the quantity of thermal energy transferred to the turbine, increase the thermal energy that reached the catalyst and shorten catalyst warm-up. This engine lacked a control to open the waste-gate on command during cold start.

This particular waste-gate is a spring-loaded, normally-closed electro-pneumatically controlled valve, which under certain circumstances allows exhaust gas to bypass the turbine. The spring holds the waste-gate shut until the compressor outlet pressure is above some critical threshold. Above this pressure, pneumatic pressure force from compressor pressure overpowers the spring and the waste-gate opens, reducing turbine mass flow and compressor boost. Without this feature, the engine could experience runaway boost where increased induction leads to increased turbine mass flow, which leads to increased induction until the engine fails. An electronic solenoid can close the waste-gate against compressor pneumatic pressure force, which increases the compressor outlet boost pressure.

For the present experiments, the waste-gate was manually opened, under the assumption that the existing electro-pneumatic control could be adapted at nominal cost to achieve the same behaviour on production units.

2.3.6 Fuel variables

Turbocharged, direct injection engines operate in a different temperature and pressure envelope than conventional naturally aspirated port-fuel injected engines. Engine knock or autoignition is a more significant limitation for turbocharged engines. Fuel delivery systems that induce significant charge cooling and fuels with high autoignition resistance mitigate the autoignition challenge. These fuels are therefore important over the entire drive cycle but may present a problem during cold start.

Fuel ethanol content

Due to favourable evaporative properties and autoignition resistance, ethanol fuel blends show considerable operational synergies with turbocharged direct injection spark ignition engines. However, fuel blends with ethanol may present emissions challenges during cold start. Compared to gasoline, ethanol has a significantly higher heat of vaporization and lower heating value. Hence for constant load, a greater quantity of ethanol will be injected, and it may be slower to evaporate causing greater emissions of unburned fuel. Road fuels have a maximum ethanol content of 70-85% because it is well known that neat ethanol has severe vaporization problems that complicate cold-start and winter driving.

Injection schedule

Compared to port fuel injection, direct fuel injection increases the amount of liquid fuel delivered into the combustion chamber. DI fuel delivery is similar to open valve injection (OVI) of port fuel injection, which is known to degrade emissions for PFI engines. One important distinction between PFI OVI and DI fuel injection is that at high fuel injection pressures typical of DI, droplet sizes are significantly smaller which accelerates fuel droplet evaporation. During cold start, fuel injection pressure may be limited, combustion chamber surfaces are cold and evaporation is problematic. Complete combustion requires effective controlled mixing of fuel and available air. Mixture preparation can also improve combustion stability (i.e. low cycle-to-cycle variability) and minimal emission of unburned hydrocarbons. Compared with port fuel injection, direct fuel injection reduces first-cycle enrichment requirements and also affords additional flexibility in fuel delivery schedule to improve cold-start engine operation.

This research explores a split injection strategy where 70-80% of fuel is delivered at a conventional timing during the intake stroke with the balance delivered late in the compression stroke. The motivation for this strategy is provided in the caption for Figure 2-5.

Figure 2-5: A common piston shape for cold-start features a bowl oriented to the fuel injector such that the piston geometry redirects fuel, alters fuel-air mixing and induces favourable center-rich, perimeter-lean fuel stratification. Establishing a rich mixture towards the spark plug improves the early stages of ignition and flame growth, which in turn, reduces the cycle-to-cycle variability of operation at late ignition timing. Image credit:[2]

2.3.7 Variables not extensively tested

Engine speed and load are relevant to engine cold-start behaviour but were not explored in detail in this research.

Engine speed

Higher engine speed can improve catalyst warm-up in several ways.

- Mass flow through the engine is proportional to engine speed,
- Heat transfer losses from combustion chamber gases have a slight negative correlation with mass flow rate (reduced residence time dominates enhanced convection for lower net losses), and

- High engine speed enhances in-cylinder turbulence which can improve combustion stability.

The drawback is that high engine speed reduces time for post-flame oxidation. Moreover, there are vehicle limits on engine speed during the cold idle that relate to lubrication, transmission input speed preceding a shift from park into drive gears and a limit on the thermal transient to which the engine is subjected. Limited data was collected at other engine speeds to estimate the impact of engine speed. The engine speed of 1200 RPM was chosen in conjunction with research sponsors from the automotive industry. Previous experience dictates it is representative of cold-start conditions.

Engine load

As with engine speed, higher engine load can improve catalyst warm-up through increased mass flow rate, reduced heat transfer losses and better combustion stability. However, at idle engine load is determined by friction: the engine will accelerate until the frictional torque (which increases with engine speed and load) equals the engine output (which decreases with speed for a fixed throttle position). In this sense, load is not truly an independent parameter. The engine load condition of constant NIMEP equal to 2.0 [bar] was chosen in conjunction with research sponsors from the automotive industry as representative of engine operation in a vehicle during the cold-start process.

The preceding material describes the conditions that are desirable during warm-up, and the engine operating parameters that can create those conditions. The next section gives some quantitative predictions of the effect of engine parameters on engine behaviour during warm-up.

2.3.8   Cold-start strategy limitations

The engine operating strategy used during cold-start must satisfy not just emissions regulations but also vehicle operation and quality constraints. This section discusses

some practical constraints on engine operation during cold-start.

Vehicle quality constraints vary for each manufacturer according to the vehicle and its intended application. The industry sponsors of this research provided broad guidelines on vehicle operation and quality constraints.

It is good engineering practice to consider all relevant practical limitations that may hinder real-world implementation. However, the primary focus of this research is emissions control and explaining engine emissions performance in terms of fundamental physical processes. Therefore this research emphasizes the constraints that have strong emissions implications.

- Turbocharger turbine limits: **(a)** According to the manufacturer, the maximum gas temperature permissible at the turbine rotor-inlet is around 900-980°C. This imposes limits on spark retard and post-cylinder oxidation (e.g. from secondary air injection). **(b)** According to the manufacturer, The internal seals of the turbine should not be exposed to a pressure differential between the turbine and compressor of more than 2-3 bar. This constrains operation with elevated exhaust back pressure.

- Some manufacturers limit the minimum intake manifold vacuum level (i.e. maximum intake manifold pressure of 0.7 [bar]). Intake manifolds are commonly used as a vacuum reservoir for power brake boosting. Insufficient manifold vacuum may produce a "soft" brake pedal and compromise perceived vehicle quality. This type of vehicle operation constraint has little direct impact on emissions. Moreover, belt-driven or electric vacuum pumps can remove this limitation, although there is a cost penalty for new hardware. In other words, in an overall comparison of diverse cold-start emissions control strategies, the manifold vacuum limitation would not be a fatal penalty for a strategy resulting in very low manifold vacuum levels.

- Cycle-to-cycle variation in engine torque is a limitation for noise, vibration and harshness (NVH). These fluctuations can cause unwanted vehicle vibration. Cycle-to-cycle torque variations are primarily caused by cycle-to-cycle variations in combustion phasing. Cycle-to-cycle variations are commonly mea-

51

sured by statistics calculated from engine data over a collection of consecutive cycles. At the suggestion of our industrial sponsors, this work quantifies cycle-to-cycle variations (i.e. of GIMEP, combustion phasing, etc.) using coefficient of variation (COV) and lowest normalized value (LNV). COV is a normalized measure of the width of the distribution calculated as the standard deviation of a sample divided by the sample mean. LNV is the minimum value of the sample divided by the sample mean. Where COV describes the distribution width, LNV describes the absolute lowest value in the sample. GIMEP was selected instead of NIMEP to avoid excessive error/sensitivity. The NVH limit on COV of GIMEP is 15-25%. Greater precision was not available due to the sensitivity of proprietary vehicle quality metrics, standards and practices. This limit on cycle-to-cycle variation has emissions implications because excessively late or variable combustion may be incomplete (partial burn misfire) and emit a large quantity of unburned fuel for that cycle. That is, conditions that lead to higher COV than the typical NVH limit on COV, often lead to partial burn misfire, which causes unacceptable excessive emissions.

The preceding section has established the way in which engine parameters can be configured for complete and stable combustion (avoiding partial-burn misfire), leading to high flow rate of high temperature exhaust gas, and low emissions concentration during cold-start. The next section examines some existing literature on the themes of mixture preparation, exhaust gas thermal enthalpy and hydrocarbon oxidation. An additional section on exhaust system design mentions some options to control cold-start emissions other than the engine operating strategies that are the focus of the present research.

2.4   Literature review

Meeting stringent engine emissions regulations requires better catalyst light-off characteristics and reducing engine-out emissions prior to catalyst light-off. Many well-studied strategies exist to accelerate the process and reduce the time to light-off,

and hence cumulative emissions during cold-start. The purpose of this section is to discuss the extensive collection of available literature. This section discusses existing strategies and technologies, and the limitations such strategies face in downsized turbocharged direct injection engines. The strategies are organized according to the mechanism of their action. They include mixture preparation, thermal enthalpy, hydrocarbon oxidation, and exhaust design.

2.4.1 Mixture Preparation

This section describes the factors affecting, and techniques to control mixture preparation. The topic of mixture preparation is important to DI due to the increased delivery of liquid fuel directly into the combustion chamber compared to PFI. Insufficient mixing or evaporation degrades emissions.

Oxygen availability

Complete oxidation requires adequate oxygen that is distributed and available to the fuel. However, excess air dilutes the fuel-air mixture and, acting as thermal ballast, decreases burned gas temperatures and usually reaction rates too. Therefore effective mixing is an important component of mixture preparation to effectively use available oxygen and support stable, complete combustion. Excess air should be used to promote complete combustion but limited to reduce the stability penalty it causes.

Charge motion

Charge motion control valves or engine intake design can induce bulk swirl and tumble motion and turbulence to promote mixing, enhance burning rate and reduce cycle to cycle variability.[17] For cold start, S. Lee et al. and D Lee et al. both found the higher burn rate permits greater delay of ignition timing, which allow more time for fuel vaporization and fuel-air mixing. [18, 19] Both sets of researchers and Wildman et al. all found that charge motion could reduce cycle-to-cycle variability, permitting substantial combustion retardation and exhaust temperature increases without

53

increase to coefficient of variation of gross indicated cycle work.[20]. They also noted that excessive charge motion could result in increased emissions, proposing local flame quenching due to excessive flame strain as a plausible mechanism. The intake manifold and intake ports in the cylinder head of the engine used in this work are designed to induce significant tumble to improve fuel-air mixing and augment burn rate. No extra charge motion devices are installed.

Split injection

Direct injection of fuel into the combustion chamber degrades emissions performance when the fuel survives the combustion process and is exhausted from the engine. However, direct injection also gives better control over fuel delivery, and advanced fuel delivery scheduling may avoid the liquid fuel problems. One way is to split the total fuel mass into several separate injection. It is hypothesized that overall penetration of the fuel may be less for several short injections than one monolithic fuel injection jet. Shorter penetration of the fuel jet promotes gas phase evaporation and can reduce the amount of fuel that strikes and sticks to in-cylinder surfaces, which contribute to engine-out emissions. Moreover, better evaporation can reduce or eliminate the enrichment necessary to obtain a given stoichiometry in the gas phase.

In practice, the injector size, performance and flow rate are dictated by operation at high loads which leads to complications at low load. At low loads and cold-start, fuel amounts are small. Small fuel amounts require the injector, which is effectively a solenoid valve, to be open for short periods of time. The lower limit of performance occurs when the injector pintle enters the ballistic regime. In contrast to long injections, in the ballistic regime, opening and closing transients dominate injector dynamics and fuel injection is not repeatable. The engine will usually still operate but the variation in fueling and injector performance cause cycle to cycle variability. For this engine during cold start, fuel delivery could almost always be divided into two, sometimes three equal repeatable pulses. The original vision of a train of many short injections could not be achieved.

One technique to maintain the same total fuel delivery but extend the injection

duration and increase the number of short pulses is to decrease fuel injection pressure. At low injection pressure, the jet velocity is low, droplets are large and the spray lasts for a long duration. At high injection pressure, the jet velocity is high, droplets are small and the spray lasts for a short duration. In terms of wetting in-cylinder surfaces there appears to be a zero-sum trade-off for injector fuel pressure. The literature suggests that fuel injection plume can collapse at sufficiently low fuel injection pressure. In this regime, evaporation is significantly compromised and considerable enrichment is necessary to promote a combustible mixture in the gas phase.

A technique explored extensively in this work involves splitting the injection in two parts to induce favourable mixture stratification. The first fuel injection contains approximately 70% of the fuel mass, is conventionally timed during the intake stroke to promote effective mixing with the air coming in from the intake valves. The second fuel injection contains the remaining 30% of the fuel mass. It is injected late in the compression stroke, shortly before ignition. The piston has a bowl designed to interact with the prevailing charge motion and fuel injection jet to direct this injection towards the spark plug. This promotes robust flame kernel development and early flame propagation which are especially vulnerable to local paucity of fuel. A secondary potential benefit is that by confining a significant fraction of the fuel to a small region of the combustion chamber, the remaining mixture is lean of stoichiometric. When this fuel is stored in engine crevices, upon its release its enhanced oxygen content will promote effective post-flame oxidation.

Special fuel preparation

Some designers have tested systems to preheat the fuel before it is injected to promote evaporation. Results are especially encouraging for fuels with slow evaporation such as ethanol. Until now packaging and power consumption have limited market adoption but at least one manufacturer has a commercial solution ready for market.[21–24]

Some manufacturers propose a dual-fuel concept wherein the engine is operated on a separate fuel, or with special fuel additives during start-up to reduce emissions. Some concepts involve gaseous fuels, such as propane or natural gas, others use liquid

fuels that have more favourable evaporative properties than gasoline, such as iso-pentane, a final group use additives such as hydrogen to enhance evaporation and ignitability for robust, complete combustion [25–27] or as a fuel for an afterburner-style catalyst pre-heater [28].

A few of these systems have made it to mass production namely the Audi 1.8 TFSI [29] and the Toyota 2GR-FSE 3.5L V6 engine [30]. Both engines are equipped with both conventional port fuel injectors (PFI) and direct injectors (DI) for every cylinder, both using a single common fuel source. The engines use PFI for cold start to avoid the issues of DI. Once warm the engines revert to mainly DI for its performance benefits. This dual injection concept is likely to be continued since the incremental cost of retaining PFI injection is low for single fuel engines. This dual injection concept may evolve with PFI injection of gasoline and DI injection of ethanol or water for mitigation of unwanted autoignition.

Valve timing

Variable valve timing is an increasingly common capability of modern engines. In engines with static valve timing, valve timing is a compromise between low RPM stability (low residuals) and high RPM breathing (long overlap). In suitably equipped engines, valve timing can be dynamically controlled to optimize gas exchange over a wider range of conditions, usually over a variety of speed and load.

Variable valve actuation technologies can independently control timing, lift and duration of valve events but those are not yet common in the market. In perhaps the most common realization of variable valve timing, an electro-hydraulic vane motor can phase the camshafts with respect to the crankshaft. This provides flexibility of when the valves open but not the lift or duration of the valve event. This technology is very common with independent control over both the intake and exhaust camshafts. The engine used for this research has dual independent cam phasing. The intake camshaft timing may be advanced from a park position when the system is de-energized. The exhaust camshaft timing may be retarded from a park position when the system is de-energized. This implies that minimum valve overlap occurs when both camshafts

are in their respective park positions, and activation of either camshaft phaser will increase the amount of valve overlap. Valve overlap drastically changes gas exchange details and has significant implications on engine operation.

The literature provides some results on the impact of valve timing on cold start, but the topic has not been extensively explored because until now common valve timing control hardware could not respond quickly enough for use during cold-start. Moreover, the role of valve timing in mixture preparation has renewed importance in DI engines for which mixture preparation is especially important. The potential emissions or operational benefits of variable valve timing during cold start are described in the following paragraphs.

Compression temperature Normally intake valve closure (IVC) occurs approximately 35-50 CAD after bottom dead center of the compression stroke to promote better volumetric efficiency at high speed and load. The effective compression ratio, which is the ratio of cylinder volume at IVC to cylinder volume at TDC, is therefore reduced from the geometric compression ratio, which is the ratio of cylinder volume at BDC to the cylinder volume at TDC. For the engine used in this research, advancing the intake valve closure from the park position increases the effective compression ratio from a value of 7.2 to 9.2, the latter being its geometric value. For an intake air temperature of 300 K, advancing the intake camshaft increases the temperature of in-cylinder gases mixture at TDC by approximately 55 K. This higher compression temperature can enhance reaction rates for robust combustion or simply contribute to additional exhaust thermal enthalpy for faster light-off.

A secondary benefit of earlier intake valve closure is a slight increase in pumping work. Since engine output torque is held constant for cold-start, an increase of pumping work necessitates an increase to gross work to compensate. Therefore the pumping work penalty, while minor, may necessitate an increment of additional mass flow of air and fuel to compensate.

Post-flame oxidation Conventional exhaust valve opening (EVO) occurs approximately 60 CAD before bottom dead center of the exhaust stroke to promote a vigorous exhaust blowdown and enhance volumetric efficiency through better scavenging of residuals. Retarding EVO extends the expansion stroke, possibly increasing the time available for post-flame oxidation before the temperature and pressure drop associated with blowdown and heat transfer to the exhaust port and manifold.

Residuals Advancing the intake camshaft or retarding the exhaust camshaft will increase the valve overlap, which is the period during which the intake and exhaust valves are both open. At part load, such as during the warm-up period after cold start, longer valve overlap leads to higher residual gas fraction. This is because during cold-start and low load operation, the pressure in the exhaust system is at or slightly above atmospheric pressure while the pressure in the intake manifold is sub-atmospheric. With both valves open, this pressure gradient can cause flow back from the exhaust into the cylinder, and from the cylinder into the intake manifold. From the point of view of emissions, internal trapping of residuals and intake backflow may be beneficial or harmful.

The exhaust gases that are drawn back into the cylinder, or re-breathed, are usually the last parcels of gas to leave crevices. They experience the lowest burned gas temperatures for the shortest period of time, likely experiencing little if any post-flame oxidation. By re-breathing them, they can be burned in a subsequent cycle and the fraction of fuel that escapes oxidation is reduced. Moreover, these unburned or partially burned species may be more reactive and promote robust, complete combustion in the next cycle.

The gases that flow back into the intake preheat the intake port and initial fuel-air mixture. As with advancing IVC, higher temperatures increase compression temperature which enhances fuel evaporation and leads to robust combustion.

On the other hand, residual gas fraction dilutes the charge. Despite higher initial mixture temperatures, residual gases act as thermal ballast and reduce peak burned gas temperatures. Dilute mixtures at lower temperature have a lower heat release

rate, which hinders and prolongs combustion. As with late ignition, combustion with high residual gas content has high cycle to cycle variability and has higher incidence of misfire.

The influence of residual gas and variable valve timing is complicated due to coupling between the residual gas temperature, combustion phasing and residual gas fraction.

2.4.2 Thermal enthalpy

Intake air heating enhances fuel evaporation and promotes late, robust combustion. Packaging and power requirements for an electrical heater sized to heat air quickly are prohibitive since an intake air heater is generally not useful for any other phase of operation of a turbocharged engine. Using heat from the exhaust and/or coolant was common to prevent carburettor icing but it is not used for modern turbocharged engines.

Ignition timing exerts significant control on the flow rate of thermal enthalpy in the exhaust. As described in a preceding section, late ignition has lower mechanical efficiency which results in higher exhaust temperature. For fixed output torque, the flow rate of air and fuel must be increased to compensate.

A great deal of research has focused on cold-start methods based on late ignition [14, 20, 31–39] Of particular interest here, Eng examines the mechanism by which engines operating with retarded spark produce reduced emissions.[14]. Eng finds that one of the most important effects of retarded combustion phasing is to increase the total amount of time during which the unburned gas mixture is above 1500 K. Early combustion phasing results in higher peak temperatures for shorter periods of time due to higher work extraction by the piston with early combustion phasing. Eng's analysis does could not determine whether post-flame oxidation occurred in the cylinder, exhaust port, runner or manifold. However, although temperatures are highest in cylinder, insufficient time and mixing occur until the runner and manifold. Min and Cheng present evidence of poor mixing between crevice gases and burned gases in the converging jet flow out of the exhaust valve.[40]. Lee and Heywood further

support Eng's conclusion with FID measurements and quenching experiments that demonstrate substantial hydrocarbon oxidation takes place in the exhaust runner and manifold.

2.4.3 Hydrocarbon oxidation

Secondary air injection (SAI) is a method of post-cylinder oxidation. The engine is run rich with 10-30% excess fuel which produces stable combustion and exhaust gas with substantial quantities of combustible gases including CO, H_2 and HCs. Air is injected into the exhaust, sometimes with a pilot source of ignition. Ma et al. and Kollmann et al. demonstrated a substantial improvement to both catalyst-in emissions of HC and CO and shorter light-off time due to oxidation of combustible exhaust components.[34, 41] The primary challenge is to induce ignition within the first few seconds after start when exhaust gases are cold and essentially non-reacting. Later work by Borland et al., then Lee et al. showed that secondary air injection close to the exhaust port was most reliable and easiest to integrate without substantial engine design changes. Substantial calibration work is required during engine design. [36, 42]

Heat release from secondary air injection (post-cylinder oxidation), is most effective when the air is injected very close to the exhaust valve stem, triggering heat release in the exhaust port, runner and manifold. SAI-induced heat release occurs upstream of the turbocharger, so the heating effect to the catalyst, which is downstream of the turbocharger would be delayed.[6, p. 179-216] The turbocharger is upstream for performance reasons and to limit exposure of the catalyst to potentially damaging high temperatures. Ignition of gases downstream of the turbocharger is significantly more challenging due to lower temperatures there.

2.4.4 Exhaust system design

Thermal losses

One way to increase the temperature of gases flowing into the catalyst is by minimizing enthalpy losses from the exhaust gases to their environment that occur between the engine exit and catalyst entrance. This includes reducing heat transfer to the exhaust port, runner, manifold and turbine. This is primarily an engine design choice, not operating strategy.

One method to limit heat transfer losses from the gas is to install the catalyst, or one of several catalysts as close to the engine as possible. This layout is present on virtually all modern vehicles. However, catalysts that are too close to the engine may suffer durability problems due to sintering caused by excessive exhaust gas temperatures and flows at high load (i.e. non cold-start) conditions. Some variations on this design employ special oxidation-only catalysts in the upstream location. Such catalysts are more robust at high temperatures, and perform adequately for cold start when NO_x is not usually a problem.

Cylinder head and exhaust manifold designs with an annular air gap around a thin-wall shield and special coatings have been successfully demonstrated as ways to limit heat transfer losses by inhibiting heat transfer from exhaust gases. These too may compromise high load performance and heat dissipation.

Catalyst designs

Electrically-heated catalysts whose warm-up occurs due to internal electrical heating have been demonstrated but are unpopular due to concerns of longevity, reliability, cost and power consumption.

Mitsuishi et al., White, Kidokoro et al. and Nishizawa et al., among others propose systems to trap hydrocarbons during warm-up via surface adsorption for later release and oxidation when the catalyst is active.[43–46] Such systems are not sufficient on their own due to performance degradation, packaging difficulties (the adsorption traps require a large surface area) and issues with water condensation which are practically

61

unavoidable during engine cold-start.

Kidokoro et al. and Nishizawa et al. describe the catalyst structures designed with thin walls and metallic substrates to have low thermal inertia for fast thermal response during warm-up.[45, 46]

2.5 Predicted engine response

This section describes computational model predictions from a GT-POWER engine model. The GT-POWER model is explained in more detail in the next chapter. It is tuned/validated from on a limited corpus of experimental engine heat release data (i.e. fuel mass fraction burn curves) taken from a similar engine in the lab before the experimental program of this research began.

The first model results explore the expected order of magnitude of changes in chemical and thermal enthalpy flow rates in response to spark timing and equivalence ratio.

2.5.1 Ignition timing and equivalence ratio

Engine simulation provides exhaust temperature and mass flow rate predictions to compute exhaust thermal enthalpy flow rate. Basic chemical equation balance and fuel physical data are used to predict chemical composition of exhaust gas from rich combustion.

The simulations are based on a constant net indicated mean effective pressure (NIMEP) equal to 2.0 [bar], which is a reasonable engine load for cold start operations. A useful reference condition is stoichiometric operation at MBT and NIMEP equal to 2.0 [bar]. This requires a manifold pressure of 0.32-0.36 [bar], MBT ignition timing of approximately 25 to 30 [CAD BTDC], exhaust gas flow rate of 5.6-5.8 [g/s] and yields exhaust gas temperature of 500-525°C.For these calculations an average molecular weight of the exhaust of 30 g/mol was assumed.

Exhaust gas mass flow rate, and exhaust gas temperature rise rapidly as ignition is retarded from MBT at constant NIMEP, as shown in Figure 2-6 and Figure 2-7

respectively.
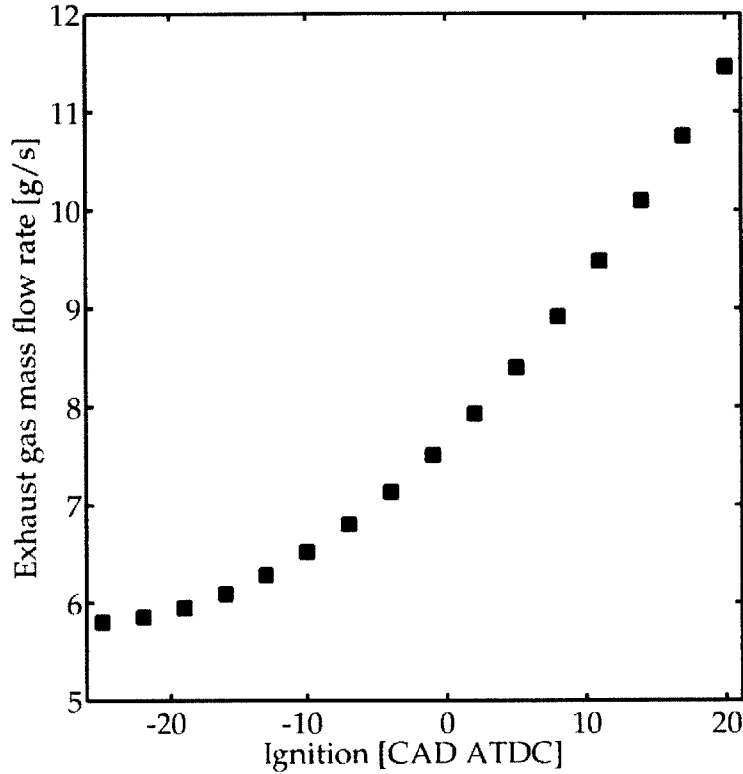
Figure 2-6: Late ignition timing leads to significant increase in exhaust gas mass flow rate for constant NIMEP=2.0 [bar] and Φ=1.

The mass flow rate and exhaust gas temperature are combined into a thermal or sensible enthalpy flow rate $\dot{Q}_{exh,thermal}$ defined in 2.3

$$\dot{Q}_{exh,thermal} = \dot{m}_{exh} \cdot c_{p,exh} \cdot (T_{exh} - T_{ref}) \tag{2.3}$$

Where $\dot{m}_{exh}$ is the mass flow rate of exhaust in [kg/s], $c_{p,exh}$ is the specific heat capacity at constant pressure in [J/(kg*K)], T_{exh} is exhaust gas temperature in°C, and T_{ref} is ambient reference temperature. $\dot{Q}_{exh,thermal}$ is a measure of the flow rate of thermal energy at the location where mass flow rate and temperature are measured.

A simple model of combustion is used to predict exhaust gas composition. Complete, stoichiometric or lean combustion ($\Phi \leq 1, \lambda \geq 1$) of hydrocarbons in air produces CO_2, H_2O, O_2 and N_2 only. Complete lean or stoichiometric combustion above is deterministic with λ as a free parameter, which Equation 2.4 shows for lean or sto-
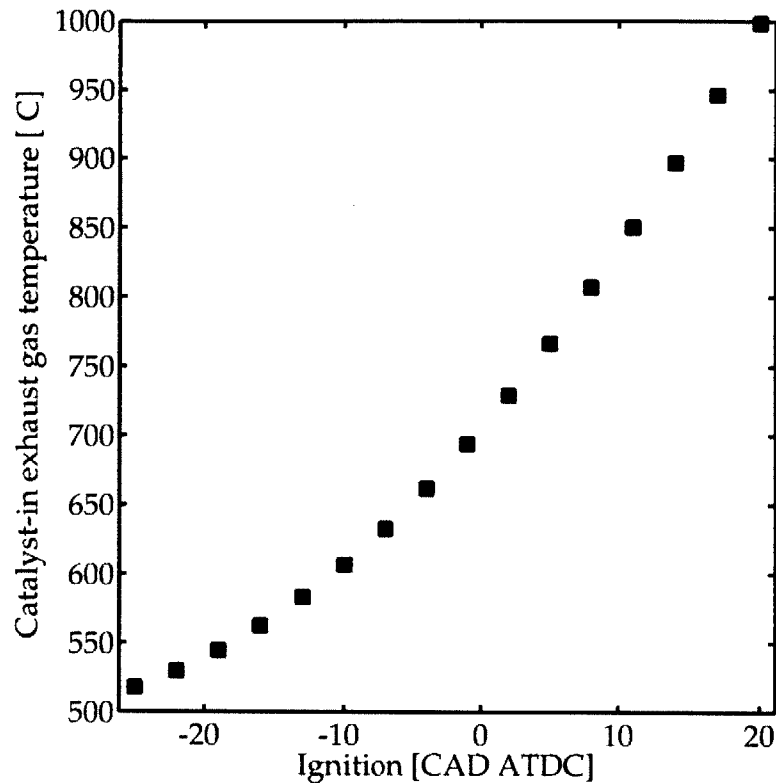
Figure 2-7: Late ignition timing leads to significant increase in exhaust gas temperature for constant NIMEP=2.0 [bar].

ichiometric combustion of iso-octane in air. The chemical formulation actually used for the fuel has a hydrogen to carbon ratio of approximately H/C=1.85.

$$C_8H_{18} + 12.5 \cdot \lambda \cdot (O_2 + 3.76N_2) \longrightarrow 8\,CO_2 + 9\,H_2O + (\lambda - 1)O_2 + 47 \cdot \lambda \cdot N2 \quad (2.4)$$
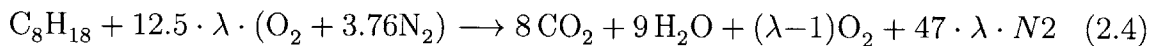
Rich operation can stabilize combustion. Rich combustion is also common with secondary air injection where unburned or partially burned combustion products provide a source of chemical enthalpy for post-cylinder oxidation. Complete oxidation of the fuel with a rich mixtures ($\Phi \geq 1, \lambda \leq 1$) does not have O2 as a product but does produces CO, and H_2 because there is insufficient oxygen to complete the oxidation of CO, and H_2 to CO_2 and H_2O respectively. Equation 2.5 shows the additional products.

$$C_8H_{18} + 12.5 \cdot \lambda \cdot (O_2 + 3.76N_2) \longrightarrow bCO_2 + cH_2O + 47 \cdot \lambda \cdot N_2 + dCO + eH_2 \quad (2.5)$$
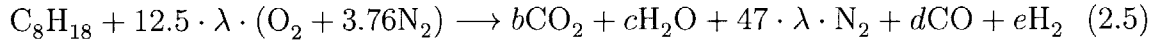
There are 4 unknown coefficients in Equation 2.5 (b-e inclusive) because there are only 3 equations from species balances (C, H, and O). The situation would be even more complicated if oxides of nitrogen, partially oxidized hydrocarbons or other trace species were admitted. This system cannot be solved because there is no information available about the ratio of CO to H_2. The water-gas shift reaction with chemistry that has been frozen at approximately 1740K yields a reaction constant $K_{wg}=3.5$ which approximates the observed species ratio. This is not a physical law, it is an empirical finding found to provide reasonable predictions of the ratio of CO to H_2 in exhaust gases of combustion or rich gasoline mixtures. Equation 2.6 is the fourth (non-linear) equation with which the system of equations can be solved to predict major combustion products of rich combustion. The exhaust composition is not that sensitive to K_{wg}. [8]

$$CO + H_2O \rightleftharpoons CO_2 + H_2; K_{wg} = \frac{[CO_2][H_2]}{[CO][H_2O]} \quad (2.6)$$
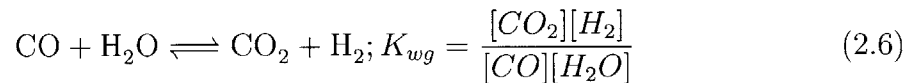
Now that rich combustion products can be predicted, it is possible to compare the flow of chemical enthalpy in the exhaust stream. Chemical enthalpy is the sum-product of each majors species mass flow rate and its respective lower heating value. Hydrocarbon species are ignored in this simplified analysis because it is assumed the fuel oxidizes completely. In real rich combustion unburned hydrocarbons are found in molar concentrations up to 1-2%, usually far less than CO.

For a slightly rich mixture (Φ=1.1) Figure 2-8 shows that chemical enthalpy in exhaust gases is significant, but that thermal enthalpy dominates for late ignition timing.

For a higher fuel-air equivalence ratio (Φ=1.3) Figure 2-9 shows that exhaust enthalpy flow rate is primarily chemical over all ignition timing.

Higher fuel-air equivalence ratio produces more CO and H_2, but rich mixtures

65
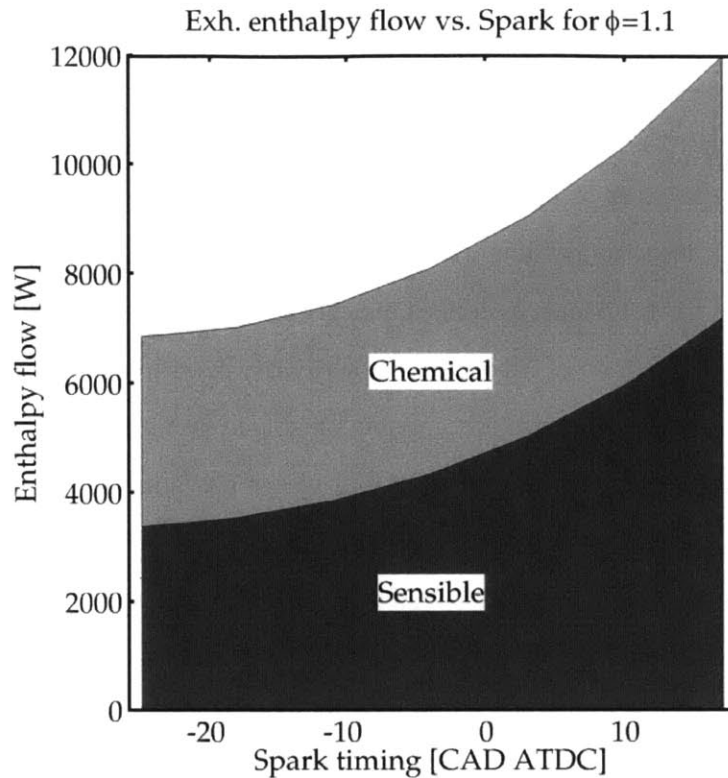
Figure 2-8: At an equivalence ratio of Φ=1.1 and early ignition timing, sensible enthalpy and chemical enthalpy flow rates are comparable in magnitude. For late ignition exhaust enthalpy flow rate is primarily sensible, or thermal in nature.

also cause lower exhaust temperatures due to greater amount of charge cooling when a greater fuel quantity evaporates and lower specific heat ratio of the fuel-rich air mixture. Figure 2-10 shows predicted exhaust gas temperature for ignition timing at different equivalence ratios.

Although rich mixtures appear to have substantially higher flow rates of chemical enthalpy, heat release from that chemical enthalpy in the exhaust (e.g. post-cylinder oxidation via secondary air injection) requires sufficiently high exhaust temperatures to ignite the CO, H_2 and other partially oxidized hydrocarbon species. Therefore late ignition for maximum exhaust temperatures is required, which confirms the need to find operating strategies that facilitate late, complete combustion.
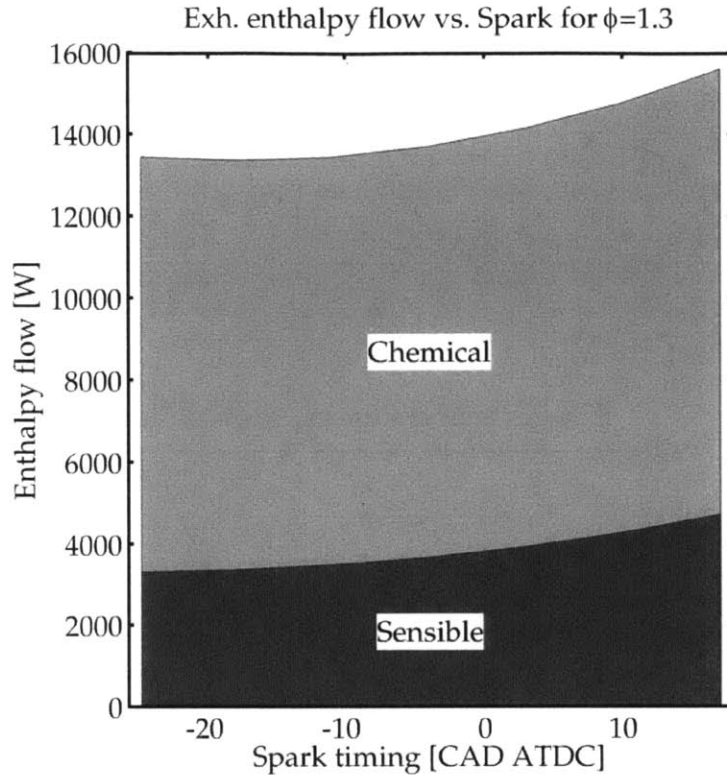
Figure 2-9: At an equivalence ratio of $\Phi=1.3$, chemical enthalpy is significantly greater than thermal enthalpy even for the latest ignition timing.

2.5.2 Variable valve timing

Intake cam phasing

The compression stroke in a spark ignition engine is sometimes approximated as isentropic compression of air. Actual measured cylinder pressure and volume data give a better fit to a polytropic compression process whose polytropic exponent during compression is 1.32-1.35 during the compression stroke. Heat transfer from the combustion chamber gases to the walls and the presence of fuel in the mixture during compression explain the discrepancy between the measured polytropic compression and idealized isentropic compression of air for which the polytropic exponent would be equal to $\gamma=1.4$.

The temperature in a later part of the stroke can be estimated from initial temperature using a model of polytropic compression in Equation 2.7.
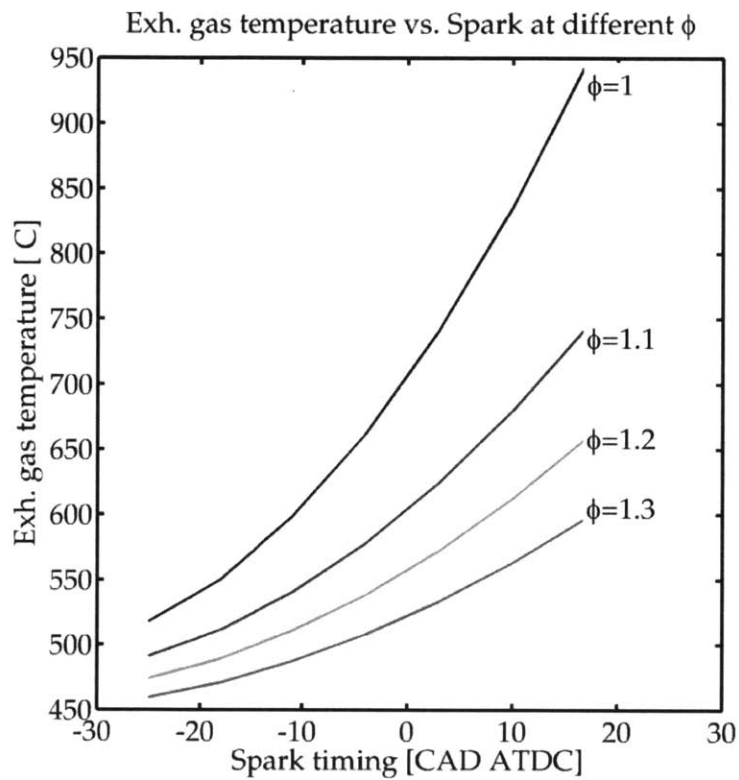
Figure 2-10: Late ignition increases exhaust gas temperature for all mixtures. Rich mixtures have lower exhaust temperatures due to increased charge cooling and reduced mixture specific heat ratio.

$$T_2 = T_1 \left(\frac{v_1}{v_2} \right)^{n-1} \tag{2.7}$$

where T_1, and v_1 are the combustion chamber gas temperature in K, and cylinder volume at the beginning of the process respectively, and T_2 and v_2 are the temperature in K and cylinder volume at the end of the process respectively, and n is the polytropic process exponent. A slider-crank model estimates combustion chamber volume as a function of crankshaft position. T_1=300K is the mixture temperature at IVC, n =1.32 is a lower bound on the polytropic exponent, state 2 is at TDC. From the camshaft park position to full intake camshaft advance, IVC ranges from 61 [CAD ABDC] to 11 [CAD ABDC]. Figure 2-11 shows that intake cam phaser advance significantly increases effective compression ratio, which is the ratio of combustion chamber volumes at IVC and TDC. For reference the geometric compression ratio is the ratio of combustion chamber volumes at BDC and TDC.
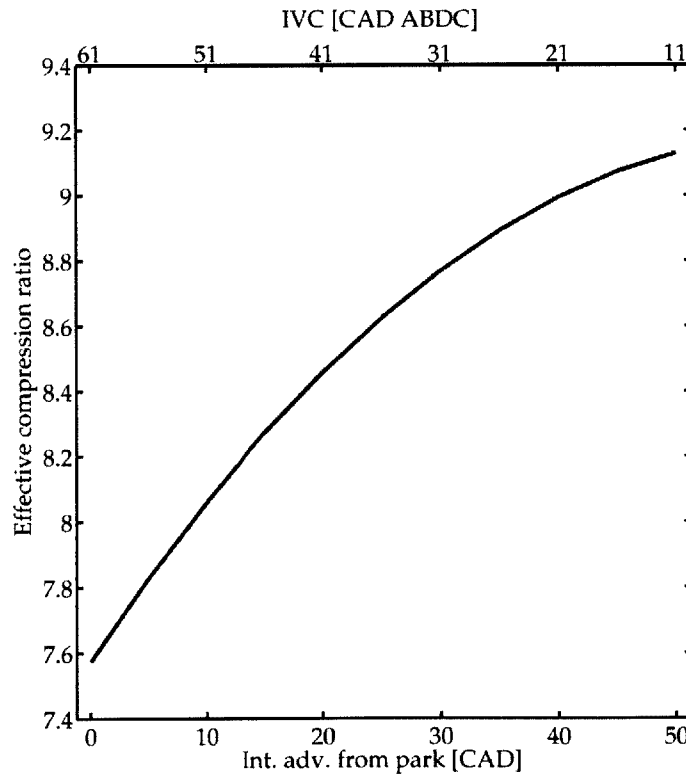
Figure 2-11: Intake cam phasing can significantly increases the effective compression ratio.

The choice of a constant mixture temperature $T_i=300K$ represents a lower limit on the the variation in mixture temperature at TDC. Effective compression ratio alone leads to modest changes in mixture temperature at TDC for fixed initial mixture temperature as shown in Figure 2-12.
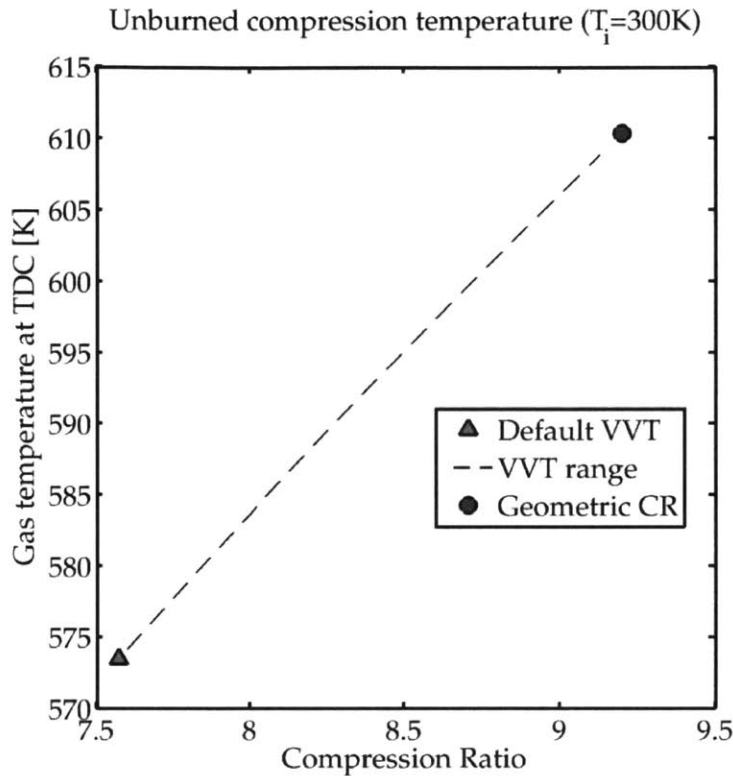
Figure 2-12: Intake cam phaser advance alone only modestly increases mixture temperature at TDC, probably insufficient to advance and stabilize combustion with late ignition timing.

For fixed duration cams, intake cam phaser advance increases the valve overlap period which increases the trapped residual fraction. High trapped residual fraction increases the initial mixture temperature and therefore mixture compression temperature at TDC. However, as a diluent high residual fraction may depress peak temperatures and pressures. The actual variation of residual gas fraction with valve timing are not yet known, so a simple model of residual fraction is used to estimate the influence of residual fraction on initial mixture temperature and compression temperature. In this model, residual gas mass fraction varies linearly from 0-20% with valve overlap and intake cam phaser advance from 0-50 [CAD]. Therefore residual

70

gas fraction is correlated with high effective compression ratio. Residual gas temperature is unknown so a range of reasonable estimates for late combustion are included. Figure 2-13 shows that residual gas fraction can significantly increase initial mixture temperature. Figure 2-14 shows that high residual gas fraction significantly increases the peak mixture temperature. The mixture pre-heating effect appears promising as a way to improve fuel evaporation and stabilize late combustion if the diluent effect of high residual gas fraction does not cause excessive cycle-to-cycle fluctuations and partial-burn misfire.
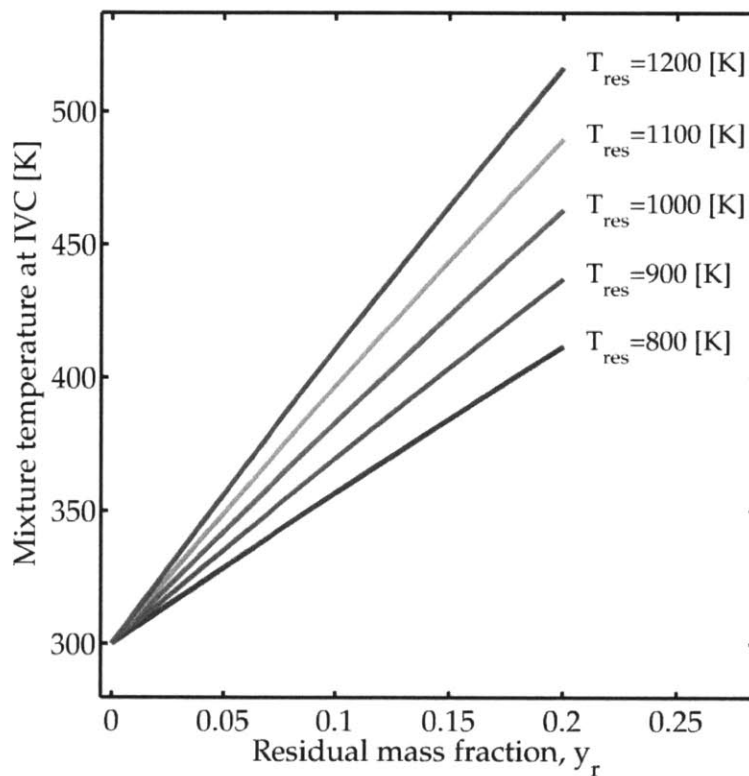
Figure 2-13: Residual gas fraction significantly increases initial mixture temperature.

Exhaust cam phasing

Exhaust cam timing can retard EVO from its base at 52 [CAD BBDC] to as late as 2 [CAD BBDC]. This extends the expansion stroke and increases work extraction by the piston and cools the gases in the combustion chamber. This reduces the flow rate of thermal enthalpy in the exhaust, but increases the length of time available for
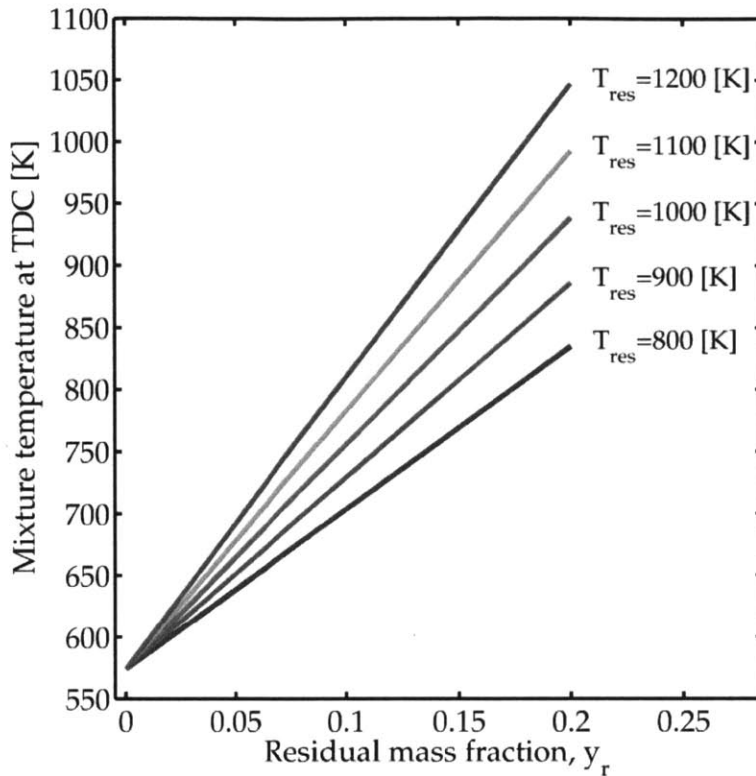
Figure 2-14: Intake cam advance increases residual gas fraction and effective compression ratio simultaneously causing a substantial increase in mixture temperature at TDC.

post-flame oxidation of unburned hydrocarbons in combustion chamber gases.

For the fixed duration cams in this engine, exhaust cam phasing retard delays EVO, which makes the expansion stroke longer. Exhaust cam phasing retaard also increases the duration of valve overlap and residual gas fraction (i.e. burned gas trapped from previous cycle). Assuming a constant temperature at the beginning of the expansion stroke of 2000K, Figure 2-16 shows that later EVO (longer expansion stroke, higher effective expansion ratio) only modestly reduces gas temperatures.

In reality, the net impact of exhaust cam phasing depends on the degree to which those residuals affect combustion. Residual gases increase the initial mixture temperature, but through dilution of reactants and added inert thermal mass, maximum temperature and temperatures through the expansion stroke are usually depressed. To account for lower temperatures due to high residual gas fraction, the temperature at the beginning of the expansion stroke is assumed to vary linearly from 2000K down

72
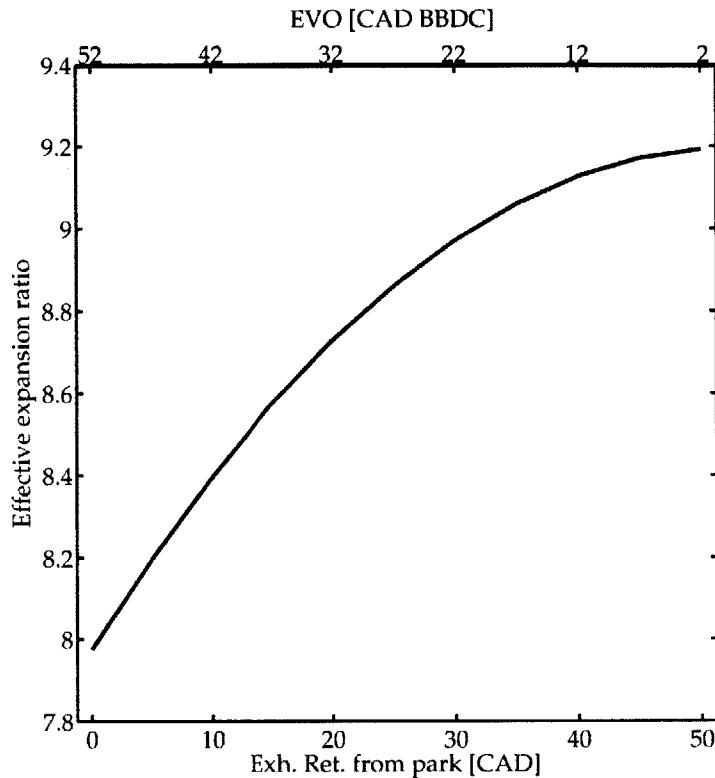
Figure 2-15: Exhaust cam phasing can significantly increase the effective expansion ratio.

to 1650K when exhaust cam phaser retard varies from 0 [CAD] to 50 [CAD]. With this assumption, Figure 2-17 shows that later exhaust cam phasing leads to significantly lower gas temperature at EVO.

Later EVO linearly increases time available for post-flame oxidation. The expectation is that high residual gas fraction from exhaust cam phaser retard will cause cycle-to-cycle variations and reduce peak gas temperatures and temperatures throughout the expansion stroke ending at EVO and therefore reduce the potential post-flame oxidation benefit. Moreover, the maximum post-flame oxidation benefit occurs for the last portions of gas to leave engine crevices, which are the same gases most likely to be re-breathed back into the combustion chamber during valve overlap period. That is, the gases that most benefit from enhanced PFO due to late EVO are least likely to end up travelling to or through the ineffective catalyst.
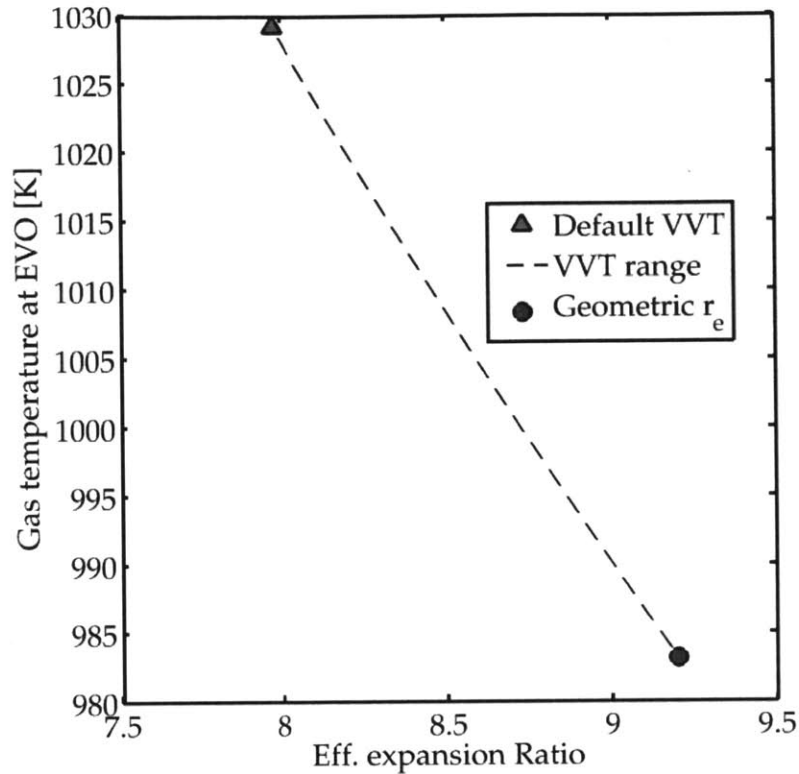
Figure 2-16: For a constant temperature at the beginning of the expansion stroke, exhaust cam phasing only modestly reduces temperatures at EVO.

2.5.3 Back pressure

Work done by the piston during the cycle to expel exhaust gases and induct fresh charge is called pumping work. For unboosted operation during cold-start, the average exhaust system pressure is usually above atmospheric by around 5 [kPa] and intake manifold pressure is usually subatmospheric by 20-70 [kPa]. Figure 2-18 contains a PV-diagram with the pumping loop labelled and shaded in red.

Pumping work mean effective pressure (GIMEP) is commonly approximated as the arithmetic difference between exhaust and intake pressures. Following from Equation 2.1, higher PIMEP requires higher GIMEP to compensate to maintain constant NIMEP. Lower intake manifold pressure, p_i and higher exhaust pressure p_e increase PIMEP. Lower intake pressure reduces air flow and results in lower GIMEP, so this fails to maintain constant NIMEP. To increase GIMEP to compensate for higher PIMEP from higher exhaust pressure, the intake pressure must increase, which de-
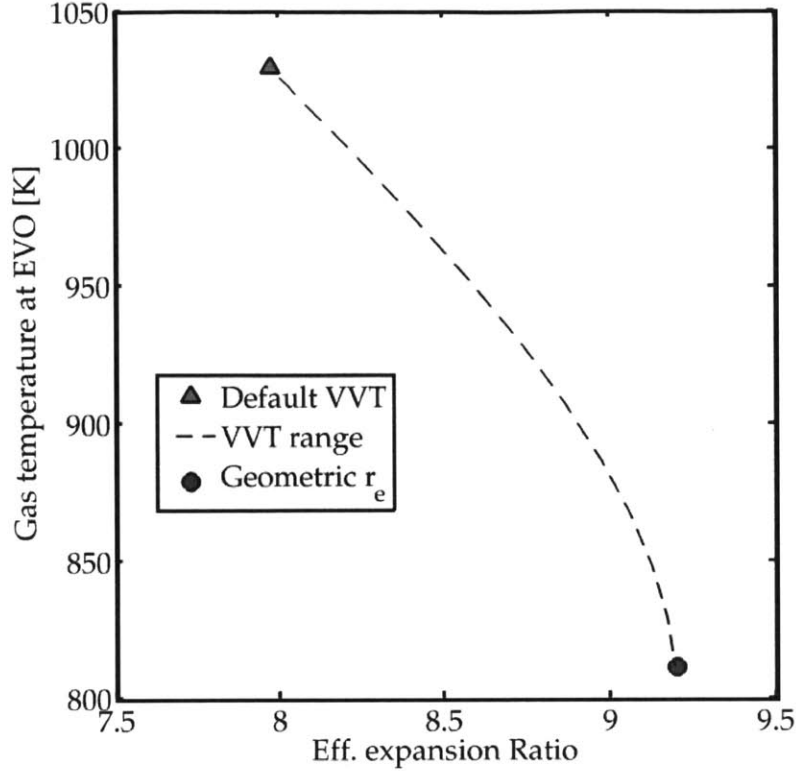
Figure 2-17: Very late EVO timing increases residual gas fraction whose added thermal mass and dilution significantly reduce temperatures at EVO.

creases PIMEP.

Referring to Figure 2-18, for fixed NIMEP the relationship between exhaust pressure and GIMEP is complicated by the purple shaded triangular region, which contributes equally to GIMEP and PIMEP and has zero net effect on NIMEP. Higher exhaust pressure shifts some area from a formerly blue GIMEP-only region to the triangle region, higher intake pressure decreases the size of the red and purple regions. The air-fuel equivalence ratio in Equation 2.8 and volumetric efficiency in Equation 2.10 can be substituted into Equation 2.1 and simplified to obtain an expression for NIMEP in terms of p_i.

$$\lambda = \frac{\left(\frac{m_a}{m_f}\right)_{actual}}{\left(\frac{m_a}{m_f}\right)_{stoich.}} \tag{2.8}$$

Where the numerator is the current air-fuel ratio by mass and the denominator is the stoichiometric air-fuel ratio by mass, which is a fuel property. Equation 2.8 can be

75

PV Diagram
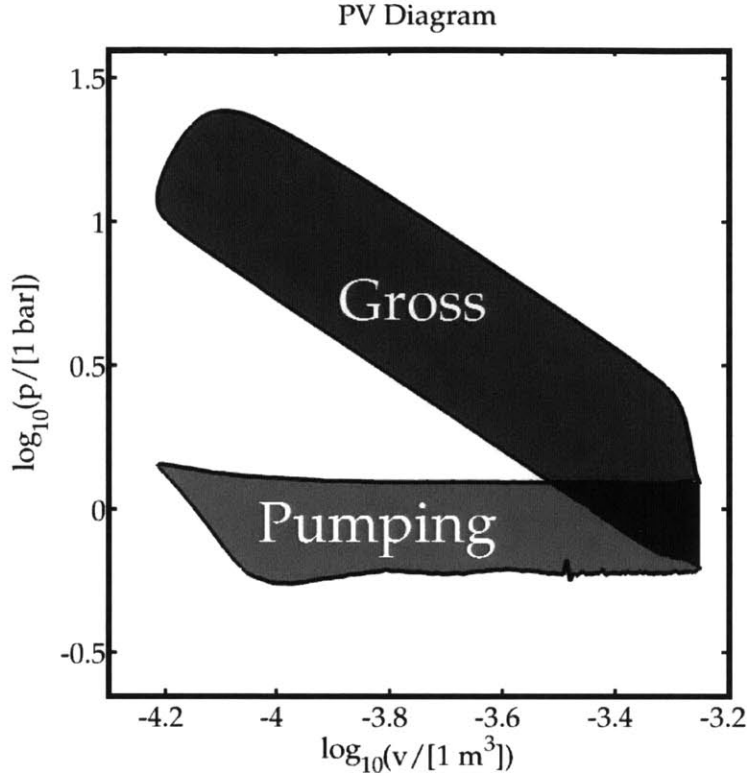
Figure 2-18: The red shaded area of the pumping loop is related to PIMEP and pumping work. The blue shaded area is the gross work loop. The purple shaded area contributes equally to both gross work and pumping work and has no impact on NIMEP. Note that log-log scale distorts the true magnitude of bound areas. For this plot, GIMEP=5.5 [bar], PIMEP=0.6 [bar] and NIMEP = 4.9 [bar].

rearranged to express fuel mass m_f in terms of air mass m_a, air-fuel equivalence ratio λ, and stoichiometric air-fuel ratio $\left(\frac{m_a}{m_f}\right)_{stoich.} = AF_{st.}$ as shown in Equation 2.9.

$$m_f = \frac{m_a}{\lambda \left(AF_{st.}\right)} \tag{2.9}$$

Then air mass m_a can be expressed in terms of intake manifold pressure p_i as shown in Equation 2.10

$$\eta_v = \frac{m_a}{\rho_{i,0} V_D} \rightarrow m_a = \eta_v \left(\frac{p_i}{R_a T_i}\right) V_D \tag{2.10}$$

Where m_a is air mass, $\rho_{i,0}$ is intake reference density, V_D is engine displacement volume, p_i is the intake manifold pressure, R_a is the universal gas constant for air and T_i is the intake manifold pressure.

Equation 2.11 incorporates the preceding equations to express NIMEP from Equation 2.1 as:

$$GIMEP - PIMEP = NIMEP = const.$$

$$\left(\eta_v \left(\frac{p_i}{R_a T_i} \right) \left(\frac{Q_{LHV}}{\lambda AF_{st.}} \right) \eta_{comb} \eta_{i,g} \right) - (p_e - p_i) = NIMEP = const. \qquad (2.11)$$

$$p_i \left[1 + \eta_v \eta_{comb} \eta_{i,g} \left(\frac{1}{R_a T_i} \right) \left(\frac{Q_{LHV}}{\lambda AF_{st.}} \right) \right] - p_e = NIMEP = const.$$

The second term in the square brackets of Equation 2.11 is always greater than unity. Therefore an increase in exhaust back-pressure p_e should be larger than the increase in intake manifold pressure p_i that counterbalances it for constant NIMEP. The preceding conclusion assumes that other parameters in the equation remain constant. For a given air-fuel equivalence ratio, the $\frac{Q_{LHV}}{\lambda AF_{st.}}$ term is a fuel property and effectively constant for all fuels in this research since it varies by only 2% between neat gasoline ($\frac{44}{1 \cdot 14.6} = 3.01$ [MJ/kg]) and neat ethanol ($\frac{26.9}{1 \cdot 9} = 2.99$ [MJ/kg]). For other parameters, this assumption depends on valve timing and valve overlap. Valve overlap affects volumetric efficiency η_v, and residuals from long valve overlap degrade combustion efficiency η_{comb}, gross indicated fuel conversion efficiency $\eta_{i,g}$ and increase intake air temperature T_i. The overriding requirement for high combustion completeness limits the variability of the second term in the square brackets. From worst-case (η_v=0.3, η_{comb}=0.95, $\eta_{i,g}$=0.05, T_i=330K) to typical values (η_v=0.85, η_{comb}=0.97, $\eta_{i,g}$=0.20, T_i=293K), the term square bracket ranges from 0.45 to 6.0 and the conclusion is that at constant NIMEP, increasing exhaust back-pressure increases exhaust thermal enthalpy flow rate by increasing GIMEP. For constant NIMEP it is difficult to predict whether the increased back exhaust back pressure and increased manifold pressure will net any increase to trapped residuals. The effect of back pressure on combustion stability must be quantified experimentally. Also, it is known that combustion at high GIMEP has advanced phasing, shorter duration and lower cycle-to-cycle variability, but the magnitude of that benefit must be quantified experimentally.

The second major effect of exhaust back pressure is how it affects the temperature of exhaust gases. During the blowdown event, combustion chamber gases undergo

expansion from the prevailing cylinder pressure to the exhaust system pressure. The expansion of cylinder gases during exhaust blowdown reduces their temperature and pressure. For constant temperature and pressure at the start of blowdown, an exhaust gas flow restriction increases the exhaust back-pressure, decreases the extent of blowdown expansion resulting in higher temperature and pressure of exhaust gases as shown in Figure 2-19.
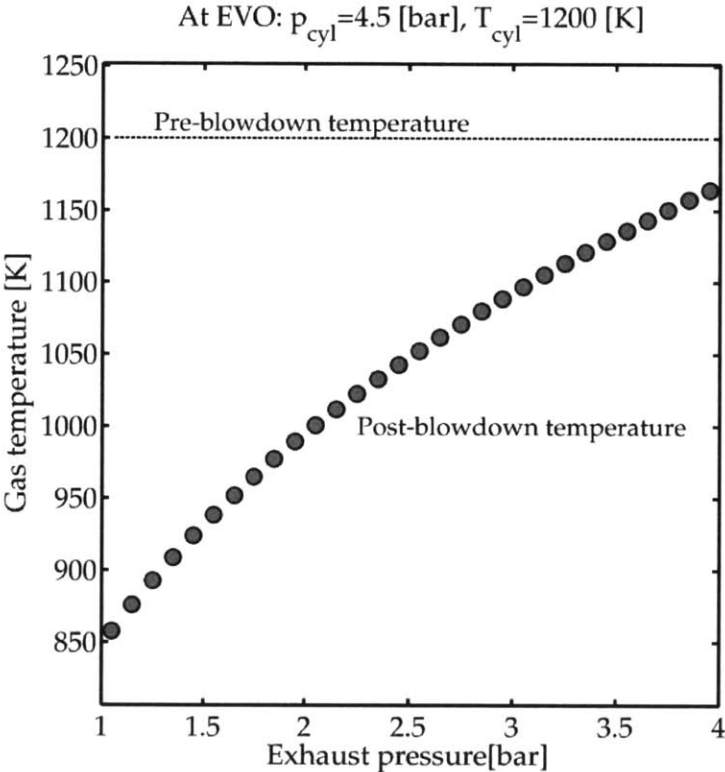
Figure 2-19: A restricted exhaust reduces the expansion of combustion chamber gases during blowdown resulting in significantly higher temperature and pressure.

2.5.4 Turbine heat transfer

Detailed heat transfer characteristics of the turbine were not available. A simple lumped capacitance model of the exhaust system is used to predict transient thermal response. The model is based on an RC-circuit analogy. The model comprises a manifold, turbine, pre-cat section and catalyst. It has the known physical properties of each component (mass, specific heat capacity, surface area). The inlet gas temper-

ature (i.e. engine-out exhaust port gas temperature) is imposed on gas entering the manifold.

The outputs of the model are component-inlet temperature predictions. Internal convective heat transfer coefficients and external convective heat transfer coefficients are estimated from literature. The convective heat transfer coefficients are then adjusted based on a limited corpus of experimental data collected from another engine. The final prediction of exhaust thermal transient shows surprising (and perhaps fortuitous) agreement with actual experimental data taken later.

At an exhaust gas mass flow rate of 10 [g/s], Figure 2-20 shows the model predicts exhaust gas at the catalyst inlet reaches a temperature of only 600K at time t=100 [s], but if the turbine is removed by setting its heat capacity to 1e-10 [J/(kg*K)], the equivalent of bolting the catalyst onto the manifold exit, then Figure 2-21 shows that exhaust gas at the catalyst inlet reaches 600K after at t=10 [s], plateauing at a temperature of 750K at t=100 [s]. Clearly the transient thermal response of exhaust gases entering the catalyst is difference, what is most significant for fast warm-up is the first 20 [s].

Over the first 100 [s] the no-turbo case increases cumulative thermal enthalpy delivery to the catalyst from 276 [kJ] to 461 [kJ], or 67% more cumulative thermal enthalpy. Most of the improvement comes during the critical first 20 [s] of catalyst warm-up. Over this period the no-turbo case increases cumulative thermal enthalpy delivery from 29 [kJ] to 56 [kJ], or a 93%. Verily the thermal mass of the turbine significantly delays catalyst warm-up and suggests that waste-gate bypass may effectively accelerate catalyst warm-up.
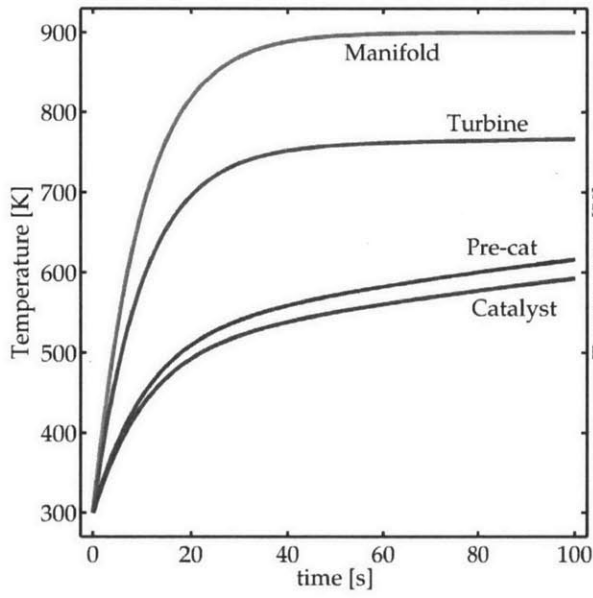
Figure 2-20: With turbine.
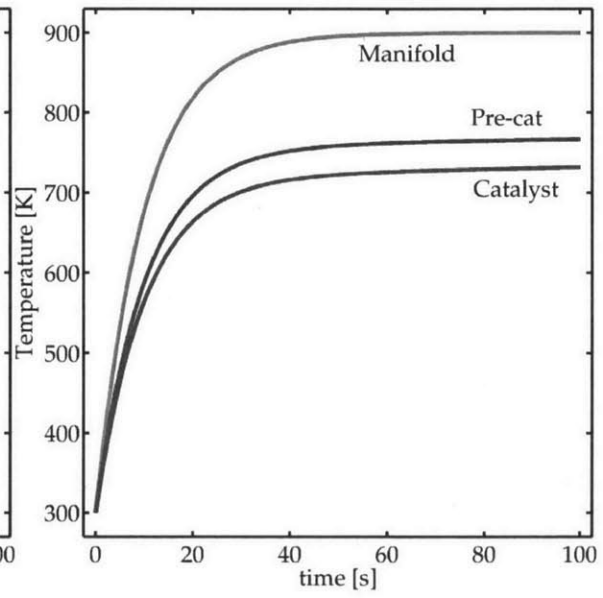
Figure 2-21: No turbine.

CHAPTER 3
EXPERIMENTAL RESULTS

THIS chapter presents experimental results from tests to characterize how unburned hydrocarbon emissions responds to changes in engine operating parameters. Experimental results are organized according to engine operating parameter. Coarse observations are presented in each section. The data focuses on factors that affect cold-start emissions performance, namely exhaust thermal enthalpy flow and exhaust hydrocarbon content. These coarse observations are the basic inputs for the exhaust system and catalyst model (detailed in the next chapter) including exhaust mass flow rate, exhaust temperature, exhaust composition (i.e. emissions data), fuel consumption rate and cycle-to-cycle variability. Some analysis and discussion of the physical phenomena and trade-offs responsible for the observed trends are included in each section. The first set of experiments relate to ignition timing.

3.1 Ignition Timing

The experimental data presented in this section were collected with one single fuel injection and stoichiometric mixture conditions according to measurements on the engine λ sensor. The data agree very well with model predictions. Figure 3-1 shows that late ignition timing increases exhaust gas temperature and exhaust gas mass

flow rate. The simultaneous increase of exhaust gas temperature and exhaust gas mass flow rate lead to a quadratic rise in exhaust thermal enthalpy flow rate. As
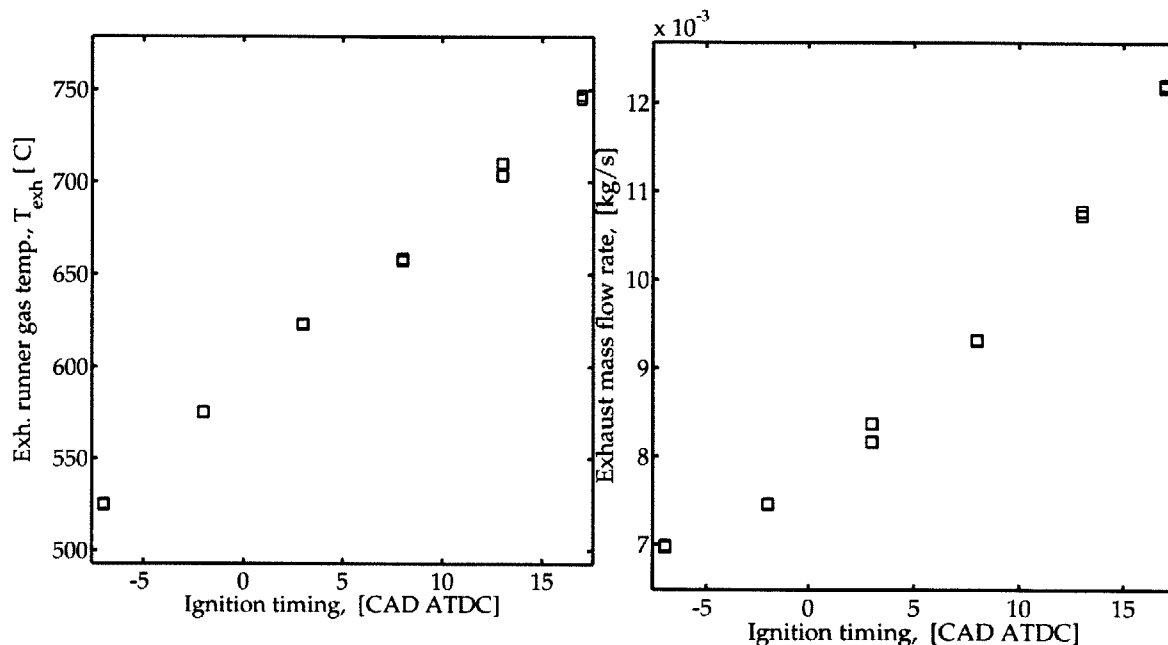
Figure 3-1: Late ignition time decreases $\eta_{i,g}$ which leads to a concomitant rise in exhaust gas temperature (left) and mass flow of air and fuel (right) to maintain a constant load.

exhaust gas temperature increases, the concentration of unburned hydrocarbons at the catalyst inlet decreases. Late ignition increases mass flow rate and decreases hydrocarbon concentration. Figure 3-2 shows that the net result is that late ignition decreases the mass flow rate of unburned hydrocarbons into the catalyst.

This very productive trend is limited by a rise in cycle-to-cycle variability. Figure 3-3 shows that late ignition causes COV to rise. This experiment shows a slope of approximately 300 [W] of thermal enthalpy flow per degree of spark retard. The next section looks at control over chemical enthalpy flow rate.
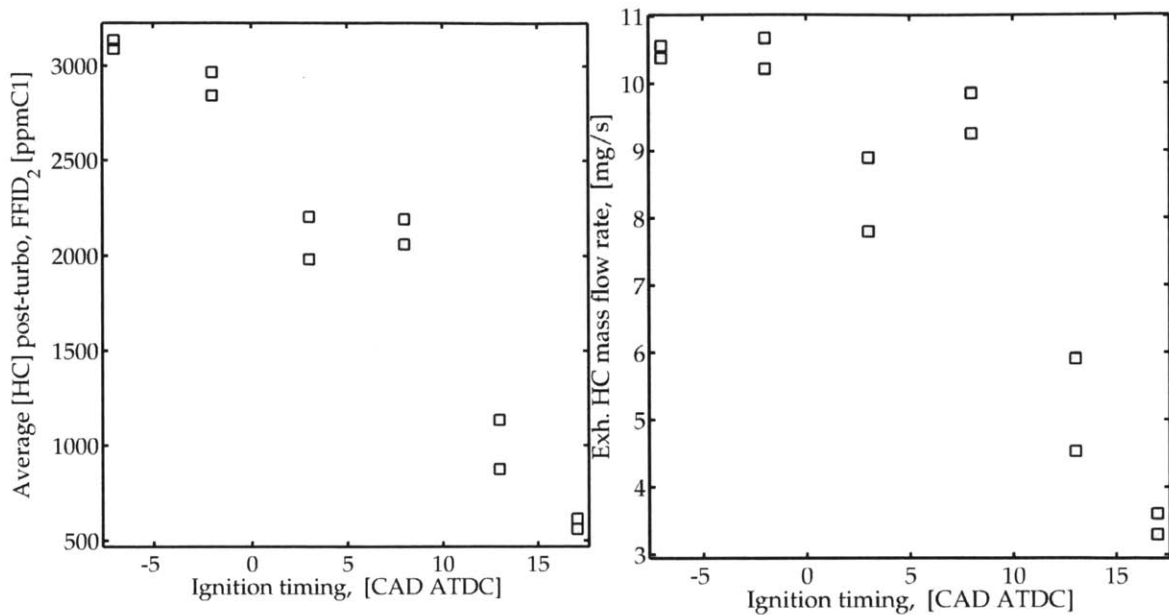
Figure 3-2: Late ignition causes hydrocarbon concentration to fall (left) at a greater rate than the mass flow rate of exhaust rises. The net result is that late ignition causes the mass flow rate of hydrocarbons to decrease (right).
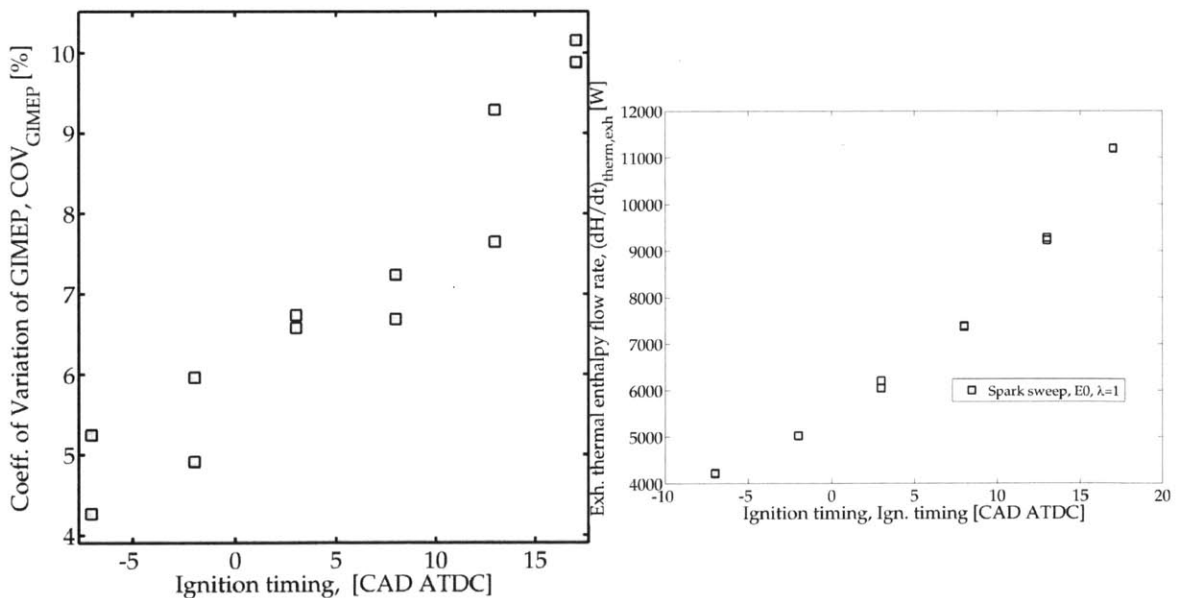
Figure 3-3: The latest ignition timing achievable for these conditions was 17 [CAD ATDC] (left). Attempts to operate at later ignition timing resulted in partial-burn misfire. At this ignition timing, exhaust thermal enthalpy flow rate is approximately 11 [kW].

3.2 Equivalence Ratio

This section attempts to quantify the chemical enthalpy gains from rich operation. The chosen range of equivalence ratios is based on the optimum engine-equivalence ratio that Lee found for secondary air injection.[42] For Lee's work, enriched operation improved stability compared to lean or stoichiometric operation. Excessively rich operation led to exhaust gas too cold to initiate heat release with secondary air. Thus Lee's optimum was a balance of stable combustion in-cylinder, and maximum heat release due to oxidation in the exhaust system. Under some conditions it appeared that different cylinders had different equivalence ratios from each other. This maldistribution of fuel and air did not affect the trends presented here. In fact, it inspired an idea for facilitating post-cylinder oxidation that is discussed in the Future Work section of the conclusions.

The chemical enthalpy flow rate for a contour map of different ignition times and equivalence ratio is presented in Figure 3-4. The stabilizing effect of rich operation is
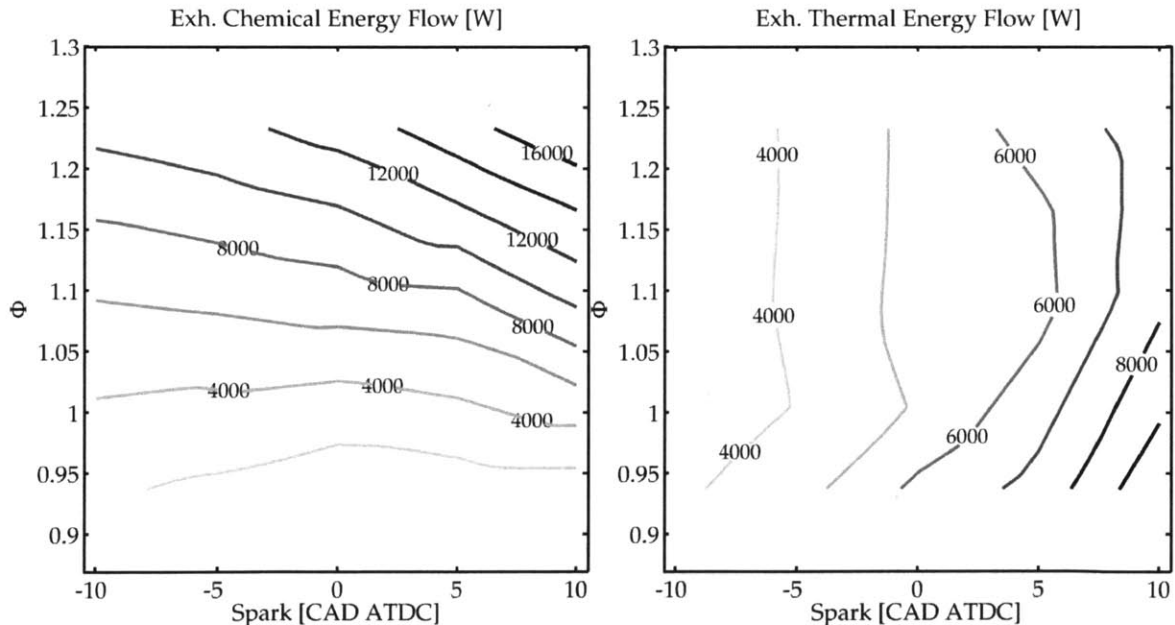
Figure 3-4: As fuel-air equivalence ratio (Φ) increases, chemical enthalpy flow rate (left) increases dramatically from a minimum of approximately 2 [kW]. Thermal enthalpy flow rate (right) shows weak sensitivity to equivalence ratio.

evident in Figure 3-5, which shows low cycle-to-cycle variability for all rich equivalence

84

ratios. Unlike the model, exhaust gas temperature appears to be relatively insensitive to equivalence ratio. However, dilute lean mixtures ($\Phi \leq 1$) have later combustion phasing, and at constant load leads to higher exhaust temperature. Figure 3-6 Rich
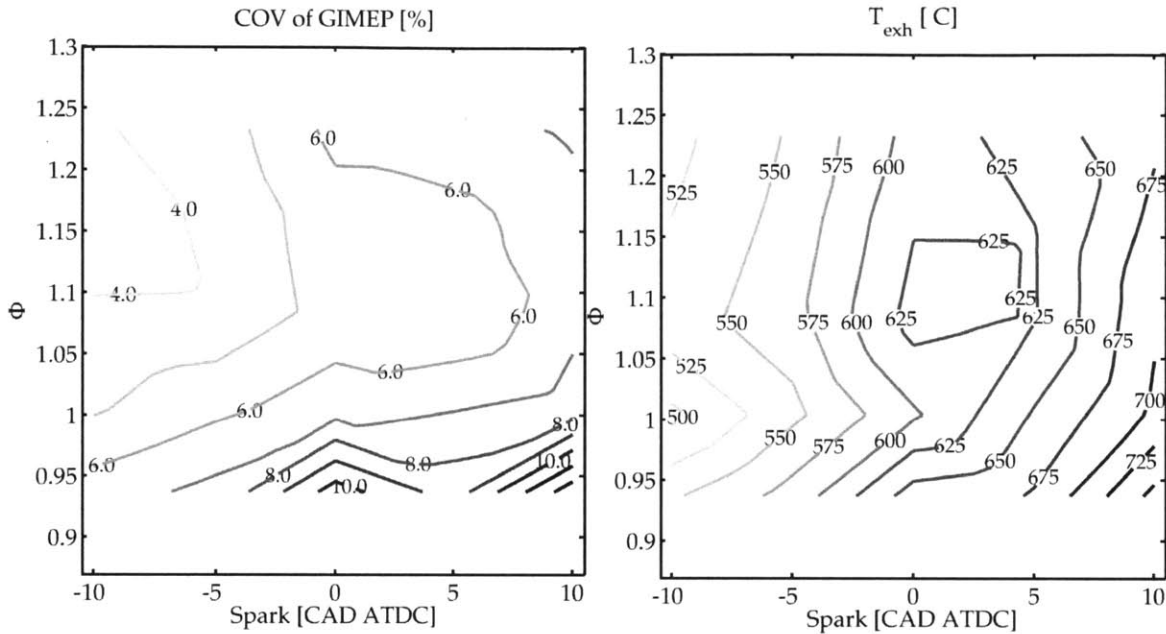
Figure 3-5: Rich mixtures ($\Phi => 1$) reduce cycle to cycle variability (left). Exhaust gas temperature appears insensitive to equivalence ratio except for lean mixtures with late ignition timing.

mixtures also increase hydrocarbon mass flow rate. Depending on the ignition timing, the mass flow rate of unburned hydrocarbons goes up by a factor of 2-6 while the total enthalpy flow rate (chemical+thermal) goes up by 2-3. The conclusion is that rich operation is effective to stabilize combustion but comes with significant increase in fuel consumption and emissions. Rich operation should not be used without some guaranteed means of post-cylinder oxidation to consume the high mass flow rate of hydrocarbons such as secondary-air injection.

The previous two engine operating parameters, ignition timing and equivalence ratio directly control the thermal and chemical enthalpy flow rates. Intake and exhaust valve timing, the next engine operating parameters considered, exert indirect influence over combustion and engine emissions response.

85
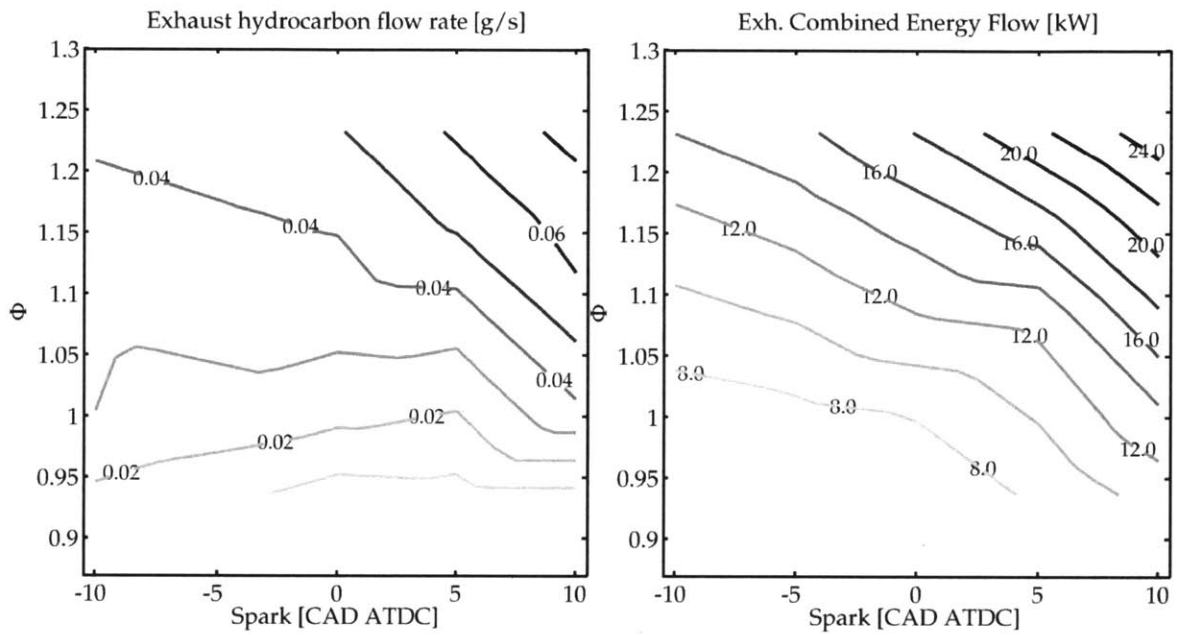
Figure 3-6: The increase of hydrocarbon mass flow rate (left) appears to outpace the rise in total enthalpy (right). This suggests that rich operation should not be used for stability without some means to oxidize the excess hydrocarbons that result from rich operation.

3.3 Variable Valve Timing

This section presents results from experiments that varied intake camshaft advance and exhaust camshaft retard. The experiments were conducted at a conservative spark timing of -5 [CAD ATDC] to tolerate instability and explore a wide range of valve timing. The findings of this series of experiments are presented as contours. A pattern emerged in the data where engine response strongly correlated with the valve overlap period.

Figure 3-7 presents the full range of valve timing available and reference gas exchange events (IVO and EVC) with contours of valve overlap as a function of intake camshaft phaser advance and exhaust camshaft phaser retard. Valve event reporting is based on reference lift of 0.25 [mm], that is, IVO is said to occur when the intake valve lift reaches 0.25 [mm].
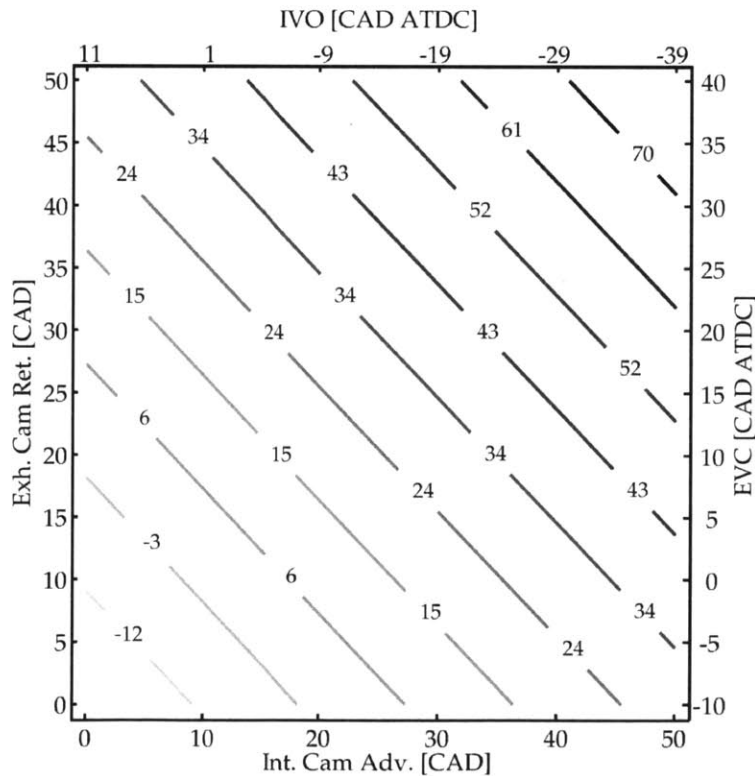
Figure 3-7: Valve overlap varies nearly symmetrically about TDC from negative valve overlap in the default position (VO=-21 [CAD]) to positive valve overlap of +75 [CAD] with both camshaft phasers at maximum travel.

The x-axis and y-axis in Figure 3-8 trace activation of the intake and exhaust

camshaft phaser respectively. The activation of either camshaft phaser increases the valve overlap period and increases the quantity of residual gas trapped in-cylinder during the valve overlap period. Figure 3-9 shows that the preheating and dilution
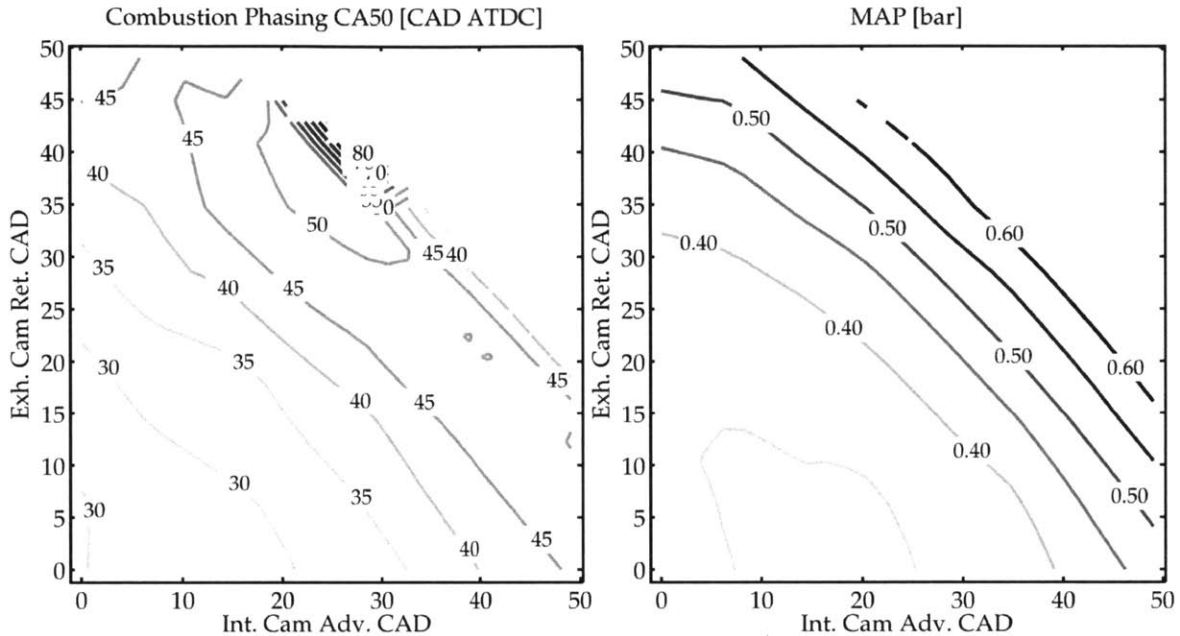
Figure 3-8: Trapped residuals displace air, then higher intake manifold pressure is required to maintain constant quantity of air and fuel to burn. However, as Figure 3-8 shows, the increased dilution due to residual gases retards combustion. The later combustion degrades efficiency and intake manifold pressure must be raised further to maintain constant load. Note the steep increase in CA50 in the top-right quadrant of left figure. This region corresponds to high cycle-to-cycle variability, for which CA50 measurements are imprecise or unreliable. The trend of late CA50 is reliable, although CA50 varies significantly cycle-to-cycle.

effect of residuals do not significantly decrease the concentration of unburned hydro-carbons in the exhaust and as a result the net mass flow rate of hydrocarbons goes up with longer valve overlap. The simple model of residual gas fraction presented in the previous chapter predicted the greatest preheating effect (and greatest emissions reduction potential) with high residual fraction. These results indicate that unburned hydrocarbon concentration is actually highest for long overlap (i.e. high residual fraction). The explanation is that high residual gas fraction increases cycle to cycle variability and the average emissions concentration goes up because of partial-burn misfire. Figure 3-10 shows the rapid increase of cycle-to-cycle variability and modest
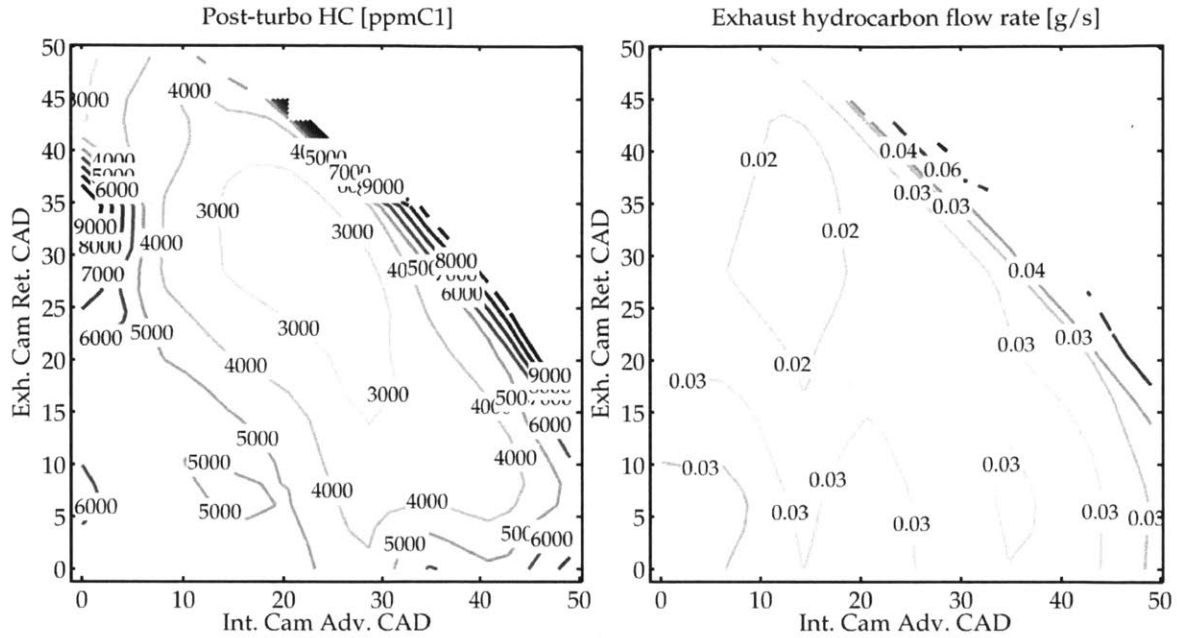
Figure 3-9: Long valve overlap increases residual gas fraction. The effect of residuals overpowers the proposed warm-up improvement mechanisms and net emissions rate is higher for long valve overlap.

increase in thermal enthalpy flow rate with valve overlap. It is concluded that the valve timing strategies investigated do not significantly improve emissions or catalyst warm-up. The reason is that excessive residual gas causes unacceptable cycle to cycle variability. Another operating parameter that may result in excessive residual gas is exhaust back pressure is the subject of the next section.
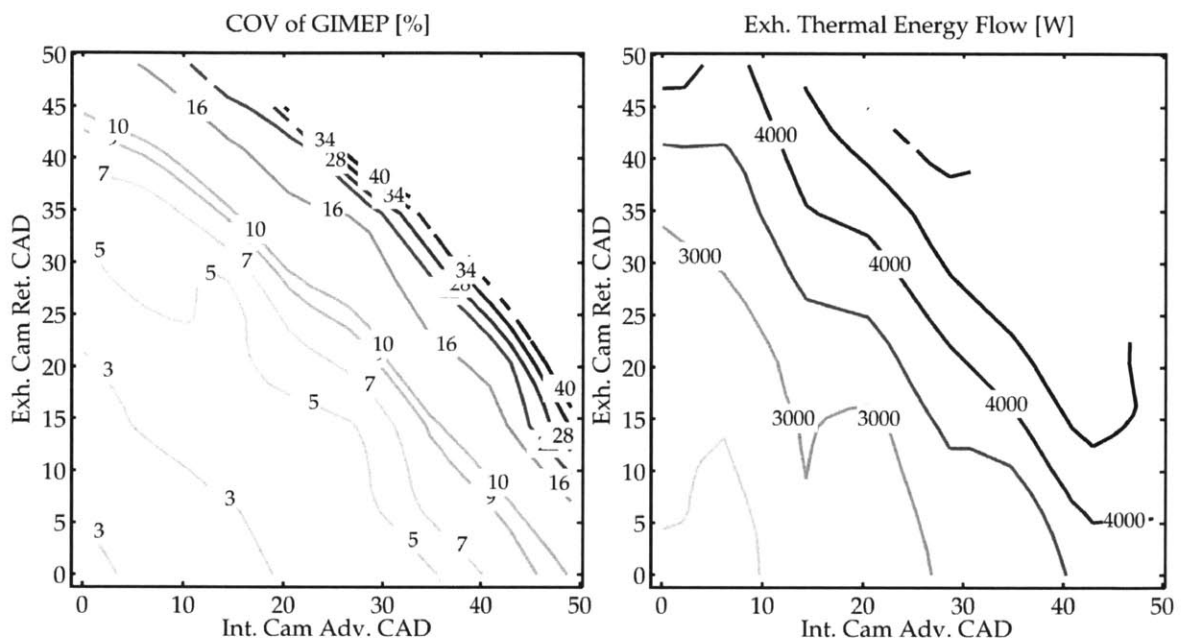
Figure 3-10: The valve timing that produces the highest flow rate of exhaust thermal enthalpy coincides with the valve timing that produces the highest cycle-to-cycle variability.

3.4 Exhaust Back Pressure

Higher exhaust back pressure increases pumping work, and alters the exhaust blowdown process in a beneficial way for hydrocarbon control during cold-start. Back pressure was raised with a valve installed to recreate the back-pressure from a catalytic converter, which this engine lacked. The effectiveness of raising exhaust back pressure at reducing engine-out hydrocarbons exceeded the author's original expectations and shed light on the post-flame and post-cylinder oxidation processes that destroy unburned hydrocarbon species that escape primary (flame) combustion in the combustion chamber. The major effects on engine operation with high back pressure are shown in Figure 3-11.
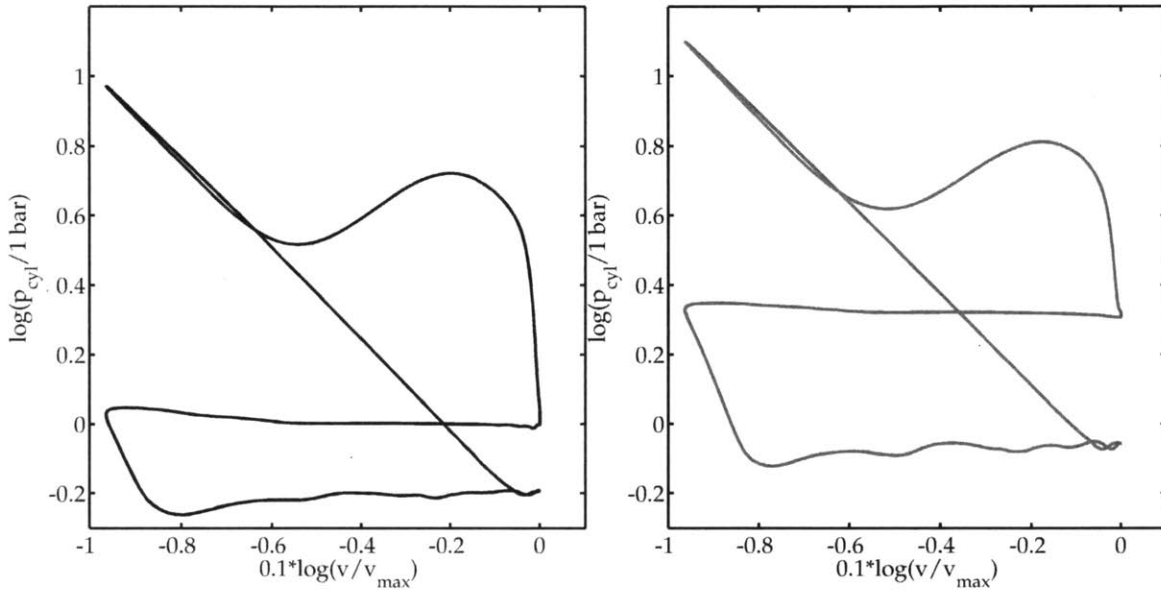
Figure 3-11: Both PV diagrams plot data at equal ignition timing of +13 [CAD ATDC] and equal engine load (NIMEP) in log-log scale. The plot on the left has $p_{exh} = 1.05$ [bar] (normal), the plot on the right has $p_{exh} = 1.80$ [bar] (high). The main effects are that high exhaust pressure case (right) has: higher pressure during exhaust stroke (upper horizontal line), higher intake manifold pressure (lower horizontal line) and, noting the log-log scale, a smaller ratio of pressure at start of blowdown to pressure at end of blowdown (~ 3.2 for left, ~ 2.5 for right).

In what follows, the exhaust pressure for a set of trials is named/specified according to the following convention. With the engine motoring at WOT, the back pressure valve is fixed in some position and the cycle-average exhaust pressure is

recorded. The valve remains fixed in this position for the series of tests. The experimental data are labelled by this nominal p_{exh} for WOT motoring. For a fixed blockage, the actual exhaust back pressure varies. The flow restriction imposes backpressure that is quadratic with exhaust gas mass flow rate. This method was chosen for the simplicity of setup and repeatability.The first set of experiments involves three back pressure levels, all with stoichiometric air-fuel mixtures.

3.4.1 Stoichiometric

Figure 3-12 shows that as ignition timing is retarded exhaust gas temperature and mass flow rate increase to maintain constant load. The actual back-pressure depends
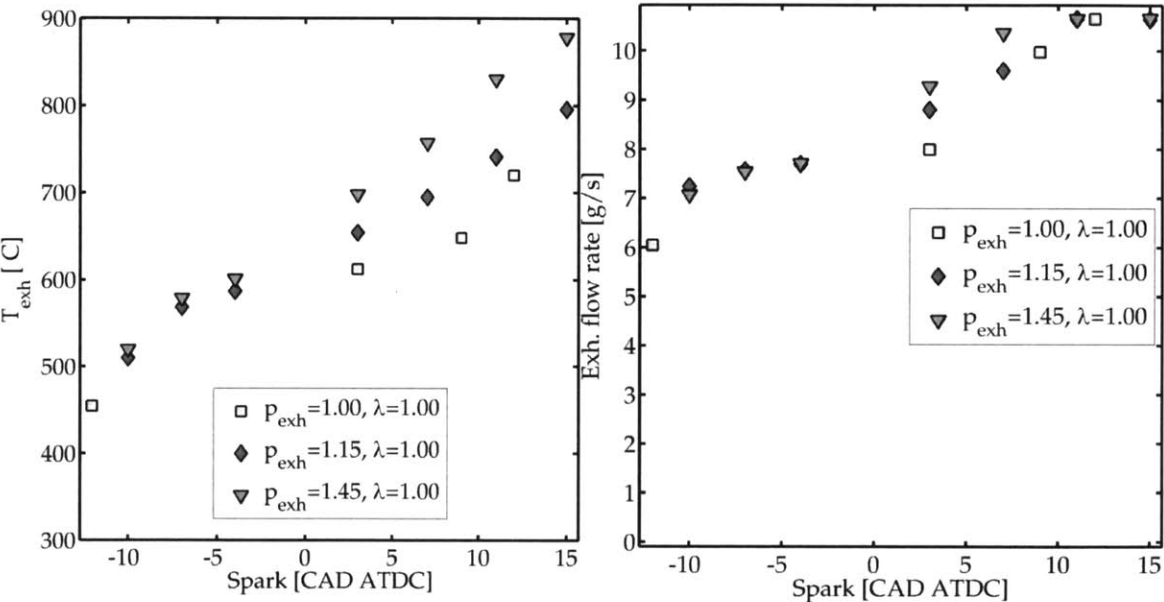
Figure 3-12: The trend from previous ignition timing experiments, later ignition timing reduces efficiency and results in substantial increases to exhaust gas temperature (left) and mass flow rate (right). The highest exhaust gas temperatures and mass flow rate correspond to the higher back-pressure cases.

on the exhaust gas mass flow rate. Figure 3-13 shows that exhaust system pressure increases with late ignition. Intake manifold pressure also increases to offset the higher exhaust pressure and maintain constant load. Taken together, the variation of intake manifold pressure and exhaust manifold pressure is expressed as PIMEP. Figure 3-14 shows that for the lowest back-pressure cases, late ignition actually causes PIMEP
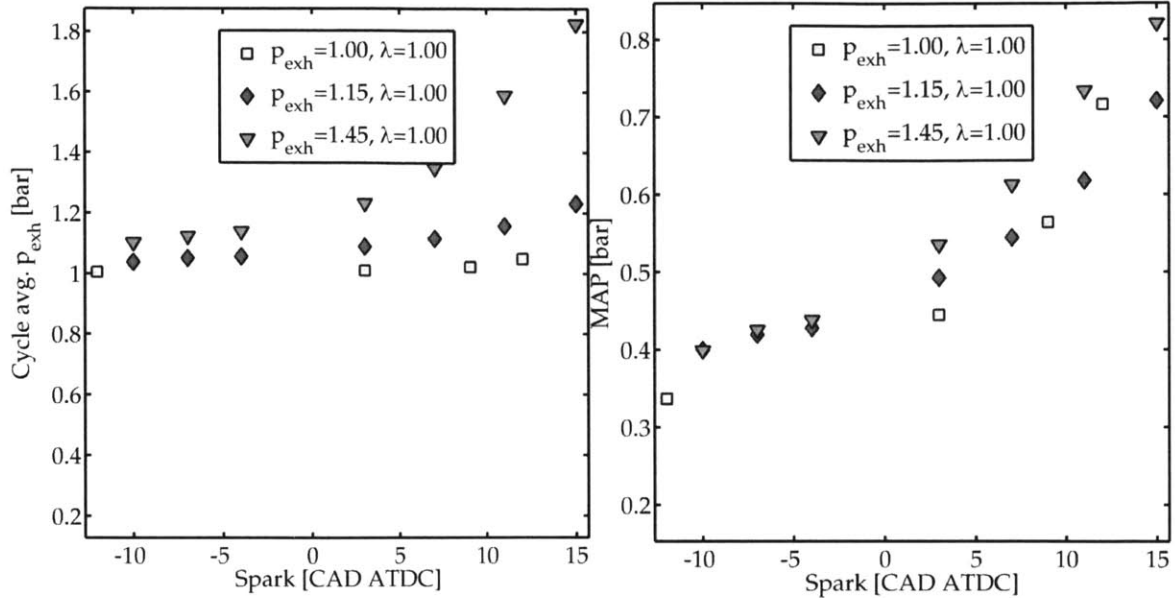
Figure 3-13: Late ignition timing causes higher mass flow rate and higher exhaust pressure (left). Higher MAP is required to overcome this additional back-pressure. (right)

to decrease. This is at odds with the model prediction from the last chapter. The discrepancy is attributed to error in the $PIMEP = (p_e - p_i)$ approximation. For the higher back pressure cases, PIMEP increases dramatically for late ignition (i.e. high mass flow) as expected. The potential drawback of increasing back-pressure is that it can result in higher residual fraction. Fox and Cheng's residual model shows that residuals are indeed higher for the high back-pressure case but the increase in residual gas fraction is quite modest. This is because high back flow increases back-flow to the cylinder during valve overlap, but high intake pressure reduces back-flow to the cylinder during valve overlap. The overall back-flow during overlap is therefore a function of the ratio of exhaust pressure to intake pressure $\left(\frac{p_e}{p_i}\right)$, which Figure 3-15 shows does not change significantly over the range of mass flow rates (i.e. ignition timing) tested. Corroborating the RGF model, plots of the combustion phasing, and burn duration in Figure 3-16 show no evidence that high back pressure leads to excessive dilution by residual gas fraction. The net result of these experiments with increased exhaust back-pressure is a drastic decrease in unburned hydrocarbon emission concentration and mass flow rate as shown in Figure 3-17. The high back-pressure case has the same

93
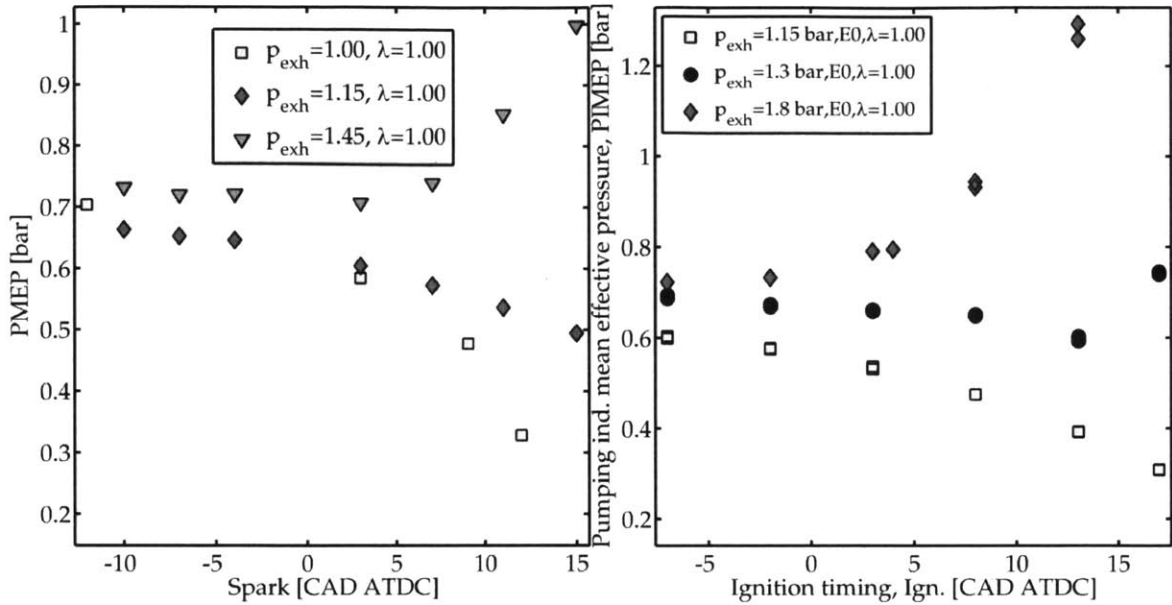
Figure 3-14: For ignition timing after TDC, high back-pressure (large flow restriction) increases PIMEP by close to 100% compared with less restricted exhaust at the same ignition timing. Note the different vertical axis scales and experimental data for these two figures.

hydrocarbon emission mass flow rate as unrestricted pressure case with ignition retarded by 5 [CAD]. The advantage of high back-pressure then is the ability to achieve high thermal enthalpy flow rate with moderate ignition delay (and a minimal stability penalty). Figure 3-18 shows that high back pressure cases exhibit comparable cycle-to-cycle variability in terms of COV and LNV. This is attributed to the nearly constant residual gas fraction, and higher GIMEP of high exhaust back-pressure cases. The latest practical ignition timing is limited by cycle-to-cycle variability. Before that limit was reached for exhaust back-pressure test, tests became limited by maximum turbine rotor inlet gas temperature limit and a melting point limit of a component in the hydrocarbon sampling system. This section concludes with Figure 3-19, which shows the dramatic increase in exhaust thermal enthalpy for the high back-pressure case. For the high-back pressure case at the latest ignition timing tested (+13 [CAD ATDC]), each 1 [CAD] increment of later ignition contributes an additional 450 [W] of exhaust thermal enthalpy, which is 50% more than the 300 [W] slope for unrestricted exhaust tests.

High exhaust back-pressure improves emissions performance (low flow rate of hy-

94
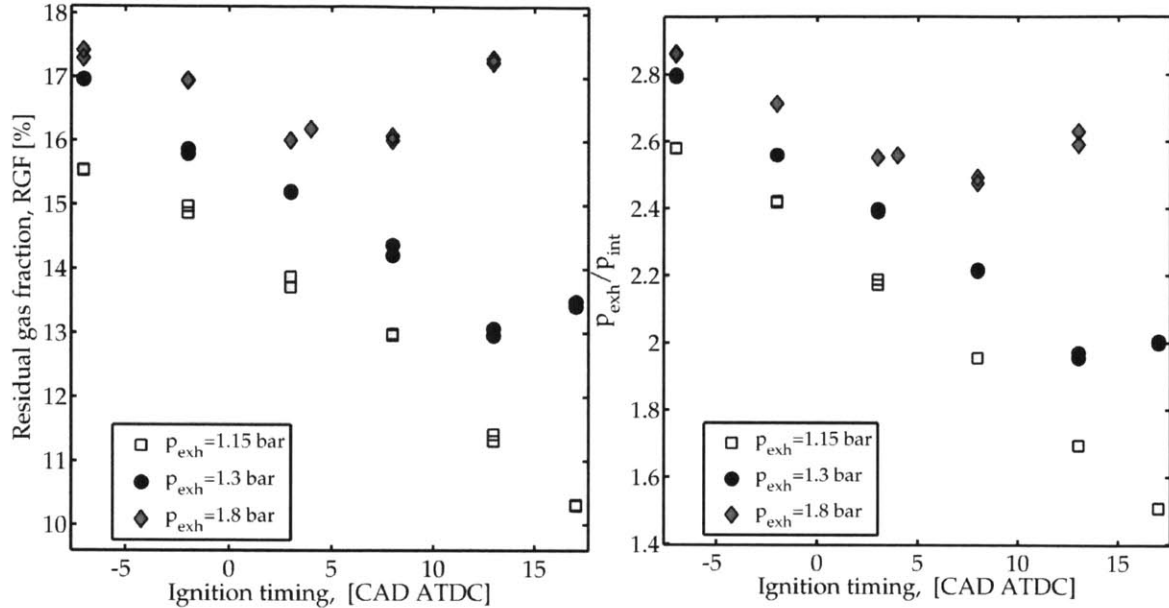
Figure 3-15: For the high-back pressure case, residual gas fraction remains relatively constant due to the competing effects of increasing exhaust back pressure (which tends to increase back-flow during valve overlap), and increasing intake manifold pressure (which tends to decrease back-flow during valve overlap).

drocarbons, high flow rate of thermal enthalpy) by altering mixture temperature profile through the engine cycle to enhance post-flame oxidation. Figure 3-20 plots several combustion gas mixture temperature profiles from engine simulations at different ignition timing ranging from -5 [CAD ATDC] to +19 [CAD ATDC]. To emphasize the effect of late ignition on exhaust gas temperatures, the mixture temperature at EVO, the average burned gas temperature from EVO to EVC, and the mixture temperature at EVC are extracted from Figure 3-20 and replotted in Figure 3-21. A critical observation about Figure 3-21 is that late ignition increases the average burned gas temperature into the 1500K region where, assuming sufficient oxygen is present, post-flame oxidation is rapid and diffusion-limited. Under these conditions, available time and available oxygen are the only factors that limit post-flame oxidation. Ignition timing later than +12 [CAD ATDC] does not significantly increase burned gas temperatures. Even if it did, later ignition would reduce the amount of time available for post-flame oxidation.

Moving now to a the role of restricted exhaust back pressure, Figure 3-22 plots several combustion gas mixture temperature profiles from engine simulations at different
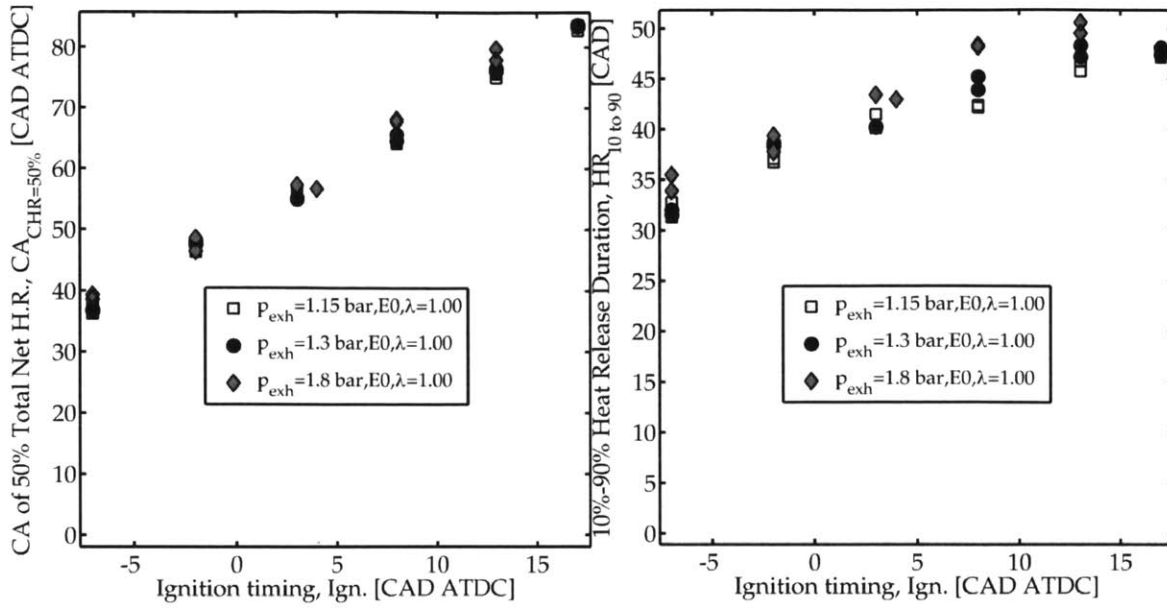
Figure 3-16: Negligible difference in combustion phasing, and burn duration support the assertion that residual gas fraction remains low for high back pressure experiments.

ignition timing ranging from -5 [CAD ATDC] to +19 [CAD ATDC] with restricted exhaust back pressure. For the sake of easy comparison, the mixture temperature profiles are re-plotted next to each other. The effect of back pressure on exhaust and burned gas temperature is plotted in Figure 3-23. The mechanism for exhaust back-pressure to improve emissions performance is clear, but there are two significant limitations. First, post-flame oxidation needs oxygen. Second, for high back-pressure tests with very late ignition, exhaust gas temperatures exceeded engine limits. The next step is to examine different equivalence ratios. This includes rich operation (excess fuel) to limit exhaust gas temperatures, and lean operation (excess air) to enhance post-flame oxidation and stay below exhaust temperature limits.
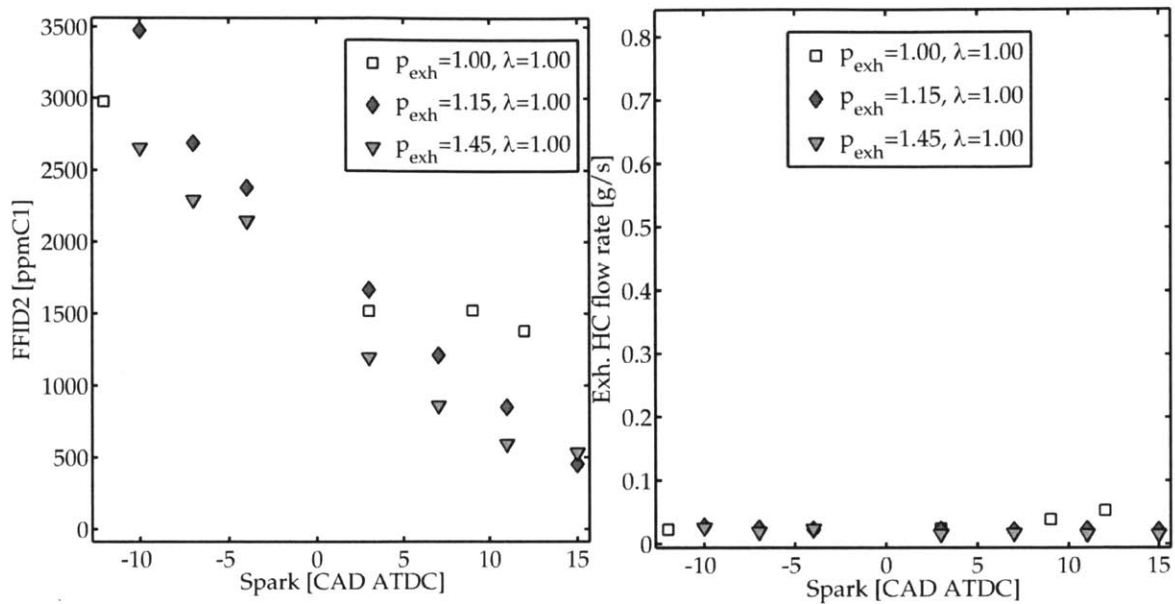
Figure 3-17: The high back-pressure case shows consistently lower concentration (left) and mass flow rate of unburned hydrocarbons (right). Hydrocarbon concentration was near the detection limit for the instrument used.
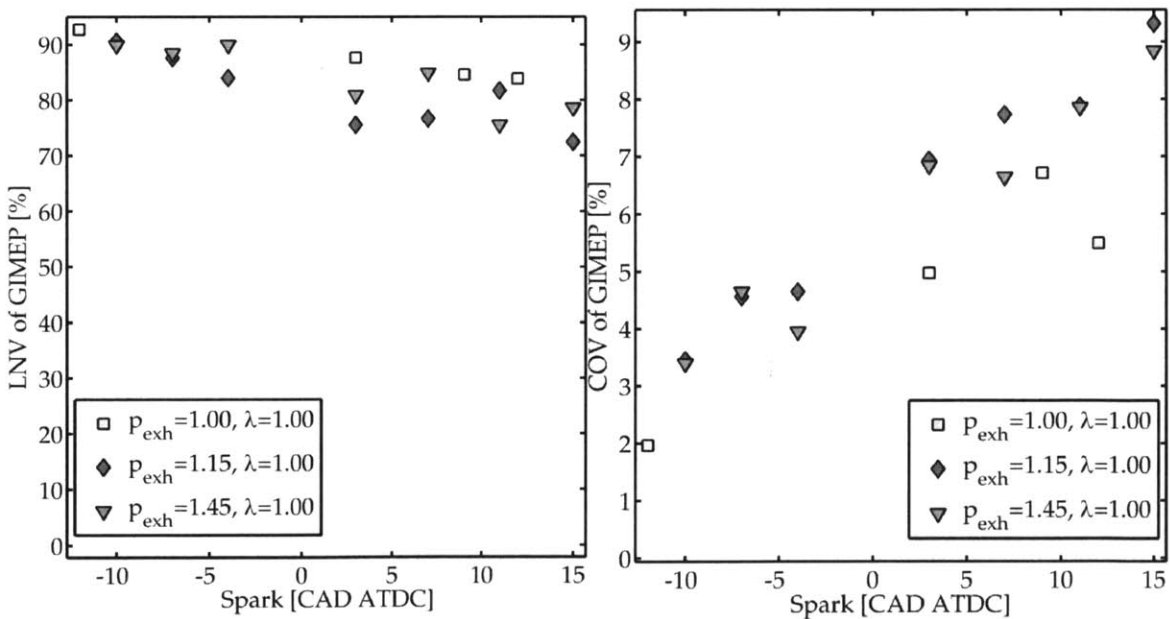
Figure 3-18: The cycle-to-cycle variability increases for late ignition. The sensitivity of cycle-to-cycle variability to exhaust back-pressure is small because for the constant NIMEP test, residual gas fraction does not increase significantly with late ignition and high back-pressure (i.e. high p_e).
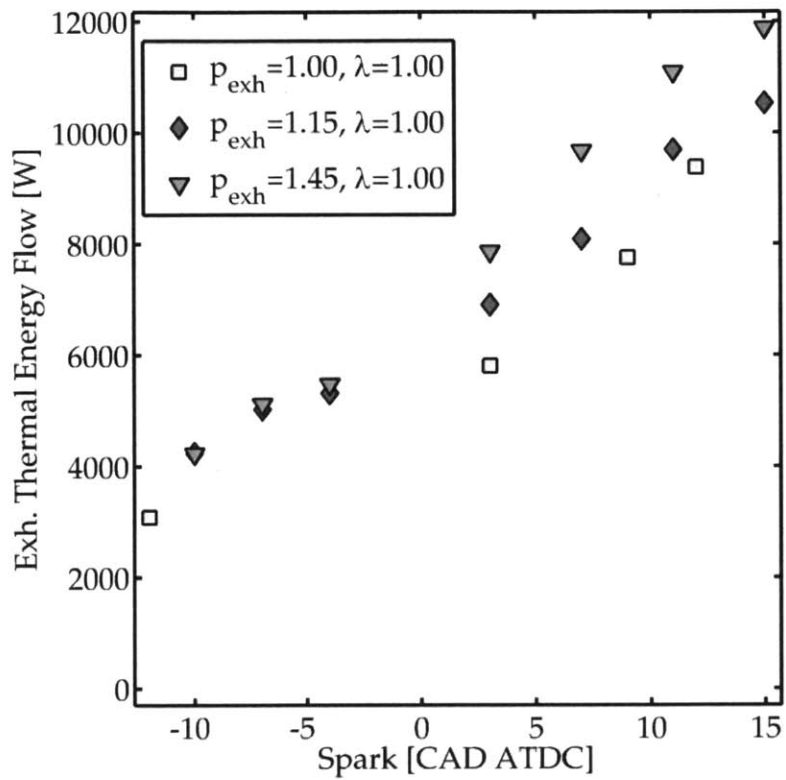
Figure 3-19: High exhaust back pressure enhances the performance of late ignition as a catalyst warm-up strategy by increasing PIMEP and hence GIMEP required to maintain constant NIMEP, and by restricting the expansion (and temperature drop) of gases during blow-down.
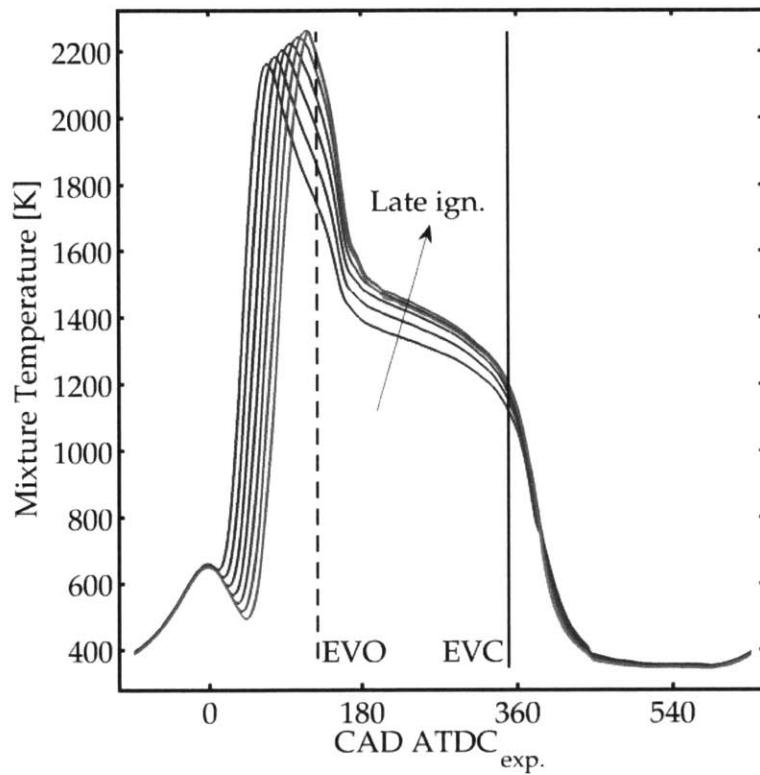
Figure 3-20: At constant engine load, late ignition increases peak gas temperatures and increases burned gas and exhaust gas temperatures (between EVO to EVC lines). The effect on exhaust gas temperature shows diminishing returns.
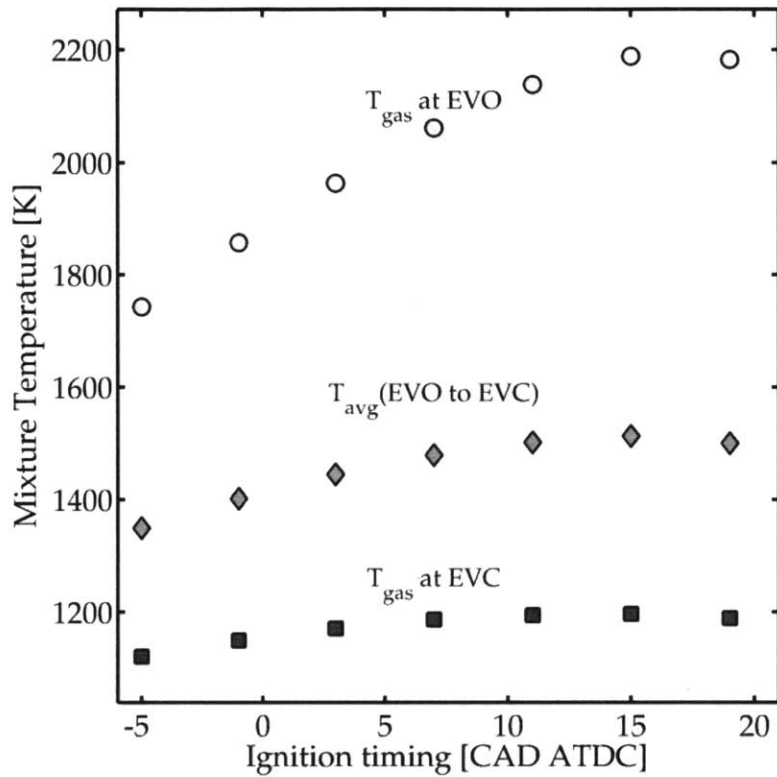
Figure 3-21: The mixture temperature at EVO is the temperature of the first (and hottest) parcel of exhaust gas to leave the cylinder. The mixture temperature at EVC is the temperature of the last (and coldest) parcel of exhaust gas to leave the cylinder. Late ignition increases the average burned gas temperature by approximately 200K.
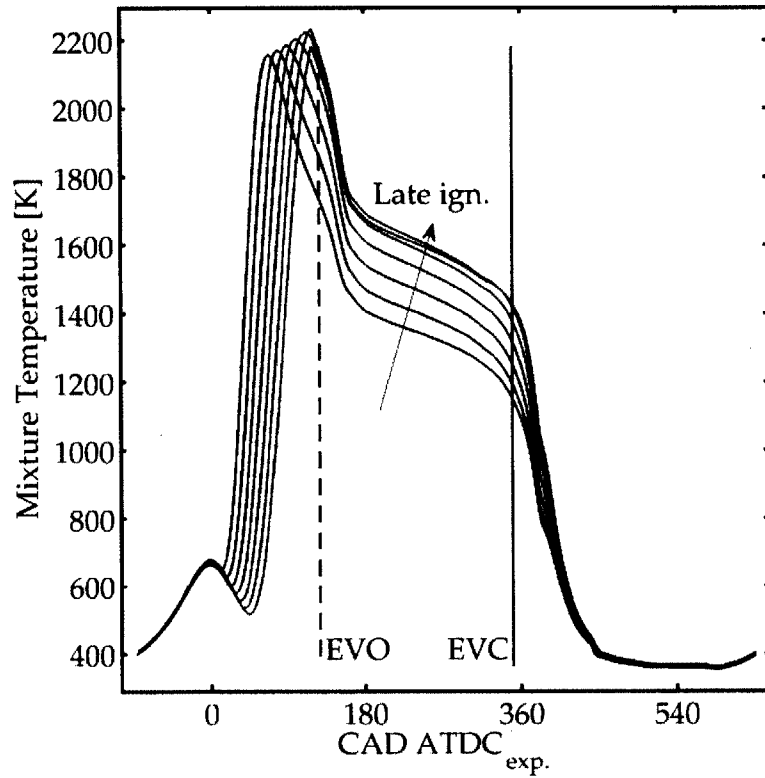
Figure 3-22: For these cases with restricted exhaust back pressure, late ignition increases peak gas temperatures but burned gas temperature (between EVO and EVC) are substantially increased for later ignition timing. This is attributed to the higher GIMEP to offset the pumping work penalty of back-pressure, and reduced expansion (and cooling) of burned gases during blowdown.

101
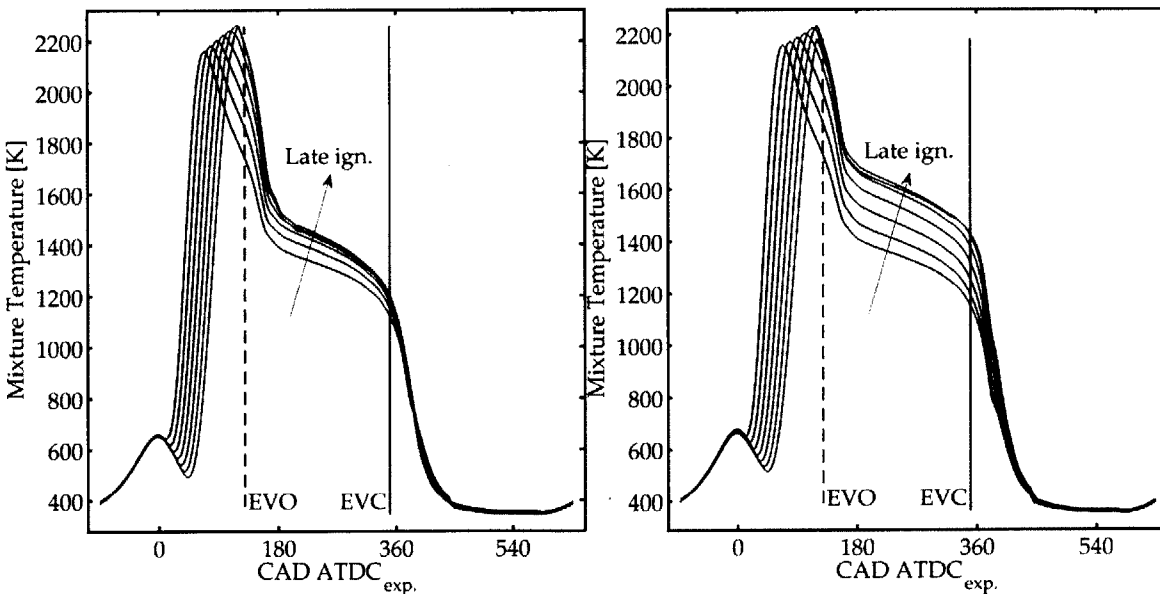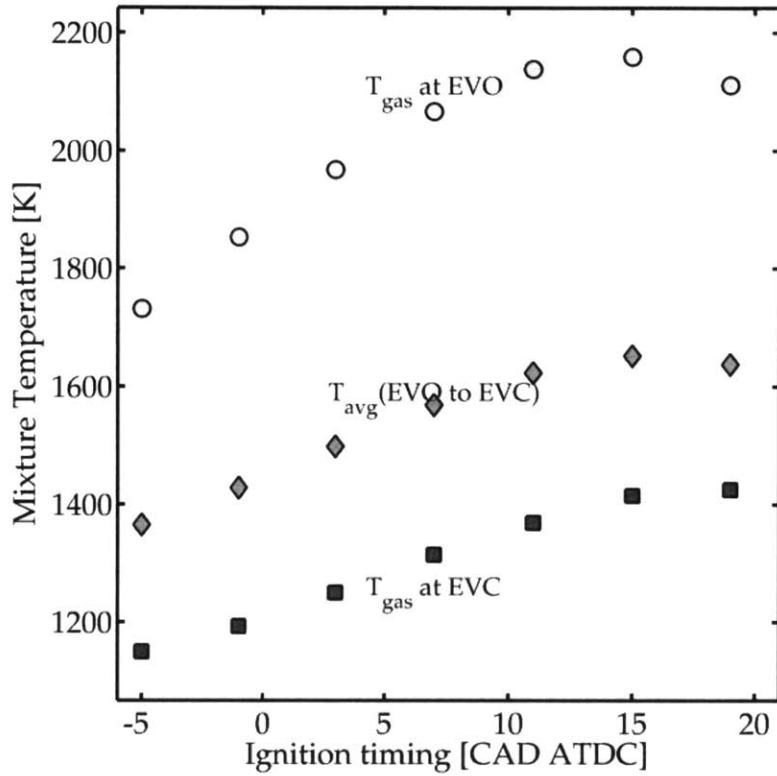
Figure 3-23: For the highest exhaust pressure case tested (p_{exh}=1.8 [bar] nominal), burned gas temperatures reach the critical 1500K threshold for diffusion-limited hydrocarbon oxidation at +3 [CAD ATDC], which is 10-12 [CAD] earlier than unrestricted exhaust. A greater portion of exhaust gases exiting the engine and mixing in the port will have high enough temperature for post-flame oxidation.

3.4.2   Equivalence ratio interaction

High back-pressure with excess air (lean fuel-air mixture) give the best emissions performance. One may initially expect lean mixtures to cause lower exhaust gas temperatures. However, the temperature decrease from lean operation is partially counterbalanced by additional post-cylinder oxidation of CO and unburned hydrocarbons that exit the cylinder. Figure 3-24 shows the dominant effect is that lean operation retards combustion phasing, which for constant load leads to higher exhaust gas temperature. Figure 3-25 shows that exhaust gas temperature and thermal enthalpy flow
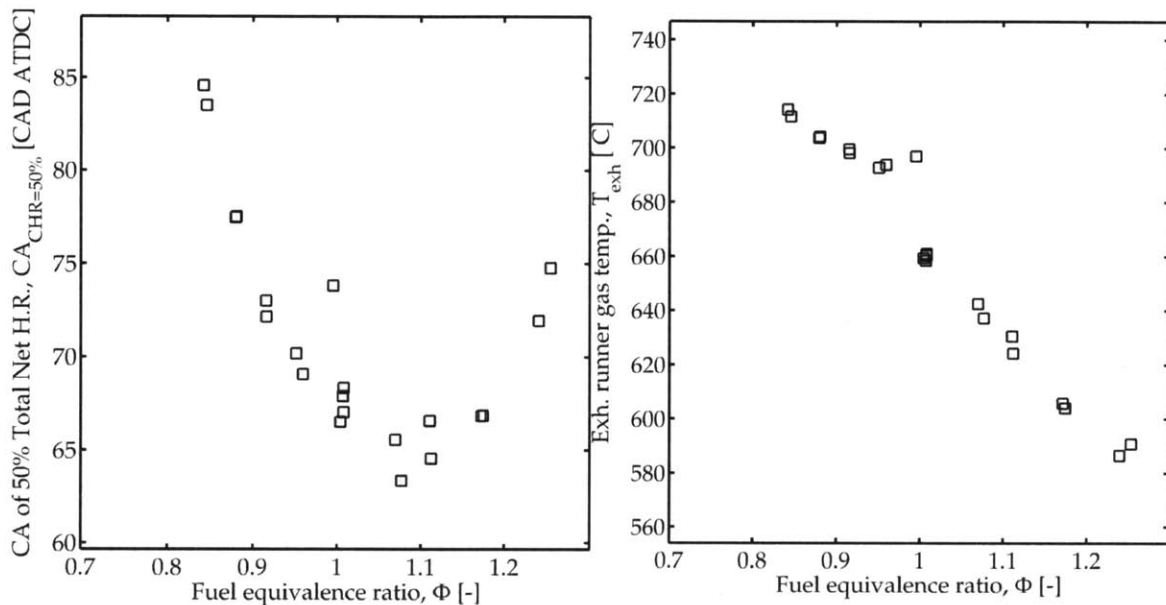
Figure 3-24: These data were collected at p_{exh}=1.05 [bar]. The trends apply equally to higher exhaust pressure. Lean fuel-air equivalence ratio ($\Phi \leq 1$) leads to later combustion phasing (left), which in turn leads to higher exhaust gas temperature (right). For rich fuel-air mixtures ($\Phi \geq 1$), the cooling effect of increased evaporative and lower specific-heat ratio lead to lower exhaust gas temperatures.

rate are higher for lean operation than a comparable stoichiometric case. Figure 3-26 provides evidence of post-flame and post-cylinder oxidation of CO and unburned hydrocarbons that escape primary (i.e. flame) combustion. The mixture dilution due to lean mixture retards combustion which is expected to cause the cycle-to-cycle variability to increase. Figure 3-27 shows that the cycle-to-cycle variability increase due to operating with 15% excess air is modest and the lean equivalence ratio offers a clear victory in terms of catalyst warm-up, but also limiting engine emissions during
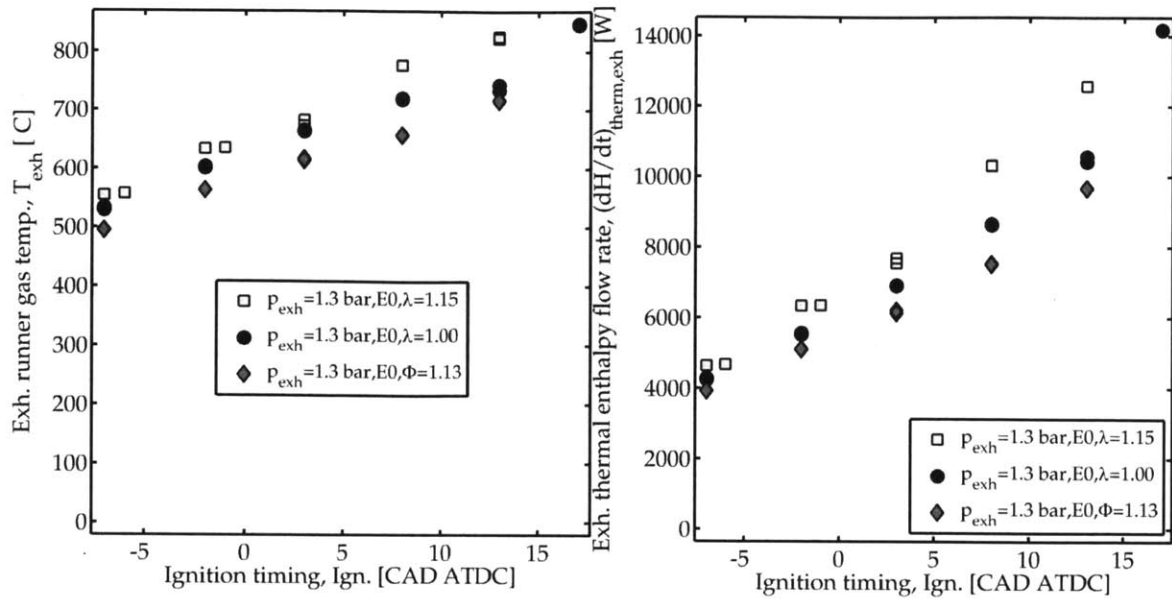
Figure 3-25: Lean operation shows consistently higher exhaust temperatures (left) and thermal enthalpy flow rate (right) due to additional post-cylinder oxidation (and heat release). Also, at equal ignition timing and constant load, lean operation will have a higher exhaust back-pressure.

cold-start. It is clear that exhaust back pressure is an effective emissions control strategy. Late ignition, lean equivalence ratio and high exhaust restriction produce high thermal enthalpy flow rates reduce emissions rate during cold start significantly. All equivalence ratios are compared in terms of combustion inefficiency in Figure 3-29. Combustion inefficiency is a measure of how much of the fuel's original heating value remains as partially oxidized or uncombusted components, namely CO, H_2 and HC. The success strategy of late combustion with excess air is more clear when Figure 3-28 is re-plotted with only lean and stoichiometric mixtures as Figure 3-29. The reader may ask what is the optimal equivalence ratio for operating with high back-pressure. Excess air improves emissions because it facilitates complete combustion. Excess air retards combustion, which at constant load leads to higher exhaust gas temperature and mass flow rate. The limit to excess air is enforced by cycle-to-cycle variability. An air-fuel mixture that is too lean will have excessive cycle-to-cycle variability, and greater probability of partial-burn misfire. Figure 3-30 shows that cycle-to-cycle variability increases linearly for lean mixtures until $\Phi = 0.88, \lambda = 1.14$, at which point cycle-to-cycle variability increases dramatically. In this case, $\Phi = 0.88, \lambda = 1.14$ is
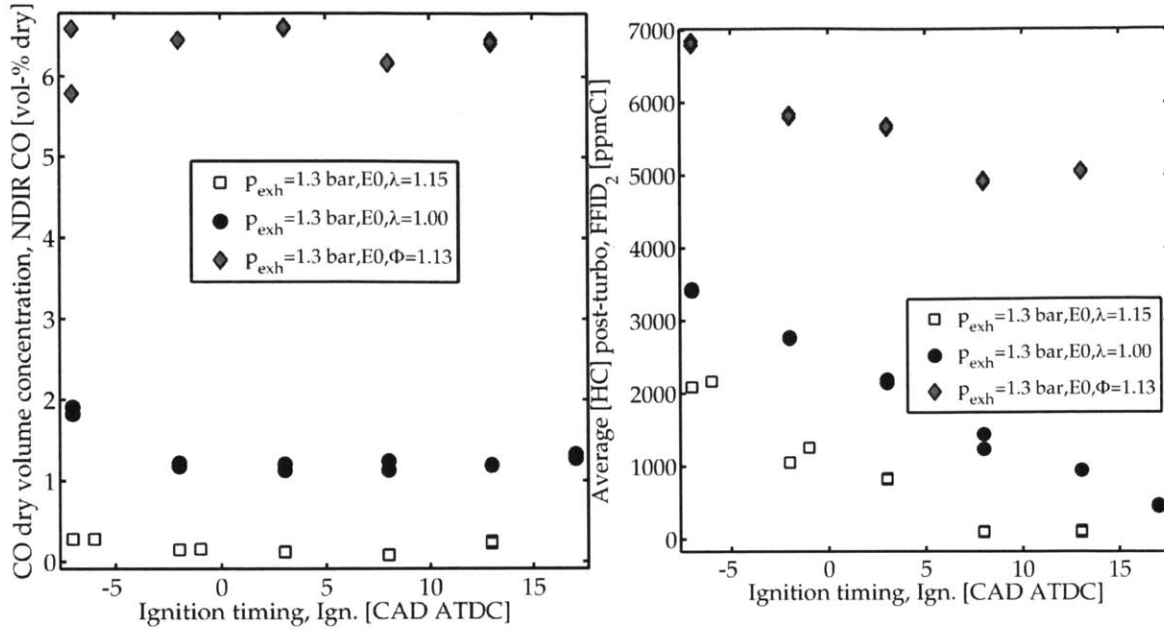
Figure 3-26: The concentration of unburned or partially burned CO and HC support the assertion that significant ongoing oxidation takes place in exhaust gases even after they have exited the combustion chamber.

the optimal equivalence ratio which provides the greatest exhaust thermal enthalpy flow while maintaining a low risk of partial-burn misfire.

Now to switch from an external engine control (exhaust flow restriction) to an internal engine control (fuel injection) the next section focuses on experiments regarding fuel injection strategy.
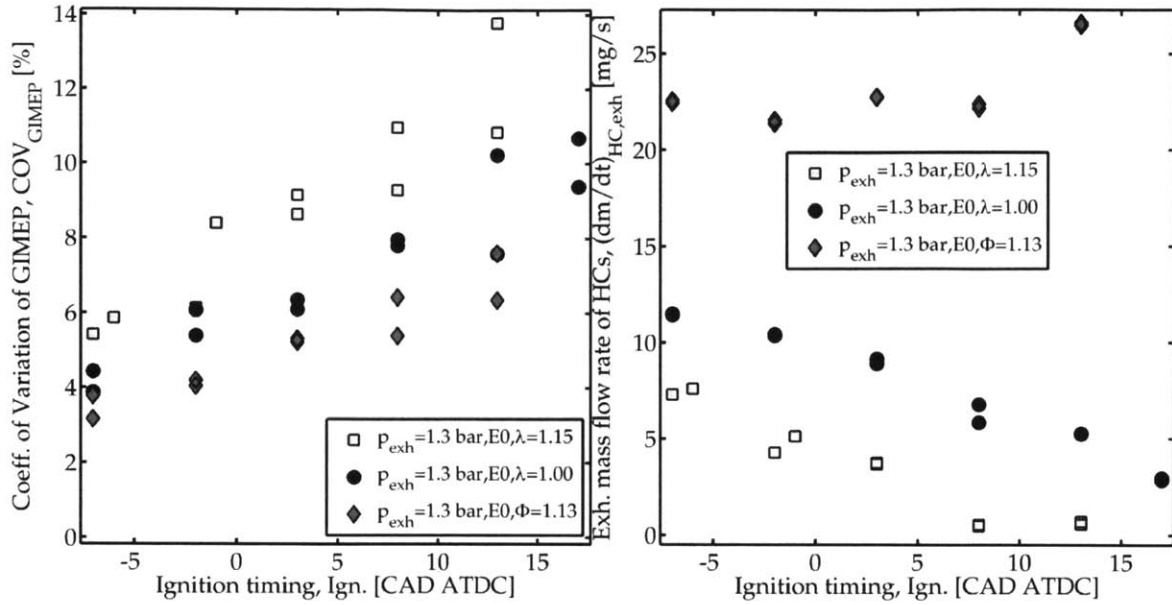
Figure 3-27: Late ignition increases cycle-to-cycle variability (left). The net result of increasing mass flow rate and decreasing exhaust hydrocarbon concentration is a dramatic decrease in exhaust hydrocarbon mass flow rate for the lean equivalence ratio down to the instrumentation detection limit.
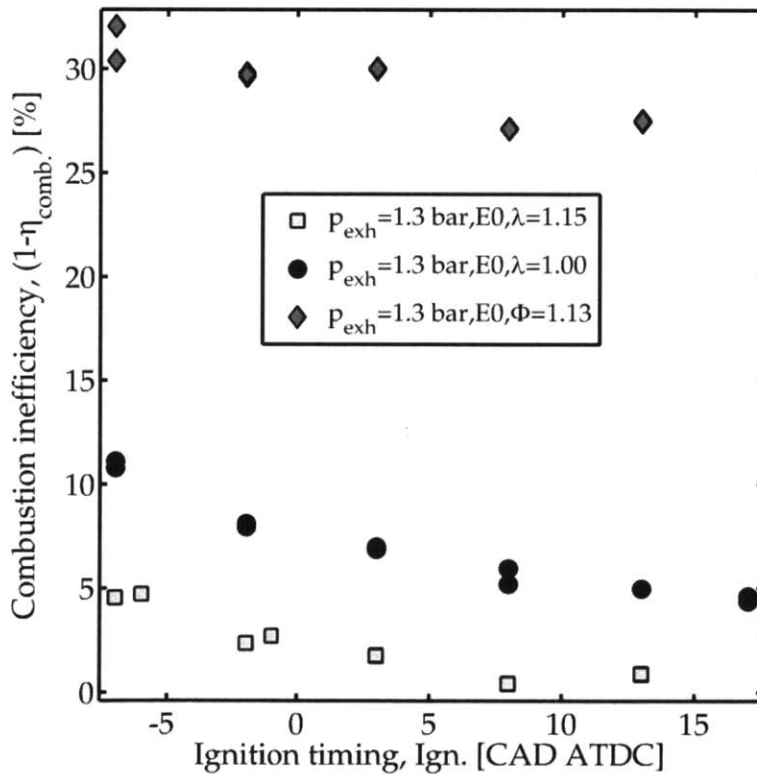
Figure 3-28: Late ignition decreases combustion inefficiency for all mixtures, excess air dramatically decreases combustion inefficiency.
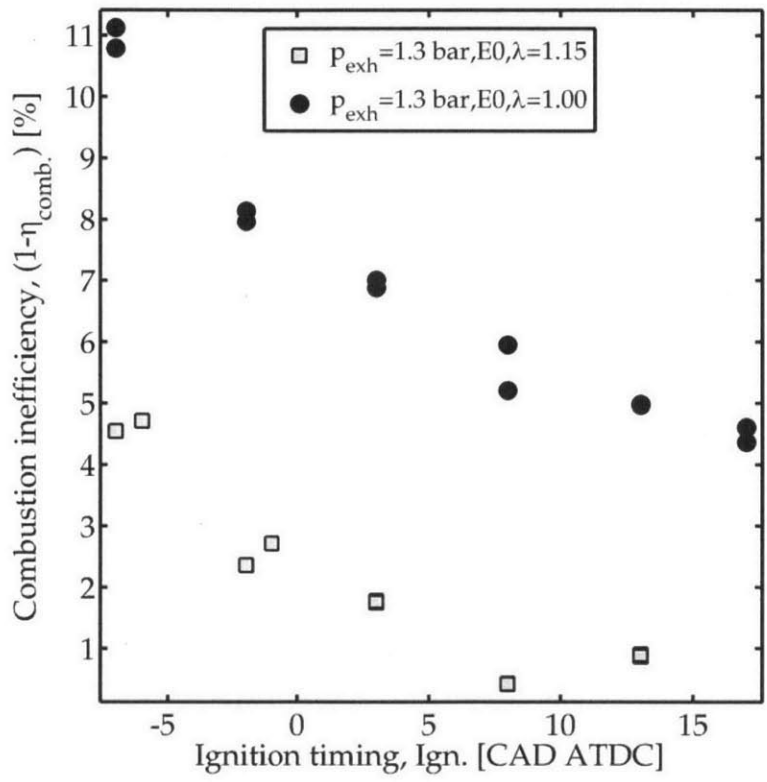
Figure 3-29: Late ignition decreases combustion inefficiency for both mixtures, the case with excess air showed combustion inefficiency near zero. This is attributed to substantial post-flame oxidation of whatever CO and HC survive primary flame combustion.
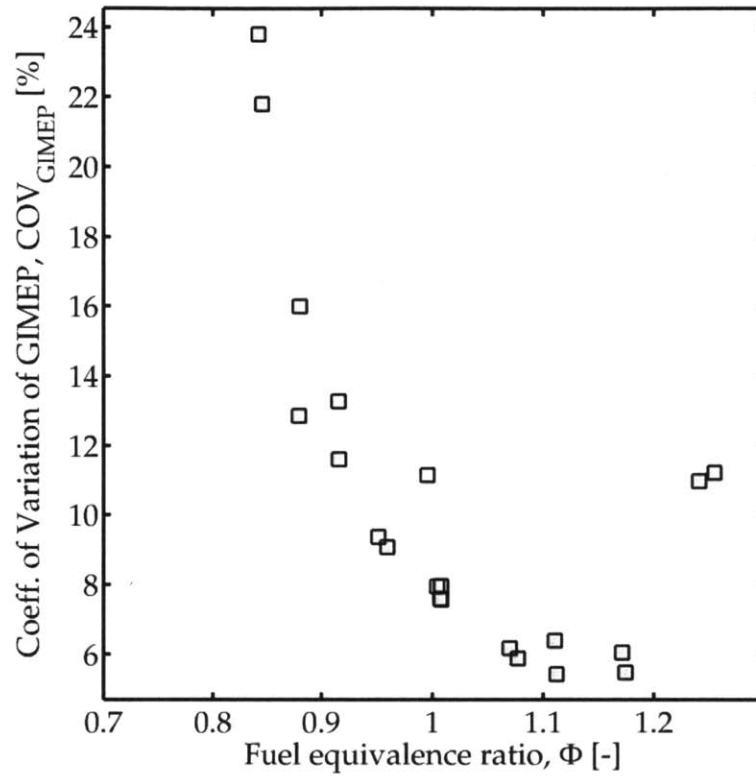
Figure 3-30: These data were collected at p_{exh}=1.05 [bar]. The trend applies equally to higher exhaust pressure. Lean fuel-air equivalence ratio ($\Phi \leq 1$) leads to later combustion phasing, which causes high cycle-to-cycle variability as measured by COV of GIMEP. Slight mixture enrichment ($\Phi \geq 1$), reduces cycle-to-cycle variability, however excessively rich mixtures ($\Phi \geq 1.2$) show higher variability as the mixture approaches its rich flammability limit.

3.5 Fuel Injection Schedule

This section describes the results of split injection experiments.

The first experiment varies the timing of the second fuel injection, which occurs late in compression stroke, for fuelling split 70%/30% by mass between first and second injections. This experiment finds that the stratification induced by split injection advances early stages of combustion heat release (in the richer mixture) and retards late stages of heat release (in the leaner mixture). The timing of the second injection alters how the fuel-spray interacts with the piston bowl. Properly timed second injections yield higher exhaust temperatures and lower emissions without a substantial increase to cycle-to-cycle variability.

The second experiment finds that a 60/40 fuel split increases cycle to cycle variability with no emissions or warm-up benefit. It was not possible to achieve reliable, repeatable operation at greater split ratios (e.g. 80/20) with this injector/injector-driver combination unless operating on fuel blends with high ethanol content. Other engine conditions being equal, fuel injection durations are longer for fuels with high ethanol content than gasoline (the heating value of ethanol is lower than gasoline so fuel injection durations are longer). An experiment with 80/20 split ratio did not show any significant difference from 70/30, for the conditions tested.

3.5.1 Split Injection

The start of injection for the intake stroke injection occurred at SOI1=80 [CAD ATDC$_{int}$]. The start of injection for the compression stroke fuel injection, SOI2 varied. The split ratio was approximately 70%-30% for the injection during intake stroke and compression stroke respectively. SOI2 timing of 100 [CAD ATDC] is effectively the same as a single fuel injection.

The late and slow combustion results in higher exhaust gas temperatures. Because later combustion reduces gross indicated fuel conversion efficiency, a greater mass of air and fuel are needed to maintain constant load. Figure 3-32 shows that late SOI2 timing increases exhaust gas temperature and mass flow rate. A com-
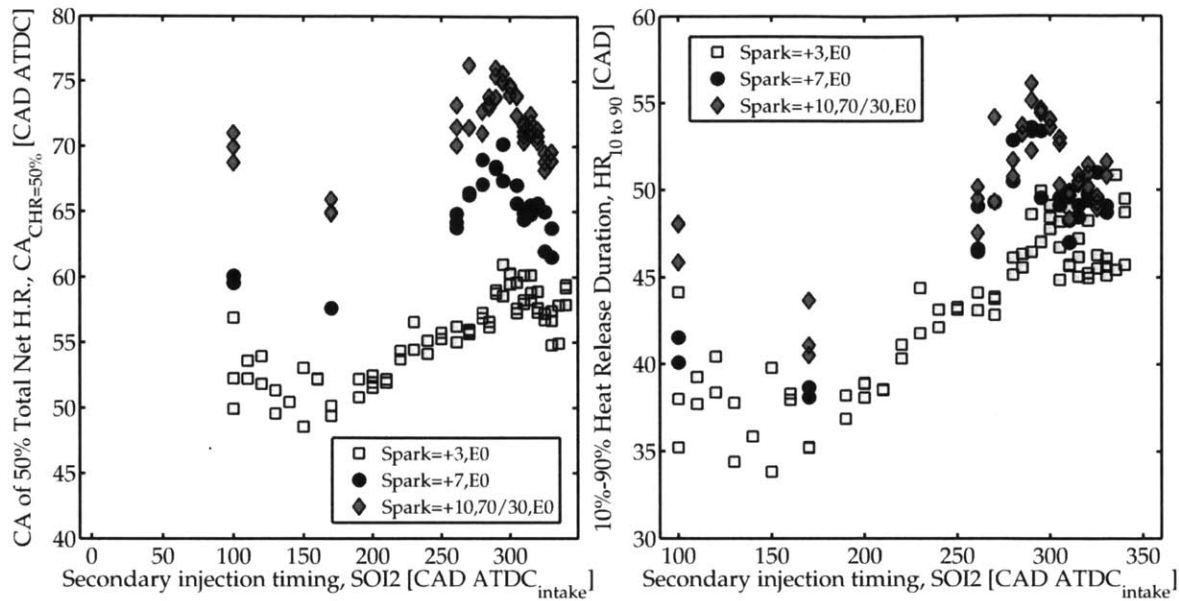
Figure 3-31: Later SOI2 retards combustion (later CA50) and prolongs heat release burn duration (longer BD1090), likely due to mixture stratification with the center of the combustion chamber enriched by the second injection, and the perimeter charge relatively lean.

mon conclusion from valve timing and late ignition experiments is that late combustion increases cycle-to-cycle variability. Figure 3-33 shows for some values of SOI2 near (SOI2~300 [CAD ATDC]), that split injection increases cycle-to-cycle variability compared to single injection. With an appropriate SOI2 the cycle-to-cycle variability penalty compared with single injection is very small. More importantly, split injection with a suitably chosen SOI2 is effective at reducing the cycle-to-cycle variability of late ignition cases. Another significant benefit of split injection is the centre-rich and perimeter-lean mixture stratification improves emissions. Figure 3-34 shows that suitably chosen SOI2 timing dramatically reduces exhaust hydrocarbon and carbon monoxide content. The preceding plots offer experimental evidence of how effective a split injection schedule can be, although there is significant sensitivity to the timing of the secondary (compression-stroke) fuel injection. The next section looks at injections split 60/40 and 80/20 in terms of (mass of fuel delivered in the intake stroke)/(mass of fuel delivered late in the compression stroke).

110
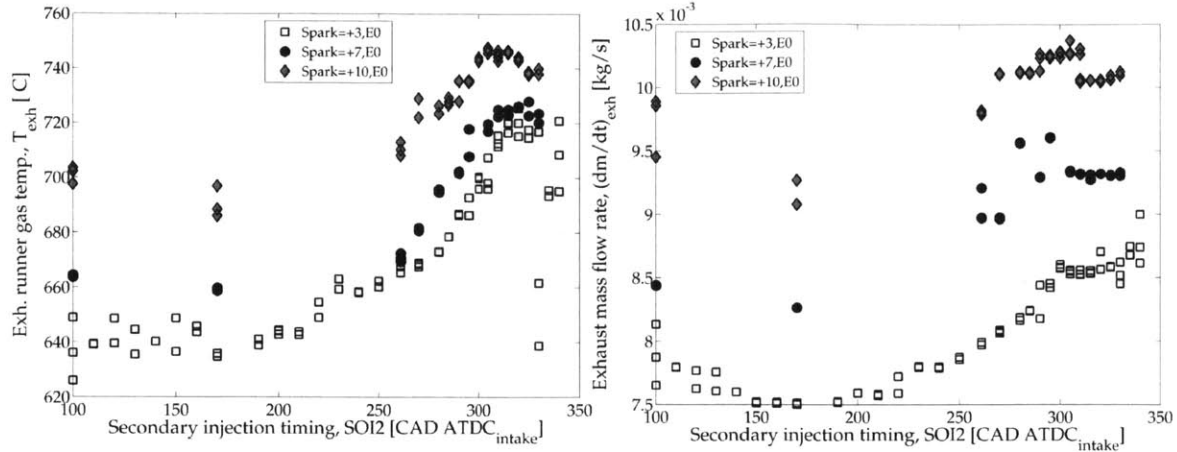
Figure 3-32: For each of three ignition timings, the 70/30 split injection strategy slows down the overall heat release, degrading fuel conversion efficiency ($\eta_{i,g}$) which results in higher exhaust gas temperatures (right) and higher mass flow rate of air and fuel (left). The shape of the curve is near SOI=320 [CAD ATDC] is the result of fuel injection spray interaction with the bowl feature on the piston crown.

3.5.2 Split Ratio

Seeing that a 70/30 fuel distribution produces a more favourable fuel-air mixture stratification than single injection (i.e. 100/0 distribution), the next section examines the benefits of a more extreme 60/40 stratification.

60/40 Split

At the risk of oversimplifying, a 60/40 fuel distribution creates two zones in the combustion chamber. The bulk of the air-fuel mixture around the perimeter of the combustion chamber is ~40% lean of stoichiometric (i.e. has only 60% of total fuel) then late in the compression stroke the core of the combustion chamber is significantly enriched by the second injection. Such extreme stratification from very rich to very lean puts both mixture zones at the edges of the gasoline flammability. The plume of fuel vapour from the second injection could "miss" the spark plug, or more simply the rich mixture is too rich and the lean mixture is too lean. Figure 3-35 shows that some late SOI2 timing values dramatically increase cycle-to-cycle variability and emissions. Still later SOI2 timings restored the engine to reliable operation with retarded combustion, higher exhaust gas temperature and lower emissions like the
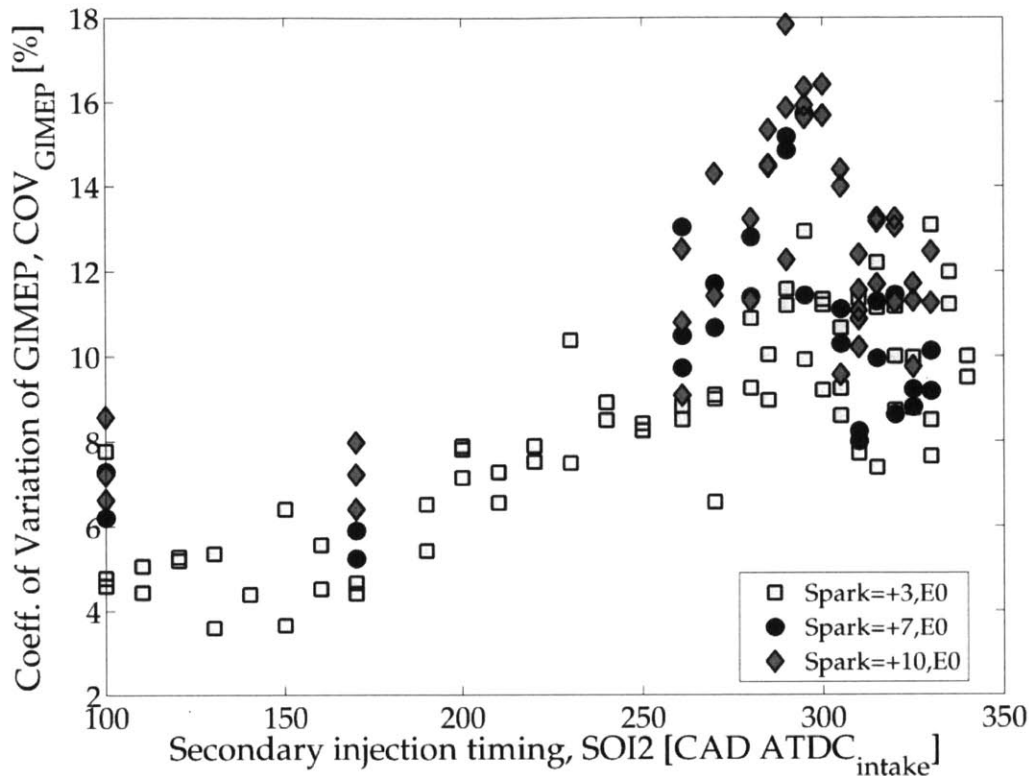
Figure 3-33: Approximately 70% of fuel is injected with SOI1 at 80 [CAD ATDC]. The balance is injected at SOI1. For SOI2 near 100 [CAD ATDC], fuel is injected in essentially one injection. Later injection results in greater center-rich, perimeter-lean stratification. In terms of cycle-to-cycle variability, a best-case SOI2 timing around 320 [CAD ATDC] optimizes fuel-spray interaction with the piston bowl. This yields optimal enrichment of the mixture near the spark plug at the time of spark.

70/30 case. This extreme sensitivity to injection timing is not desirable in a cold start strategy, especially since 60/40 confers no additional cold-start performance benefit relative to 70/30. It was established that a 70/30 fuel split ratio performs well, while a 60/40 fuel split ratio renders the engine excessively sensitive to SOI2 timing. The following section presents some results on an 80/20 split ratio.

80/20 Split

Lest the reader lose spirit in examining split ratios, now is a good time to point out that 80/20 is the practical limit for this set of injectors. The second fuel injection pulse (the 20% pulse) is at the minimum performance limit. The injector/driver combination on this engine cannot achieve reliable operation with any shorter pulse

112
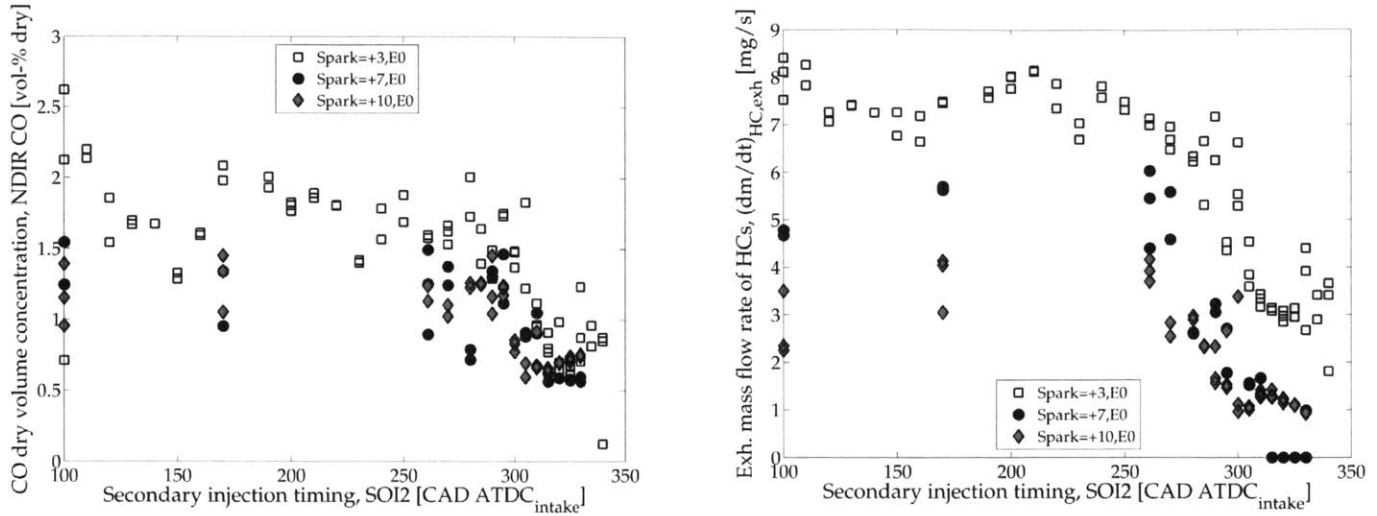
Figure 3-34: For each of three ignition timings, with appropriate SOI2 timing, the 70/30 split injection strategy leads to reduction in CO (left) and hydrocarbon mass flow rate (right). The proposed mechanism is that 70/30 split leads to leaner crevice gases. When the lean crevice gases exit the crevice in the expansion stroke and mix with burned gases, the higher oxygen availability improves post-flame oxidation.

(e.g. for a 90/10, or 70/15/15 triple injection).

Figure 3-36 indicates that the 80/20 split injection is less sensitive to SOI2 than both 70/30 and 60/40 injection split ratios. This is not surprising since only a small fraction of fuel contained in the second. At their ideal SOI2 timing, the 80/20 distribution reduces emissions less than 70/30. This is consistent with the proposed lean crevice gas mechanism. The topic of mixture preparation stays but the focus changes from how the fuel is delivered to the chemical make-up of the fuel.
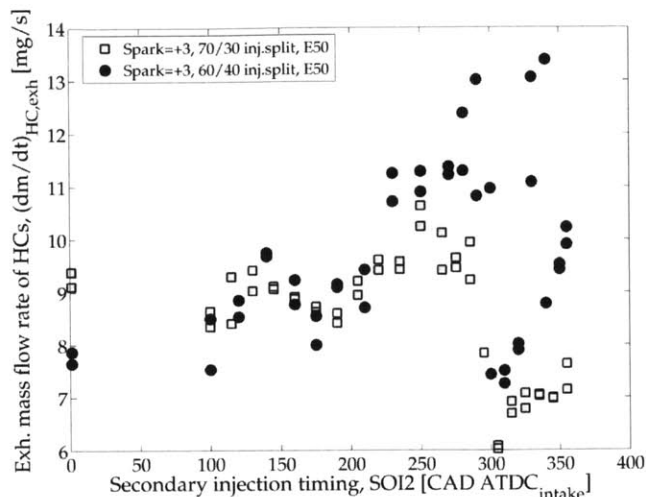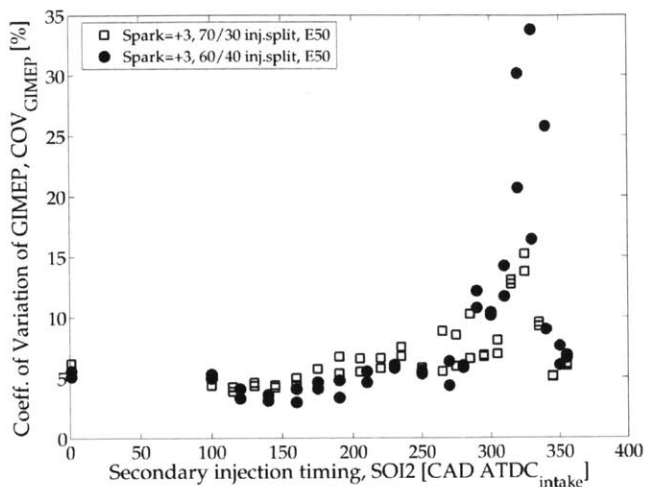
Figure 3-35: A 60/40 split ratio increases the engine's sensitivity to SOI2 timing compared with a 70/30 split ratio. Some SOI2 timing values, while acceptable for 70/30 resulted in severely incomplete combustion (i.e. NIMEP<0) and large spikes in hydrocarbon emissions. It is concluded that 60/40 ratio is too sensitive to SOI2 timing.
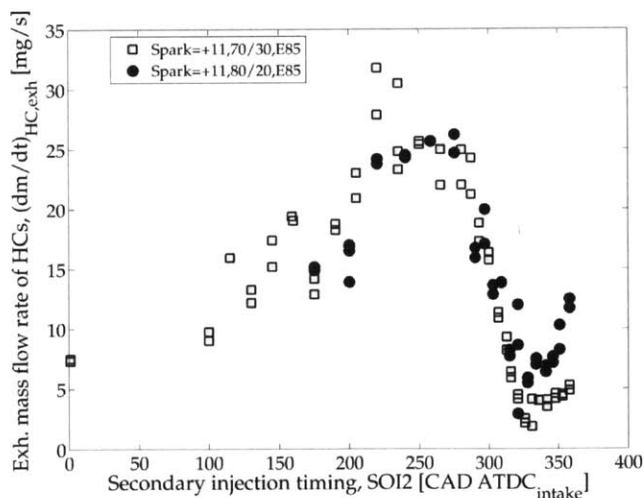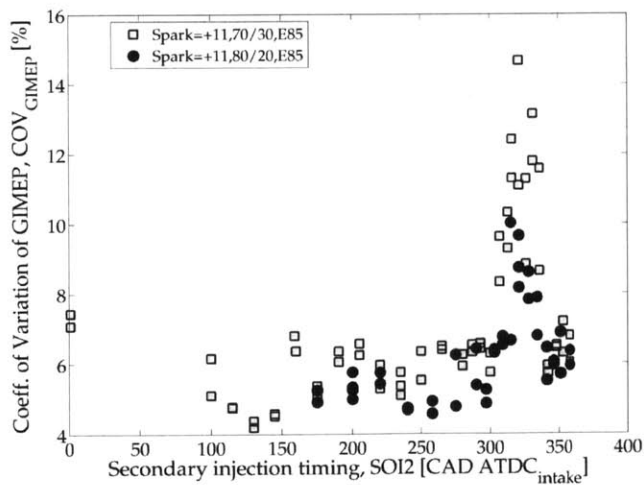
Figure 3-36: In terms of CCV (left), the 80/20 split ratio is less sensitive to SOI2 timing than 70/30 split ratio.

3.6 Fuel ethanol content

In this work ethanol blends are named for the volume percent ethanol. E0 is neat gasoline, E30 is a mixture containing 30% by volume ethanol, balance gasoline. E100 is neat ethanol. In the marketplace it is common for fuel manufacturers to use different base gasoline to compensate for different blend fractions of ethanol. For example, it is typical for the base gasoline in an E85 mixture to have low autoignition resistance because the final E85 fuel mixture's autoignition resistance will be improved by ethanol. The variation of gasoline base stock complicates the analysis of emissions. For this research ethanol blends were prepared using 99.99% pure anhydrous ethanol and a constant base gasoline (Haltermann HF0437).

Results for E0, E30, E50 and E85 are presented below. The initial expectation was that fuels with high ethanol content (e.g. E85) would have poor emissions performance for two reasons. First, ethanol's lower heating value is approximately 35% less than that of gasoline so a greater mass of fuel must be injected. Second, on a mass basis the heat of vaporization of ethanol is approximately four times greater than gasoline. This means compared with gasoline, the ethanol fuel evaporation process may be slower (or incomplete), and will result in more cooling in the combustion chamber. Original expectations were partially correct but overly pessimistic. Ethanol blends performed satisfactorily in cold-idle testing.

Comparing E0 with E85 to get a sense for the extreme differences, Figure 3-37 shows that the combustion phasing of E85 is more advanced (happens sooner) than gasoline, and the burn duration of E85 is significantly. Figure 3-38 compares the exhaust temperatures for E85 with that for gasoline. Since both tests are carried out at essentially the same ignition timing, this change in combustion phasing and duration substantially lowers exhaust gas temperature for E85 compared with gasoline. The lower exhaust temperature of E85 are also at least partly attributable to additional evaporative cooling of the air-fuel mixture in the combustion chamber due to ethanols significantly higher heat of vaporization.

115
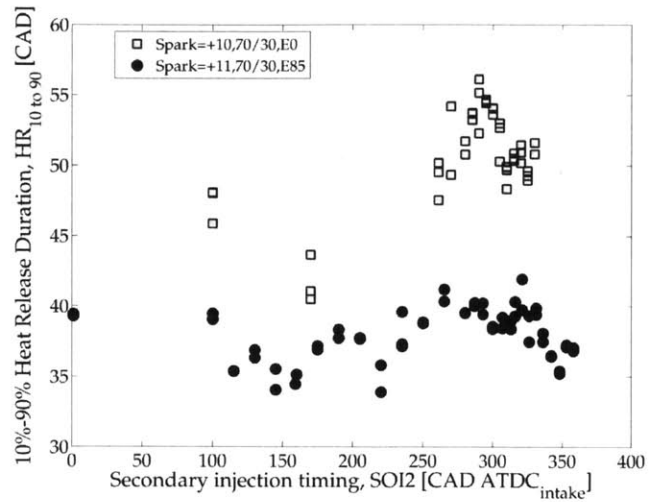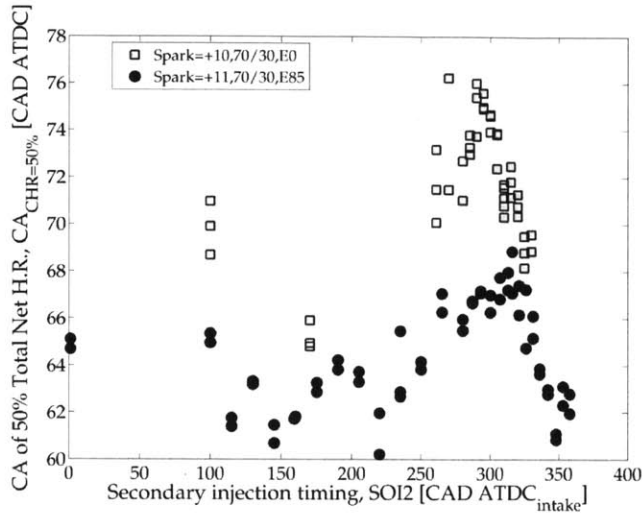
Figure 3-37: Despite the greater mass of E85 fuel injected, E85 50% total heat release point was 6-10 [CAD] more advanced than E0 (left). Partially as a consequence of earlier phasing, E85 also had a shorter burn duration (i.e. faster burn, right) despite a 35% greater fuel mass injection.
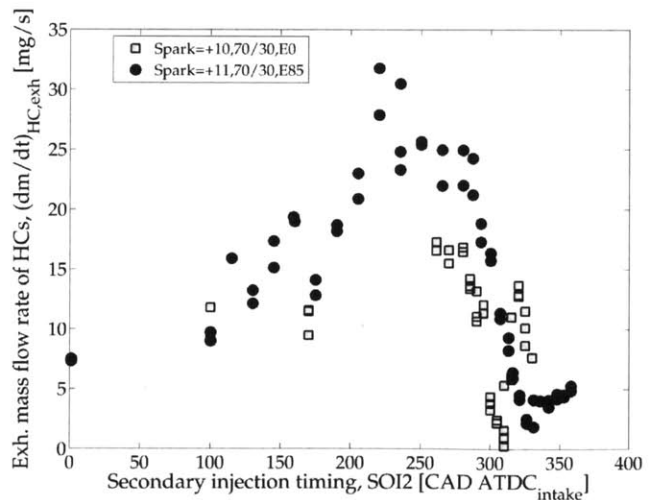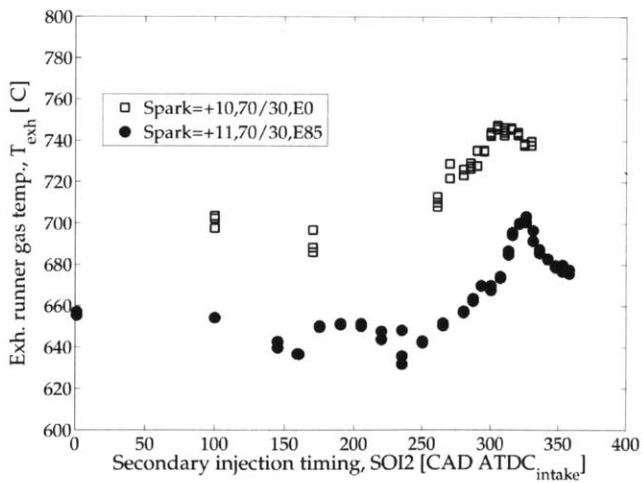
Figure 3-38: Despite the greater mass of E85 fuel injected, E85 hydrocarbon mass flow rate is comparable to E0 mass flow rate emissions. This is attributed to the simpler faster chemical kinetics of oxidation of ethanol. Also, the stoichiometric air fuel ratio of E85 is around 30% less than that of gasoline. Ethanol mixtures are likely to be locally less rich which helps with combustion completeness.

3.7   Other

This section briefly summarizes minor experimental results for themes not explored in detail. The first experiment shows unburned hydrocarbon emissions are insensitive to fuel injection pressure for the conditions tested. The second experiment shows that using the waste-gate to provide a shortcut bypass for exhaust gas from the exhaust manifold to the catalyst is only minimally effective.

3.7.1   Fuel pressure

Figure 3-39 shows the modest sensitivity of engine emissions to fuel injection pressure for the conditions tested. The insensitivity is due to a trade-off in jet momentum,
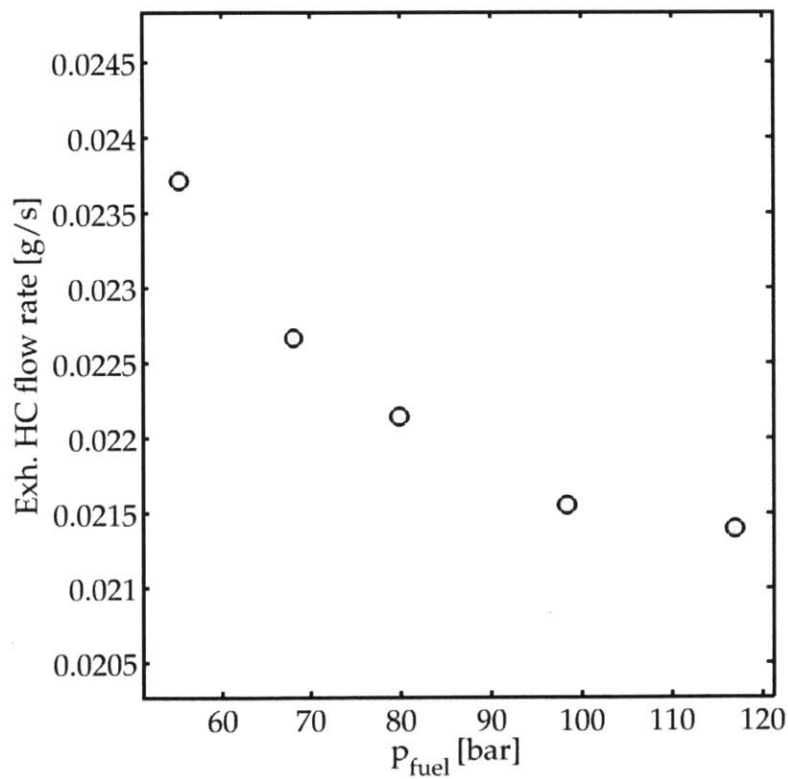
Figure 3-39: The mass flow rate of unburned hydrocarbon emissions decreases modestly as fuel injection pressure increases, probably due to smaller droplets evaporating more completely before primary combustion.

droplet size and injector duration. For constant injected fuel mass, higher injection pressure (e.g. 100 [bar]) leads to smaller droplet size distribution sometimes measured

by Sauter Mean Diameter (SMD), and higher jet momentum for a shorter injection (i.e. pulse width) duration. Small droplets evaporate more quickly but high pressure may lead to more fuel jet penetration and the fuel spray may hit the combustion chamber wall and form a liquid surface. Testing at high pressures shortens total fuel injection durations, causing prohibitively small injection durations for the 30% injection during 70/30 split injection experiments. In contrast, lower injection pressure (e.g. 20 [bar]) leads to larger droplet size distribution, lower jet momentum and a longer injection duration. Large diameter fuel droplets produced by low fuel injection pressure take longer to evaporate. Fuel that does not evaporate may wet the wall. Excessively low pressure may cause the fuel injection spray to collapse. Tests used a nominal fuel injection pressure of 5.0 [MPa].

3.7.2 Waste-gate bypass

Opening the waste-gate did not significantly improve catalyst warm-up. Figure 3-40 shows that transient thermal warm-up was nearly identical regardless of the position of the waste-gate. The waste-gate passage is small diameter and has low lift. When open the waste-gate valve redirects the exhaust gas flow towards the wall of the pipe leading to the catalyst, which may enhance local wall heat transfer for the pipe wall. Waste-gate valve design could be improved, or a second waste-gate valve added for better operation during cold-start turbine bypass.

118
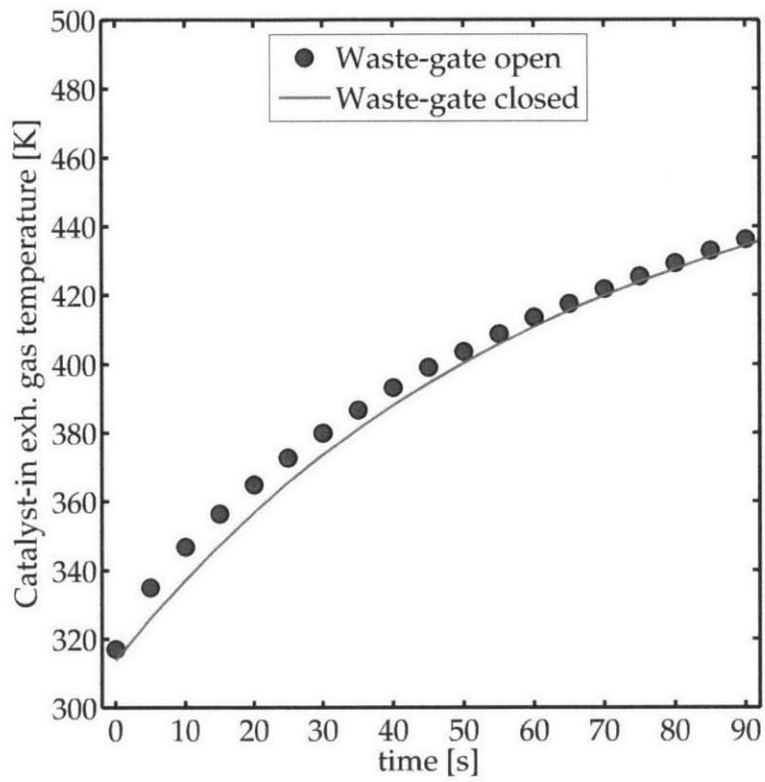
Figure 3-40: The temperature of exhaust gas at entering the catalyst is only modestly improved under the condition tested.

This page intentionally left blank

CHAPTER 4

EXHAUST SYSTEM AND CATALYST MODELS

THE previous chapter presented various engine-out experimental data. These experiments offer insight into operational trade-offs that apply to engines configured for fast catalyst warm-up and low emissions during the warm-up period. The focus of this chapter is to estimate the time duration of the warm-up period so that emissions and fuel consumption totals may be estimated. Hydrocarbon emissions totals are an effective criterion to judge warm-up strategies because hydrocarbon emissions regulations restrict the cumulative emissions over the test cycle.

This chapter reviews the reasoning for estimating emissions data with a computational model, describes the computational models in detail then concludes with some model results.

4.1 Strategy

Cold-start emissions are modelled with an exhaust system thermal model and a transient model of an automotive three-way catalytic converter. The exhaust system thermal model is a physically-based model and since the convective heat transfer physics are simple, the model provides excellent fidelity with experimental results.

Five reasons contribute to the decision to model the catalytic converter:

1. Catalyst formulations vary between manufacturers. Detailed experimental char-

acterization of one formulation, whose details may be confidential, is not widely applicable.

2. Simulation eliminates the effects of catalyst ageing during an extensive experimental program.

3. It is difficult to maintain consistent initial conditions (e.g. oxygen storage, residue from previous tests) between tests for an extensive experimental program.

4. Existing computational models already have reasonable predictive accuracy.

5. The numerical model permits a "look inside" the catalyst without complicated or expensive instrumentation.

4.2   Models

Two engine system simulation models are used in this research. The first is an engine model to probe engine performance and estimate quantities that are difficult-to-measure repeatably or with sufficient temporal resolution. The second engine system simulation model is the exhaust and after-treatment model which simulates the transient thermo-chemical warm-up process of a hypothetical cold-start. These two models are described in greater detail the their respective sections which follow.

Both engine system simulation models are constructed, evaluated and post-processed in Gamma Technologies GT-SUITE, which is a commercial simulation package for engine and vehicle systems. GT-POWER is a component of GT-SUITE optimized to simulate 1-D thermal/fluids physics of internal combustion engines and other vehicle systems.

4.2.1   Engine model

Project sponsors supplied a detailed GT-POWER model of the engine, intake and exhaust systems. The model was modified to reflect the as-built details of plumbing and geometry of the experimental engine. The intake air components between the

compressor-outlet and throttle body are omitted. They are replaced by a reservoir at the inlet of the intake manifold. This accelerates computational convergence and permits the user to specify that intake manifold air pressure and temperature exactly match experimentally measured values. It has a negligible effect on gas exchange. Figure 4-1 shows a schematic of the detailed GT-POWER model. GT-POWER does
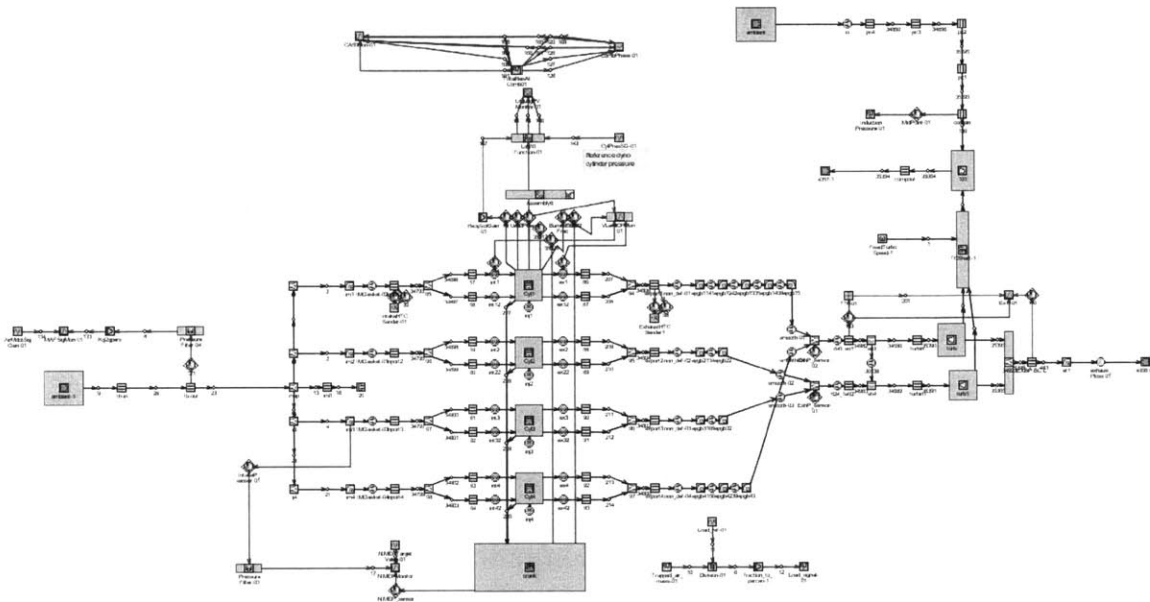
Figure 4-1: This engine model does not include a throttle body or the stock charge air cooler. It has been modified to replicate the experimental engine for which intake air temperature and humidity are controlled.

not have models for chemical kinetics of combustion. It can interface with kinetic solvers, or the user can specify combustion characteristics through a user-defined mass-fraction fuel burn profile. For the present work, experimentally derived burn profiles (from engine combustion chamber pressure and volume data) are input to GT-POWER. The solver "imposes", rather than simulates, the heat release from combustion. GT-POWER uses the heat release schedule and correlations for working physical fluid thermo-physical properties to predict temperature and pressure of gases in the combustion chamber.

For each simulation GT-POWER iteratively solves mass, momentum, and energy conservation equations for the engine system, and each cylinder. This includes the following processes and phenomena:

- Gas exchange comprising air in, exhaust out, back-flow from exhaust to intake, short-circuit from intake to exhaust

- Fuel injection: for evaporative cooling, and mixture specific heat ratio

- Compression stroke with net work transfer from piston to combustion chamber gases

- Combustion with a prescribed heat release schedule (scaled by the fuel amount, related to air intake density and user-specified fuel-air equivalence ratio)

- Expansion stroke with net work transfer from combustion chamber gases to piston

- Other: heat transfer from combustion chamber gas to combustion chamber walls, piston-cylinder friction, heat transfer from exhaust gases to exhaust system components

The GT-POWER model must be empirically tuned and validated with experimental data to properly model combustion chamber heat transfer and account for phenomena such as blowby. The validation procedure is to run a simulation whose parameters are set with experimentally measured values for:

- Intake air pressure (MAP),

- Fuel-air equivalence ratio (Φ),

- Burn profile: CA50 timing, 10%-90% burn duration (BD_{10-90}), and

- Valve timing (IVO and EVC).

Then, compare experimentally measured values with model-predictions of:

- Air mass flow rate,

- Engine load (NIMEP), and pumping work (PIMEP)

- Exhaust gas temperature at the exhaust manifold-inlet.

A visual comparison of the PV diagram which verifies fidelity of gas exchange details and the polytropic constants the for compression process and expansion process. That is, for a PV diagram plotted in log-log scale, the slope of data points during compression and expansion strokes. The slopes of these lines may be affected by

124

mixture properties or combustion chamber heat transfer. The engine model was validated across a range of engine load values of NIMEP from 1.5 to 3.5 [bar], and ignition timing from -30 to 20 [CAD ATDC]. Across this range of conditions, more than 85% of simulation predictions were within ±5% of nominal experimental values, and more than 95% were within ±10% of nominal experimental values.

The validated model can be used to estimate temperatures, pressures, flow rates and engine performance data with good fidelity. In this research it is primarily as a tool to estimate combustion chamber burned gas temperature, which is difficult to measure with high temporal resolution repeatably in a running engine.

The second engine system model is the exhaust and after-treatment model, which comprises two sub-models:

1. A thermal model of the exhaust components from the engine cylinder head outlet to the catalyst inlet including the exhaust manifold, turbocharger turbine and pre-catalyst pipe.

2. A chemical kinetic and 1-D flow model of the catalytic converter

The next sections describe the inputs, outputs and assumptions of each sub-model.

4.2.2   Exhaust system thermal model

The exhaust system thermal model is constructed in GT-POWER, shown schematically in Figure 4-2. The model contains geometric and material property details of actual engine exhaust components. The turbine object in GT-POWER models the mechanical operating characteristics of the turbine as an expander, not the thermal behaviour that is germane to cold-start warm-up. The thermal response of the turbocharger is modelled with a surrogate whose thermal mass and heat transfer properties match the actual turbine. The geometric and material properties are measured then tuned from transient thermal tests involving the actual turbine.

The inlet conditions for the model are user-specified from experimentally measured exhaust gas mass flow rate and final temperature after a 300s warm-up starting from cold. Exhaust gas composition is assumed constant with respect to time. Over the
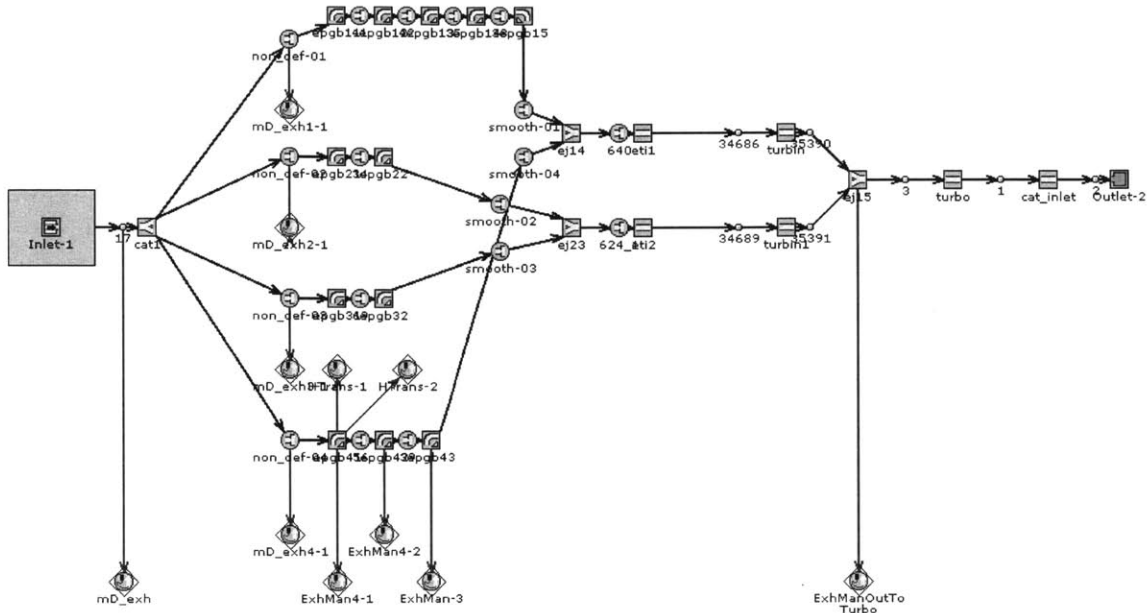
Figure 4-2: This model is used to predict the temperature drop between the engine outlet (exhaust manifold inlet) and the catalyst-inlet.

course of warm-up, exhaust gas thermal properties do not change significantly due to high fraction of N_2 for the range of equivalence ratios in this research. The model assumes ambient conditions of 25°C for external natural convection.

Figure 4-3 shows that the model predicts the transient temperature of exhaust gases, measured at the exhaust manifold inlet, over the desired interval with good agreement. The time-dependent predicted temperature of exhaust gases at the catalyst inlet from the exhaust system thermal model is used as input for the catalytic converter model. The mention of time-dependent temperatures raises the issue of the thermocouple error correction, which is now addressed.

Thermocouple error correction

Thermocouples introduce two types of error in this research. The first error is that thermocouples lag actual temperature of the medium in which they are submersed by some time related to the size and construction of the thermocouple. The second error is that thermocouples reach an equilibrium temperature offset by some amount due to conduction and radiation losses from the thermocouple bead.

126
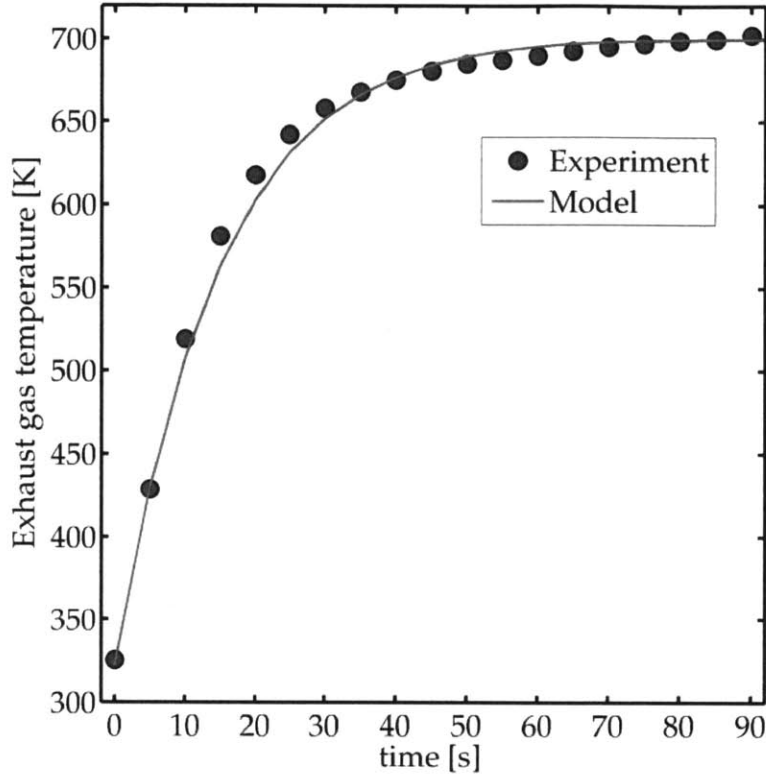
Figure 4-3: The tuned exhaust thermal model accurately predicts the transient temperature profile of exhaust gas at the exhaust manifold inlet during warm-up.

Transient Response Thermocouples do not measure instantaneous exhaust gas temperature. There is a characteristic response time or delay due to the thermocouple's finite heat capacity. In other words, the thermocouple itself must heat up (which takes finite time) before it registers a temperature change. Using geometry and material properties and knowledge of the convective field in the exhaust (from GT-POWER) it is possible to estimate a true gas temperature from a transient thermocouple reading. GT-POWER can report true gas temperature and thermocouple temperature from a virtual thermocouple "installed" in the model. These features were used to convert transient experimental thermocouple recordings around the exhaust system (e.g. post-turbo, pre-cat, etc.) to estimated true-gas temperature data to more accurately characterize the exhaust system thermal model. Figure 4-4 shows that errors due to transient response. Since the exhaust manifold runner thermocouple was fitted with an aspirated radiation shield, a transient correction for the exhaust manifold runner thermocouple was not applied. Such a shield was necessary
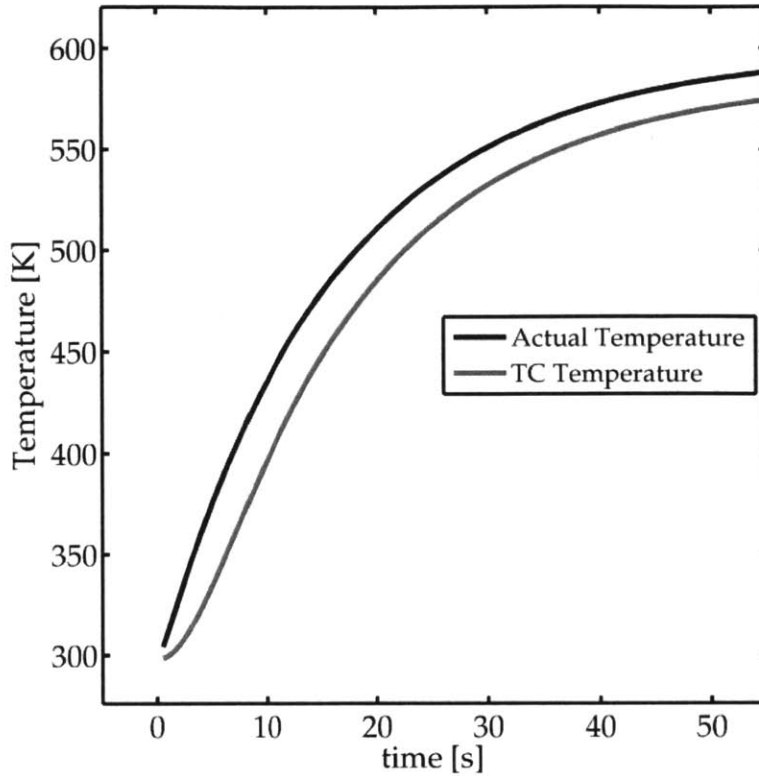
Figure 4-4: At 10[s] the difference between the true gas temperature and thermocouple reading is can be on the order of 40K, put another way the thermocouple lags the actual gas temperature by approximately 3.5[s].

because radiation is a potential source of significant error in thermocouple readings of exhaust gas.

Thermocouple losses   After the transient the thermocouple bead reaches some equilibrium temperature. For hot engine exhaust gas, the thermocouple reading is somewhere between the gas temperature and the wall temperature. The bead loses energy to its surroundings due to conduction along the thin thermocouple probe, which acts like a fin, and to the walls via radiation. The thermocouples used in this research had a length to diameter ratio greater than 100 so conduction losses along the thermocouple are ignored. Radiation losses from the thermocouple bead to the internal surfaces of the exhaust system are significant for exhaust gas temperatures above ~800-900K.[47] Temperatures in the exhaust manifold runner whose thermocouple are above this threshold, which motivated the use of a radiation shield

128

to reduce radiation losses. Thermocouples downstream of the turbocharger did not surpass this threshold.

With transient thermal data newly corrected for thermocouple errors, and experimental engine emissions data from the previous chapter it is time to examine the catalyst model.

4.2.3   Catalyst model

The catalytic converter model is based in GT-POWER, shown schematically in Figure 4-5. It simulates transient chemical kinetics, oxygen storage and 1-D flow. The model predicts reaction rate (species conversion), heat transfer, surface temperature at points that are spatially resolved in 1-D (streamwise along converter), time-resolved from cold at $t = 0$[s] to $t = 300$[s]. With kinetic parameters chosen from the literature, the model can predict cumulative catalyst-out hydrocarbons that agree with experiments for FTP and NEDC drive cycles.[48]
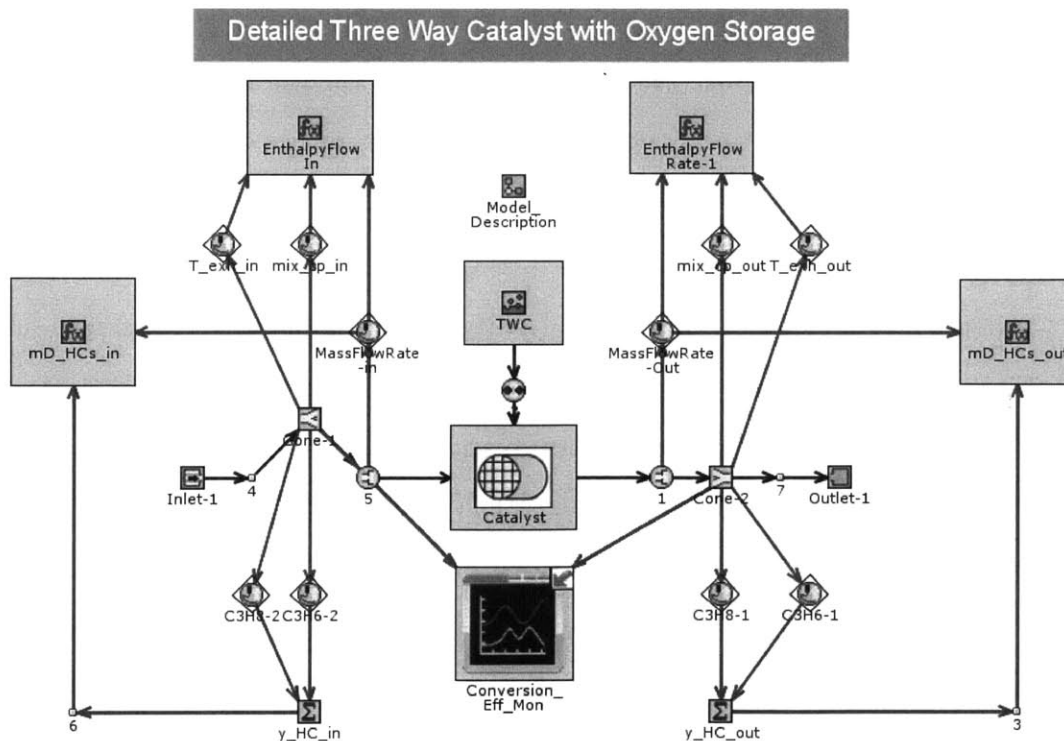
Figure 4-5: The model simulates transient thermal and chemical processes during cold-start. The catalyst inlet is on the left side, the outlet is on the right side.

Configuration

The three-way catalyst has physical parameters to describe cerium (CeO_2 and Ce_2O_3) and platinum group metal (PGM) loading and active surface site density.

The kinetic scheme contains 15 reactions, 9 for PGM sites and 6 for cerium. The model accounts for an inhibition function between CO and C_3H_6 (propylene), and the water-gas shift equilibrium. The kinetic scheme is adapted from Ramanathan and Sharma, [48], which show broad similarities to other schemes in the literature. [49–59]

Inputs

The model assumes ambient temperature as its initial condition and the following inputs, all of which may vary with time:

- Mass flow rate of exhaust gases taken from experimental measurement
- Exhaust gas temperature (taken from experimental catalyst-in measurement)
- Exhaust gas composition: [CO, CO_2, N_2, O_2, H_2O, H_2, C_3H_8, C_3H_6, NO_2, NO]

The hydrocarbon species are broken into "fast" reacting hydrocarbons (propylene C_3H_6 in this case) and "slow" reacting hydrocarbons (propylene C_3H_8 in this case). Experimental hydrocarbon measurements quantified total hydrocarbons (i.e. were not broken down by species) so a fixed ratio of 85% fast, 15% slow was used as recommended by the literature.[57, 60, 61]

The concentration of NO and NO_2 were not measured during experiments. For most operation with a cold engine at low or part load NO_x concentration is low. Therefore NO and NO_2 concentration is set equal to 10 [ppm]. The author cautions that with high intake manifold pressure, late ignition and lean air-fuel mixture, NO and NO_2 may be substantially higher than 10 [ppm].

4.3 Results

The catalyst-out cumulative hydrocarbon predicted by the model agree well with published data. An important caveat of the current modelling effort is that "cumulative emissions" in the present work do not include two documented sources of hydrocarbons from real vehicles.

1. Unreacted hydrocarbons condensed or adsorbed on the surface of the catalyst from the previous engine shutdown.

2. Emission of unburned fuel during the cranking and start-up transient that precedes cold idle.

The aforementioned hydrocarbon sources would simply increase every model prediction by some constant offset and the trends presented here for cold-start fast idle remain valid.

4.3.1 Thermal trends in catalyst warm-up

Under typical catalyst warm-up conditions, the leading edge of the catalyst warms up first and fastest. With sufficient residence time, it would also be the first of any part of the catalytic converter to catalytically facilitate surface reactivity. Heat transfer to the turbine of a turbocharged engine reduces the flow rate of thermal enthalpy delivered to the catalyst. With slower warm-up, the question is whether the catalyst warms more evenly, and how much heat release from surface reactions in the leading edge contribute to subsequent warm-up of downstream catalyst sections.

Simulation results show that the leading edge is always at the highest temperature and becomes reactive first. This suggests that heat transfer near the leading edge is still rapid enough to activate the entry region first. What was not known was how much of the catalyst was in "the entry" region, that is whether the first 25% is critical, or just the first 5% in the streamwise direction. Depending on how hot the entry region becomes, and how quickly it warms up two cases may prevail:

1. The leading edge is hot enough that its oxidation is limited only by diffusion

and residence time. Thermal energy from heat release from reactions at the leading edge of the catalyst cascades downstream, advected by exhaust gas to heat and activate subsequent portions of the catalyst.

2. Heat transfer at the leading edge is slow enough that the surface temperature of the catalyst substrate is flattened by axial conduction within the catalyst substrate. Lower and more uniform catalyst surface temperature lead slow the rate of heat release from surface reactions. Cumulative thermal energy released induces light-off and cascading energy release at some distance from the leading edge.

Axial temperature profiles along the simulated 1-D catalyst are plotted for late ignition (i.e. high mass flow, high temperature) and early ignition (i.e. low mass flow, low temperature) in Figure 4-6 describe cases 1 and 2 respectively. The trends mentioned
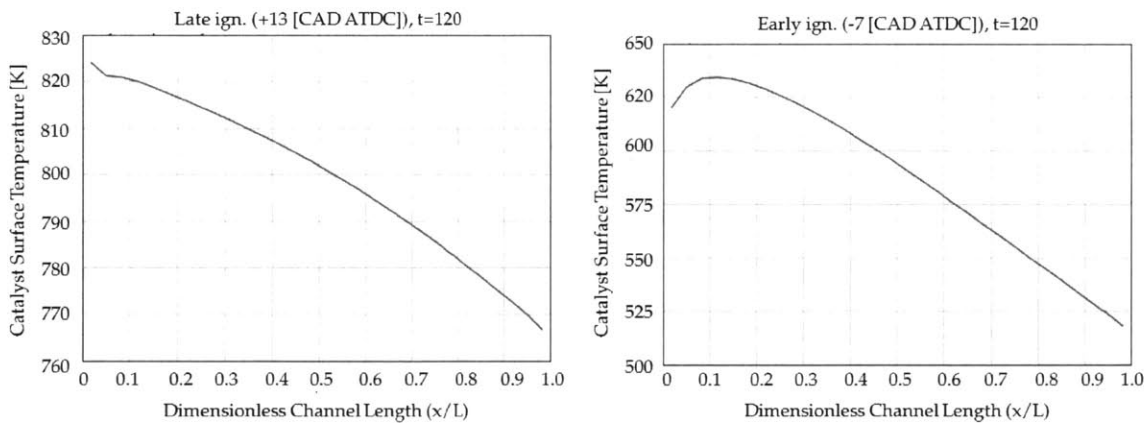
Figure 4-6: These data are extracted at $t = 120$ s, before the catalyst has reached thermal or chemical steady state. High flow and high temperature exhaust from late ignition (left) lead to rapid heat release in the entry region which cascades downstream. Low flow and low temperature exhaust from early ignition (right) lead to a more gradual transfer of thermal energy from catalyst surface reactions to gas and a light-off location at some distance downstream from the leading edge

above may be exploited by rapidly heating only a small entry region of the catalyst. After the entry region is heated, exothermic release from catalytic reactions will sustain activity there and transfer thermal energy downstream (mainly by advection due to the bulk flow). This is another reason to prefer high flow rate of exhaust gas rather than a hypothetical low flow rate, low emissions rate configuration. In fact, many

practical three way catalysts are designed with multiple bricks. The properties of the first brick are adapted to resist high temperatures during operation and cold-start without sintering or thermal deactivation. The first brick may also have different washcoat formulations or PGM loading density.

Having looked at the thermal behaviour of the catalyst, now the chemical behaviour of the catalyst during warm-up is examined.

4.3.2 Chemical reactivity

Figure 4-7 shows the transient evolution of the chemical reaction rate of the propene (C_3H_8), the fast reacting hydrocarbon, for an early ignition timing and a late ignition timing, in consecutive streamwise volume elements of the catalyst. The exact location of each volume element in the catalyst is not the important feature, just the development and distribution of reactivity. With some insight into the thermochem-
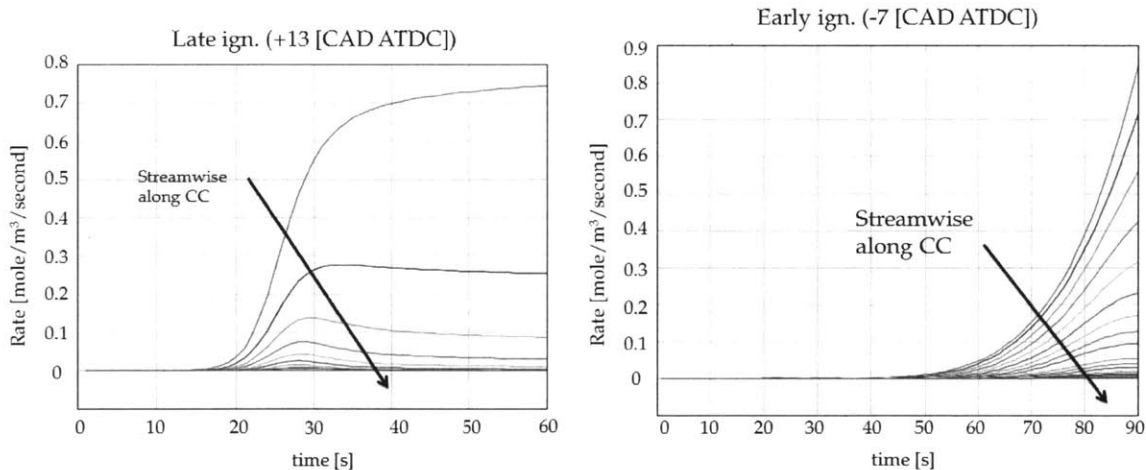
Figure 4-7: Upstream volume elements react first, but the late ignition case (left), the first 3 volume elements (3cm) corresponds to 95% of all oxidation at t=40s. In contrast, for early ignition (right), even heating of entry sections causes a more even reactivity distribution, even up to 90s. Note that both plots share a nearly equal vertical axis scale but the late ignition case (left) has a shorter horizontal axis scale than the early ignition case (right).

ical details of the catalyst model, we now discuss the criterion to decide when the catalyst is "warmed up". The introduction of this thesis quoted a 250°C activation temperature, but what has to reach 250°C for the catalyst to perform adequately?

Another common activation criterion is the time until hydrocarbon conversion efficiency ($eta_{conv} = 1 - \frac{m_{HC,out}}{m_{HC,in}}$ reaches a threshold value of 50%. The former is simpler while the latter is defined in terms of actual emissions control. Aside from emissions during warm-up, the actual time to warm-up is important because it dictates whether the catalyst is ready soon enough to handle the demanding high-load transients that occur 25s after cold start in the emissions test. Figure 4-8 shows that, for the range of light-off behaviour modelled in this research, these criteria are well correlated. With a
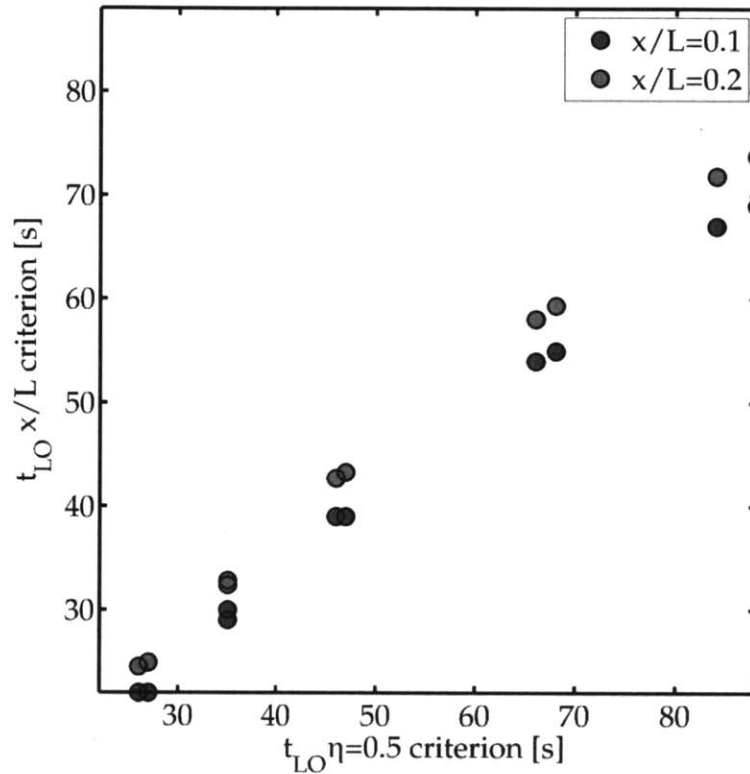
Figure 4-8: The thermal criteria plotted on the vertical axis are the time until a specified location ($x/L = 0.1$ and $x/L = 0.2$) reach the light-off temperature. These criteria are plotted as a function of the time until $\eta_{conv} = 50\%$

thoroughly understood model, we can now move to comparing emissions performance of different cold-start strategies.

4.3.3 Emissions predictions

The exhaust and after-treatment model simulates the emissions performance of warm-up strategies from experimental data. In the early stages of this research, a trade-

off was expected between two types of strategies. One, with slow warm-up, but low hydrocarbon emissions rate. A second with comparatively fast warm-up, but comparatively high emissions. In practice, post-flame oxidation in burned gases was found to be quite important. Under the cold-start fast idle constraint of constant engine load, strategies for fast warm-up entail high exhaust gas temperature and high exhaust mass flow rate. High exhaust gas temperature facilitate post-flame oxidation. The net result is fast warm-up and low hydrocarbon emission rate. In other words, the envisioned slow warm-up, low emissions strategies can't compete, because emissions are not low enough and fast warm-up strategies lead to low emissions via post-flame oxidation.

Although the model can predict cumulative catalyst-out hydrocarbon emissions for an arbitrary matrix of engine-out hydrocarbon emissions rate and engine-out exhaust gas temperatures, in practice catalyst-in conditions are confined to a narrow region of the full test space in Figure 4-9 Late ignition timing plays a dual-role in minimizing catalyst-out emissions during cold-start due to higher thermal enthalpy flow rate of exhaust gases, and enhanced post-flame oxidation. No other strategy provided equal benefit, so catalyst model predictions are restricted to rapid warm-up strategies involving late ignition timing. Figure 4-10 shows predicted hydrocarbon emissions for 10 experimental conditions over a 300 s warm-up simulation. The cumulative mass of emissions data from Figure 4-10 is re-plotted in Figure 4-11 to show that later ignition decreases cumulative emissions. Because of unacceptable cycle-to-cycle variation at later ignition times, the trend of emissions and light-off time can't be extended to provide still faster warm-up and even lower emissions. Fortunately, this research revealed that higher exhaust back pressure reduces emissions that does not require such late ignition timing. Figure 4-12 shows emissions predictions for late ignition trials with standard and increased exhaust back pressure. With accurate predictions of how long the catalyst takes to warm up, and cumulative emissions over that period, the next task is to estimate the fuel consumption over that period. Despite the short duration of cold-start, for equivalent emissions performance engine manufacturers prefer fuel-efficient emissions control strategies.

135
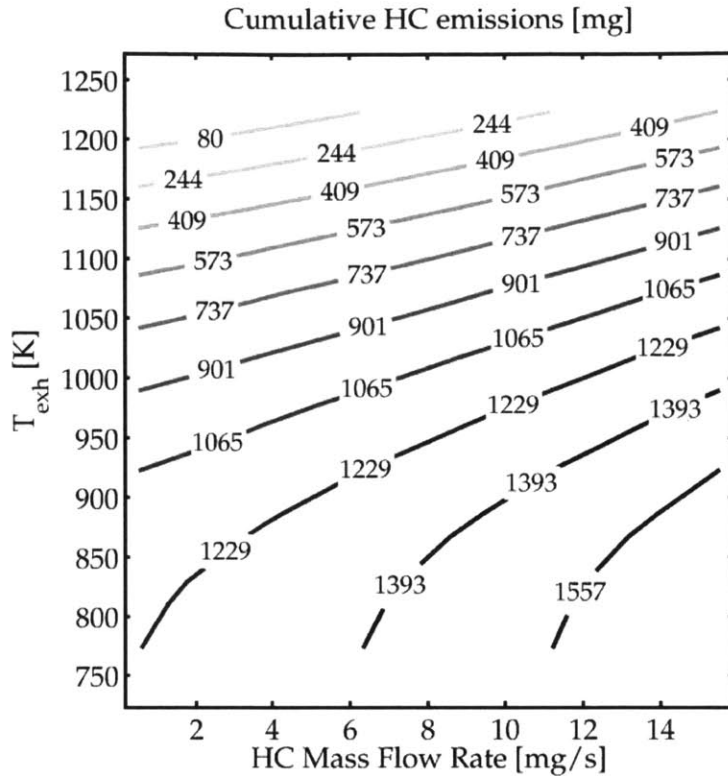
Figure 4-9: Practical warm-up strategies try to approach the top left region where warm-up is fast and cumulative catalyst-out hydrocarbon emissions are low. MBT timing would be located in the bottom right quadrant.

4.3.4 Fuel consumption results

Using engine speed data, fuel mass injected per cycle from engine experiments is converted to a fuel consumption rate. The fuel mass injected per cycle, light-off time and total fuel consumption during warm-up are plotted for high exhaust pressure experiments in Figure 4-13. The research and computational models appear to point a way forward in cold-start emissions control. However, as with all computational models, some uncertainty remains in the fidelity of the catalyst model. The next section examines model sensitivity.

4.3.5 Uncertainty Quantification

The results of this research are subject to two sources of uncertainty. One is error in experimental measurements. The second are modelling errors. Thermocouple

Cat-out Cumulative HC mass evolution
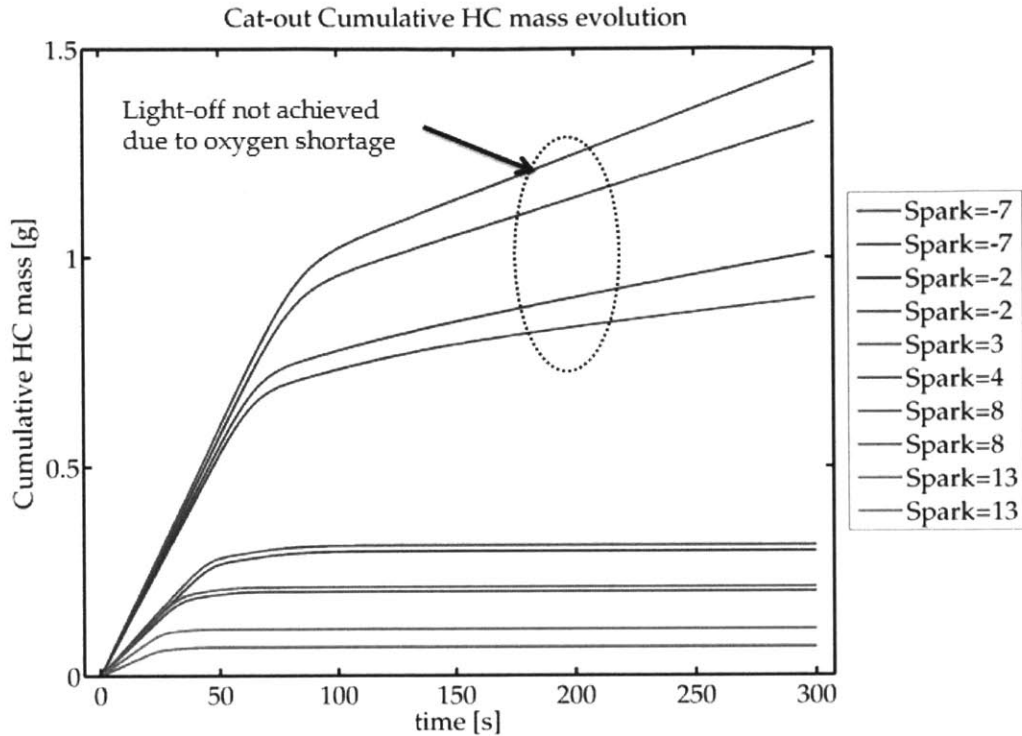
Figure 4-10: Emissions rate and cumulative emissions are lower for late spark cases (red). Some experimental cases failed to warm-up due to insufficient oxygen, possibly from poor air-fuel equivalence ratio control.

measurement error has already been discussed. For the catalyst model, the main issues are:

- The catalyst model uses two hydrocarbon species (propane and propylene) to represent hydrocarbon gases. How accurate are its predictions for exhaust gas containing oxygenates (e.g. formaldehyde from combustion of gasoline blended with ethanol)

- Most automotive catalysts operate near atmospheric pressure. In the high exhaust pressure cases, pressure in the catalyst approached 3 bar. The unknown role of exhaust gas pressure and density in the catalyst. Some literature suggests species competition for active sites and self-inhibition at high pressure.

- The catalyst model is 1-D, which means some work is needed to relate its predictions to those of a real 3-D monolith. It is not known the extent to which different light-off strategies alter that relationship (e.g. flow pattern,

137
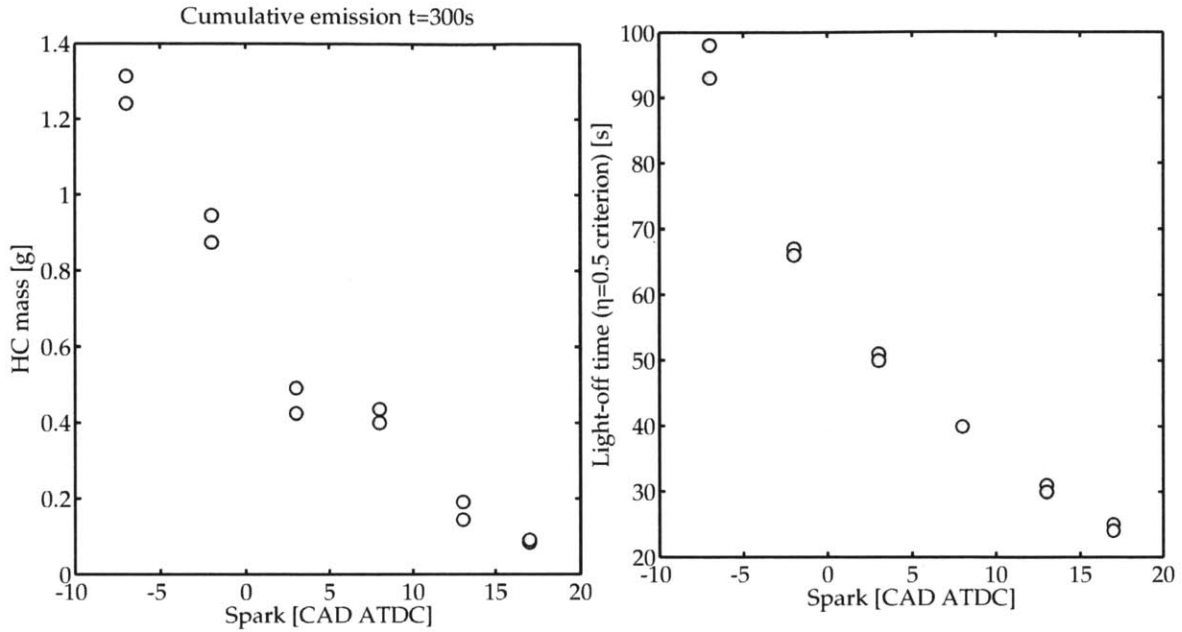
Figure 4-11: Late ignition decreases cumulative hydrocarbon emissions through faster warm-up (shorter light-off time) and reduced emissions concentration arising from better post-flame oxidation.

temperature distribution, etc.)

The following table describes the uncertain experimental parameters with mean values and standard error. Then these are grouped into two test casts, one for "fastest warm-up" and another for "slowest warm-up". Table 4.1 summarizes the results, which indicate the model is modestly sensitive to experimental uncertainty.

Table 4.1: Sensitivity Analysis

-	$\dot{m}_{exh}$	T_{exh}	HC	CO	t_{LO}	HC total
Units	g/s	°C	ppm_{C1}	vol-% wet	s	mg
Fast	11	825	1100	1.3	28.5	381
Measurement and error	10±0.5	800 ± 25	1000±100	1±0.3	30	400
Slow	9.5	775	900	0.7	31	394

The bulk of the work is complete. The next chapter summarizes the results of this research and proposes some future directions for this topic.

Cumulative emission t=300s
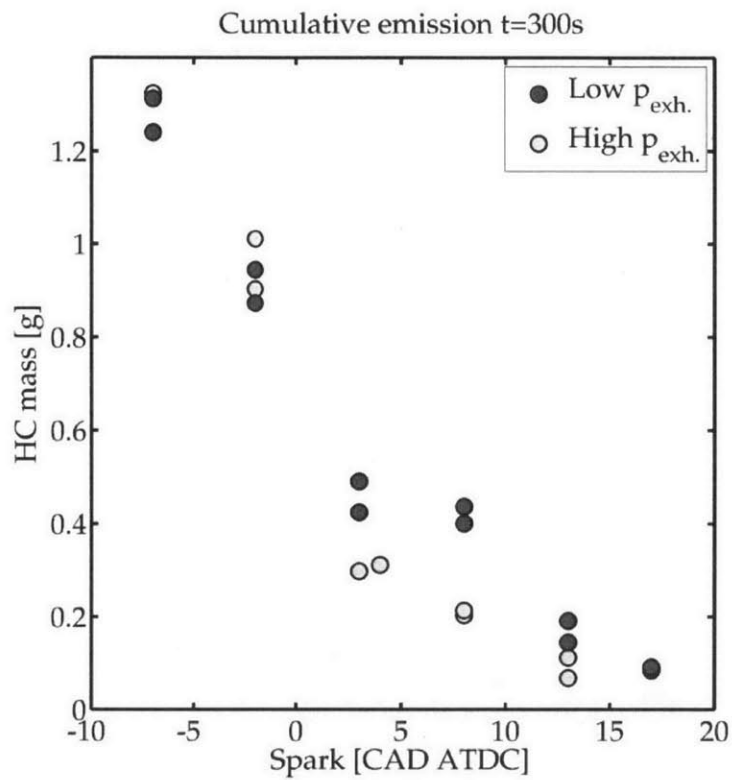
Figure 4-12: For stoichiometric mixtures, the high back pressure case consistently outperforms the standard back pressure emissions performance. Lean mixtures to exploit enhanced post-flame oxidation are predicted to offer still-better emissions performance.
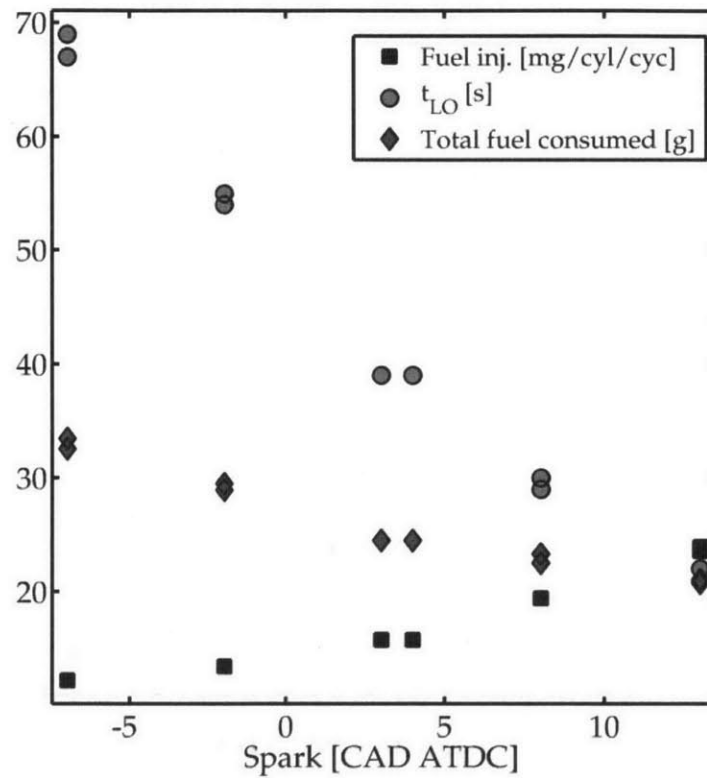
Figure 4-13: For late ignition at fixed load, exhaust mass flow rate and temperature are higher, both which accelerate catalyst light-off. Total fuel use goes down, probably because the hotter exhaust is able to induce cascading light-off.

CHAPTER 5

CONCLUSIONS

THIS thesis reports a broad survey of experimental engine research on methods to control cumulative catalyst-out unburned hydrocarbon emissions from turbocharged, direct injection spark ignition engines during cold start. The preceding chapters examined sources of engine-out emissions of unburned hydrocarbons, control strategies in the literature, findings from engine experiments and catalyst simulations. This thesis concludes a description of the work performed, a summary of the major findings and some recommendations for future work on the topic of emissions control for turbocharged DISI engines during cold-start.

5.1 Summary

This research set out to characterize the emissions behaviour of turbocharged DISI engines. The objective was a control strategy for catalyst-out emissions of unburned hydrocarbons during cold-start. Emissions control for gasoline engines aims to accelerate the warm-up process of the catalytic converter and maintain low emissions during warm-up. The research focused on the fast-idle portion of cold-start. The idle period is repeatable, a large contributor to cold-start emissions, a particular challenge for DI fuel engines and extended by the thermal warm-up delay caused by the turbine. The research had three components:

1. Engine experiments with varied engine parameters including ignition timing, equivalence ratio, fuel injection schedule, valve timing and exhaust back-pressure were conducted. Fuel blends with ethanol were also tested (since ethanol fuel blends have performance and efficiency synergies in turbocharged DISI engines). Exhaust thermal enthalpy flow rate (for fast catalyst warm-up) and emissions data (for low emissions) were recorded during engine experiments.

2. A calibrated 1-D engine simulation to probe the thermophysical processes that were not measured or measurable during experiments.

3. An exhaust system model containing a 1-D thermal model of the exhaust system (from engine to catalyst) and 1-D catalytic converter model with thermal/flow and three-way catalyst chemical kinetics details. The exhaust aftertreatment model used experimental data to simulate the warm-up process. The simulations estimate cumulative catalyst-out hydrocarbon emissions and fuel consumption over the warm-up cycle.

5.2 Findings

A high flow rate of thermal enthalpy in the exhaust gas is necessary to accelerate catalyst warm-up. High thermal enthalpy flow rate comes from a high mass flow rate and/or high exhaust gas temperature. Operating at a fixed engine speed and output load during cold idle, reduced fuel conversion efficiency is needed to produce more mass flow rate and high exhaust gas temperature for high thermal enthalpy flow rate.

Engine experiments show that late and slow combustion heat release cause fuel conversion efficiency to decrease. The following techniques cause late and/or slow combustion heat release:

- Late ignition timing.

- A lean air-fuel ratio. Air dilution delays combustion and leads to facilitates higher post-flame oxidation.

- An appropriately stratified fuel-air mixture. A locally-rich mixture near the spark plug (at the time of ignition) reduces cycle-to-cycle variation and facili-

tates later ignition timing or globally leaner mixtures.

- High residual gas fraction, i.e. from long valve overlap. Residuals dilute the fuel-air mixture which delays and slows combustion. Late combustion from high residual gas fraction leads to only modest increases in exhaust gas temperature and modest decreases in engine-out hydrocarbon concentration with comparatively high cycle-to-cycle variation.

The risk of partial-burn misfire increases with late and/or slow combustion no matter the engine parameter used to delay or slow combustion. Partial-burn misfire causes engine roughness and even a single misfire event emits a significant and unacceptable contribution of unburned hydrocarbons. Therefore partial-burn misfire must be avoided.

High exhaust gas temperature not only helps accelerate catalyst warm-up, but also help to oxidize hydrocarbons that do escape primary (flame) combustion. From engine experiments and simulations, it is concluded that post-flame oxidation in the combustion chamber and exhaust system play a critical role in decreasing the quantity of catalyst-in emissions of hydrocarbons (and other unburned or partially burned products) that escape primary (flame) combustion. It is further concluded that strategies for fast warm-up are preferred to strategies for slow-warm-up with low-emissions, since post-flame oxidation that accompanies fast warm-up results in low emissions too.

Major findings from ignition (spark) timing experiments:

- Ignition as late as +20 [CAD ATDC] was possible (with single injection) before misfire.
- For each CAD of spark retard, exhaust gas temperature at the exhaust manifold inlet increases by approximately 9.2°C, exhaust gas mass flow rate increases by 0.24 [g/s], COV of GIMEP increases by approximately 0.25%-points, catalyst-in hydrocarbon flow rate decreases by 0.3 [mg/s].
- Late ignition experiments were limited by partial-burn misfire.

Major findings from fuel-delivery schedule experiments:

143

- A split injection of 70% fuel delivered at regular timing during the intake stroke, and 30% of fuel delivered late in the compression stroke creates a mixture that is center-rich, perimeter-lean. Center-rich near the spark plug reduces cycle-to-cycle variation. Perimeter lean reduces the amount of fuel trapped in combustion chamber crevices.

- Engine behaviour and emissions were relatively insensitive to injection timing of the first injection (70%) for conventional timing in the intake stroke.

- Engine behaviour and emissions were relatively insensitive to injection timing of the second injection (30%) for when it occurred early in the intake stroke.

- Engine behaviour and emisions were very sensitive to second injection timing late when it occurred in the compression stroke. Cycle-to-cycle variability peaked for second injections starting (SOI2) at 300 [CAD $ATDC_{intake}$], and decreased to a minimum at $\sim$ 330 [CAD $ATDC_{intake}$].

- A ratio of 60/40 had higher peak cycle-to-cycle variations than 70/30. It is theorized that a 60/40 split ratio leads to a rich zone that is too rich and lean zone that is too lean for effective flame propagation.

- A ratio of 80/20 was difficult to achieve with gasoline, and showed smaller emissions and stability benefits than 70/30.

Restricting exhaust flow to increase exhaust back-pressure causes exhaust gas temperature at the engine-outlet to increase. Higher exhaust pressure necessitates higher intake manifold pressure to maintain constant engine load. At constant air-fuel equivalence ratio, higher intake pressure increases the amount of fuel injected (and burned) and maximum temperature achieved in the combustion chamber. Higher exhaust pressure also alters the exhaust blowdown process. The net effect that high exhaust back pressure (p_{exh} = 1.80 [bar] for WOT motoring at 1200 [rpm]) leads to significantly higher temperature during late expansion, and greater post-flame oxidation which lead to lower emissions. The most significant improvements came with restricted exhaust and lean air-fuel mixtures (Φ = 0.87, λ = 1.15). The lean mixture delays combustion and facilitates post-flame oxidation. For equal cumulative

catalyst-out emissions, a high exhaust pressure with lean mixture had significantly lower cycle-to-cycle variation, i.e. risk of partial-burn misfire. It is concluded that exhaust flow restriction (i.e. high exhaust back pressure) can be an effective way to improve warm-up and reduce emissions. The use of high exhaust back-pressure is limited by turbine rotor inlet temperature limits, which may be alleviated by a modified waste-gate to bypass more exhaust gas from the exhaust manifold, around the turbine to the catalyst.

The potential for valve timing to improve cold-start emissions was limited on this engine. Neither intake cam advance, nor exhaust cam retard alone lead to significant emissions improvements. When used simultaneously, intake cam advance and exhaust cam retard lead to long valve overlap period. Long valve overlap increases residual gas trapping during the valve overlap period. Excessive residual gas causes cycle-to-cycle variability and misfire. It is concluded that exhaust valve overlap must be minimized.

The main conclusions from the study of ethanol blends are:

- At the same ignition timing, ethanol blends produce lower exhaust gas mass flow rate and lower engine-out exhaust gas temperature than gasoline. This contributes to slower catalyst warm-up.

- The mass flow rate of engine-out unburned hydrocarbons from E30 and E50 ethanol blends are comparable to gasoline for the conditions tested.

- For equal ignition timing, E85 showed the highest emissions rate of any fuel blend tested. This contributes to higher emissions during catalyst warm-up.

- For the same ignition timing, ethanol blends had lower COV than gasoline due to shorter burn durations and advanced combustion phasing.

Using the waste-gate as a bypass valve for exhaust gas to flow from the exhaust manifold to the catalyst-inlet did not significantly improve warm-up for the condition tested.

The simple 1-D catalyst model was able to predict vehicle-out cumulative hydrocarbon emissions that agree with data in the literature. The common 50% hydrocarbon conversion efficiency criterion for judging when the catalyst is operational corre-

145

lates with a simpler thermal criterion for warm-up. Namely, the time for a location 10% or 20% along the catalyst in the streamwise direction to reach a characteristic surface temperature of 250°C. This criterion is easier to measure experimentally.

The turbine can delay cumulative enthalpy flow to the catalyst during the first 30 [s] of warm-up by up to 93%. Even with slow warm-up, the catalyst model predicts that the monolith heats first and fastest in the entry region. Heat release due to surface reactions in the entry region warms downstream sections by advection in the bulk flow.

The engine and exhaust thermal and aftertreatment models in this work could be used to test design changes when emissions regulations become more strict, or to predict hydrocarbon emissions in response to particulate matter control strategies.

5.3 Recommendations and Future Work

Research is never finished. Some ideas for future explorers of engine emissions control are listed below.

Cascading Light-Off Cold-start strategy should aim to warm the entry region of the catalyst to induce rapid heat release in the entry region of the catalyst thereby starting a cascading light-off. This objective suggests a preference for maximum exhaust gas temperature over maximum exhaust gas mass flow rate. This has implications on the use of secondary air injection for cold-start. High flow rates of secondary air could significantly increase exhaust gas mass flow rate, reduce catalyst-in emissions but negatively affect light-off through reduced catalyst-inlet exhaust gas temperature.

Modelling tools The exhaust thermal and catalyst kinetic model should be integrated into one model. At the time of writing, the solvers for each component were not compatible. Some experimental research should examine the role of exhaust gas density and pressure in catalyst chemical kinetics during cold-start conditions, and

146

how to incorporate oxygenates (from unburned and partially burned ethanol) into cold-start catalyst modelling.

Larger waste-gate bypass Design changes to turbocharger waste-gates. Heat transfer (losses) from the exhaust gas to the turbine could be reduced with a waste-gate or bypass design that permitted more exhaust gas to shortcut from the manifold to the catalyst inlet.

Secondary air Although it requires extra equipment, secondary air injection could enhance post-flame oxidation and the mass flow-rate of gas in the exhaust. A related idea is to apply individual cylinder equivalence ratios. That is, run two cylinders rich and two cylinders lean. They could mix and effect significant heat release in the exhaust. A related idea is to vary the equivalence ratio cycle-by-cycle, alternating between rich and lean to send "slugs" of mixture for downstream mixing and reaction.

Other emissions DISI engines also emit large quantities of particulate matter (PM). Hydrocarbon control strategies should be harmonized with PM control strategies. NO_x, oxides of nitrogen, normally form only at very high temperatures and load. Some of the strategies discussed this thesis may produce significant NO_x emissions. Future work in this area should monitor NO_x.

Sum of deltas This work surveyed a broad array of engine control strategies, but tested and analyzed only a small subset of all possible engine parameter combinations and permutations. Configurations that are a superposition of strategies may provide further benefits. Two configurations of interest:

1. Moderately late ignition timing (+10 [CAD ATDC]), 70/30 split injection (for stability), late EVO (for longer time for post-flame oxidation), very high exhaust back pressure (~ 2.0 [bar]) and 15% excess air ($\lambda = 1.15$).

2. Moderately early ignition timing (+5 [CAD ATDC]), 70/30 split injection (for stability), early EVO (to reduce expansion for low conversion efficiency and high

147

exhaust gas temperature), very high exhaust back pressure ($\sim$ 2.0 [bar]) and 15% excess air ($\lambda = 1.15$).

Appendices

This page intentionally left blank

APPENDIX A

EXPERIMENTAL SETUP AND PROTOCOL

This appendix contains provides detail on the experimental engine setup, experimental protocol, specifications of the standard cold-start operating point, data collection frequency and experimental shutdown procedure used in this research. The purpose of this section is to offer detail about the testing conditions for later researchers to duplicate or put the present results in context.

A.1 Experimental Setup

This section describes the engine and auxiliary equipment used to conduct experiments for this research. The first portion describes the base engine and its subsystems. The second portion describes instrumentation and data acquisition systems. The final portion describes the basic experimental protocol and engine preparation during research.

A.1.1 Engine setup

This section describes the basic engine test apparatus beginning with features of the base engine.

Base engine

The experimental setup was designed and built for the purposes of cold-start emissions experiment. It consists of a 2009 model year GM LNF Ecotec engine. The LNF is a 2.0L inline 4-cylinder, turbocharged, direct injection gasoline spark ignition engine. This engine and its successors are available in a number of vehicles under a few nameplates. Table A.1 provides engine layout and geometry information of the engine used in this research.

Engine modifications

A cylinder pressure transducer mounting port with flame arrestor was added to each cylinder of the engine cylinder head. The intake manifold was modified to incorporate

Table A.1: LNF engine layout and geometry information

Engine type	In-line 4 cylinder
Displacement [cc]	1998
Bore [mm]	86
Stroke [mm]	86
Wrist pin offset [mm]	0.8
Connecting rod [mm]	145.5
Compression ratio	9.2:1
Fuel system	Side-mounted gasoline direct injection
Valve configuration	16 valve DOHC, dual cam phaser 35.1 mm intake valve diameter 30.1 mm exhaust valve diameter
Max. torque	350 N·m at 2000 rpm
Max. power	260 kW at 5300 rpm

a port fuel injection (PFI) system and taps for measuring temperature and pressure in the intake runner of cylinder #4, the cylinder closest to the flywheel, farthest from the serpentine belt pulley. The exhaust manifold was modified to incorporate ports for sample, temperature and pressure measurement. Due to concerns around melting or prematurely ageing/sintering catalyst bricks during prolonged tests, a hollow catalytic converter housing was constructed and a gate valve was used to impose a comparable pressure restriction on exhaust gas flow. The ring gear from the original engine flywheel was transplanted to a larger flywheel. The new flywheel had a higher polar moment of inertia to damp RPM fluctuations during operation with high cycle-to-cycle torque variability. Reduced RPM fluctuations made dyno speed control easier and prolonged the life of the compliant rubber element in the driveshaft connecting the engine to the dynamometer.

Active valvetrain

The production engine incorporates variable valve timing (VVT) by means of hydraulic camshaft phasing units, one each on the intake and exhaust camshafts. An electrohydraulic valve regulates oil pressure within the hydraulic phaser. Differential oil pressure across the vanes in the phaser to advance or retard. This type of

camshaft phaser changes the timing of valve events relative to the crankshaft but does not change the lift or duration of the valve event. In other words, these phasers give control over *when* the valves open, but not the length of time for which they are open. This engine has an advancing intake cam phaser, and a retarding exhaust cam phaser. When the system is not energized the intake camshaft and intake valve timing return return to a fully retarded default timing, while the exhaust camshaft and exhaust valve timing return to a fully advanced default timing. Intake and exhaust cam phasing are continuously variable with a range of approximately 50 CAD. Figure A-1 and Figure A.1.1 show valve lift curves superimposed on a cylinder pressure (one cycle) trace with camshaft phasers in the default and full travel positions respectively. During a true cold-start, it is possible that the cam phasers and pro-
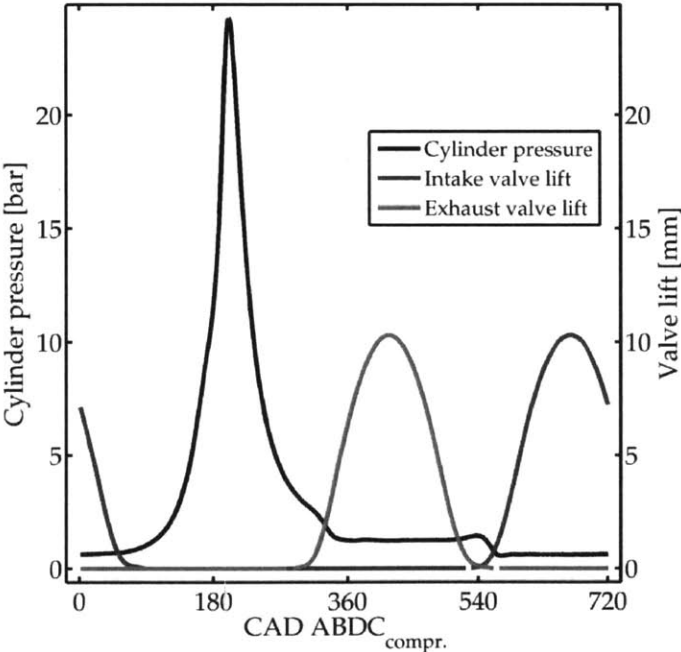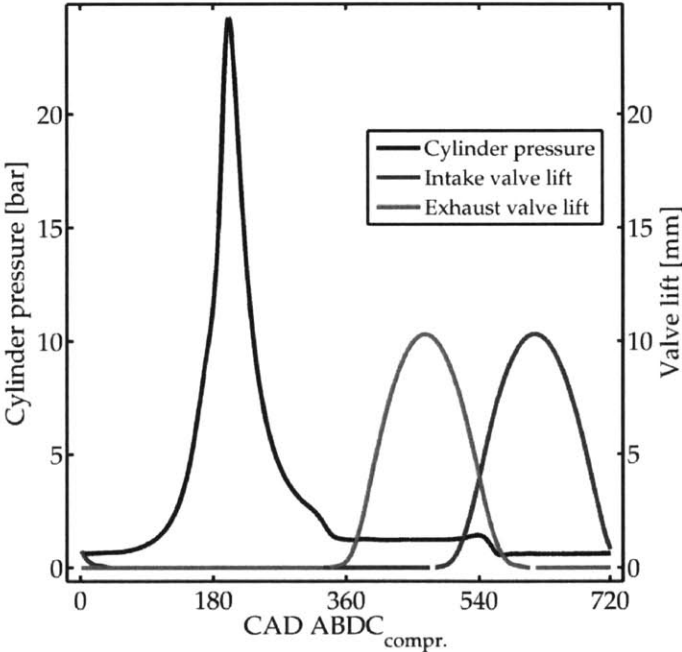
Figure A-1: Default   Figure A-2: Full travel

duction controller may not be fully reliable and responsive until well into cold-start operation due to oil flow, pressure and viscosity limitations at low engine speed. For the purposes of this work, that limitation was ignored and cam phasers were used as if they would be instantly operational on a production engine. Table A.2 summarizes the park and maximum phaser valve timing.

154

Table A.2: Basic valve timing and lift (cam phasers inactive)

		Opens	Max opening	Closes
Intake valve	Base timing	$+11°\text{ATDC}_{compr.}$	$+126°\text{ATDC}_{gas.ex.}$	$+61°\text{ABDC}_{compr.}$
	Max advance	$-39°\text{ATDC}_{compr.}$	$+76°\text{ATDC}_{gas.ex.}$	$+11°\text{ABDC}_{compr.}$
	Lift [mm]	0.25	10.3	0.25
Exhaust valve	Base timing	$+52°\text{BBDC}_{exp.}$	$-125°\text{ATDC}_{gas.ex.}$	$-10°\text{ATDC}_{compr.}$
	Max retard	$+2°\text{BBDC}_{exp.}$	$-75°\text{ATDC}_{gas.ex.}$	$+40°\text{ATDC}_{compr.}$
	Lift [mm]	0.25	10.3	0.25

The custom PC engine controller measured cam position using the OEM cam position sensors and crankshaft encoder to a resolution of 1 CAD. The feedback control on cam phasing is executed once per engine cycle. The control is accurate to within +/- 1 CAD. If a desired cam position is outside of the 50 CAD range of the valve phaser, the base position can be adjusted mechanically within the engine to allow the desired position to be reached. However, the cam profiles and valve timing are set to maximize engine performance and optimize emissions control over a broad operational window not just cold-start emissions management.

Intake and exhaust systems

The intake system was fitted with a mass flow meter (EPI Flow MPNH 8716) and an air-water intercooler acting as a condensation dehumidifier. The working fluid of the liquid side of the intercooler was a mixture of ethylene glycol and water cooled to 0°C such that the air exited at a known humidity. The production engine has an air-to-water (i.e. air to engine coolant) intercooler between the turbocharger compressor outlet and the throttle body. This intercooler was removed since it would be largely inactive during simulated cold-start.

The electronic throttle body was controlled by a custom microcontroller host H-bridge PWM controller to maintain user requested throttle plate angle, intake manifold pressure (MAP) or NIMEP. The latter two modes were used infrequently because cycle-to-cycle variations in combustion phasing and gas dynamics resulted in
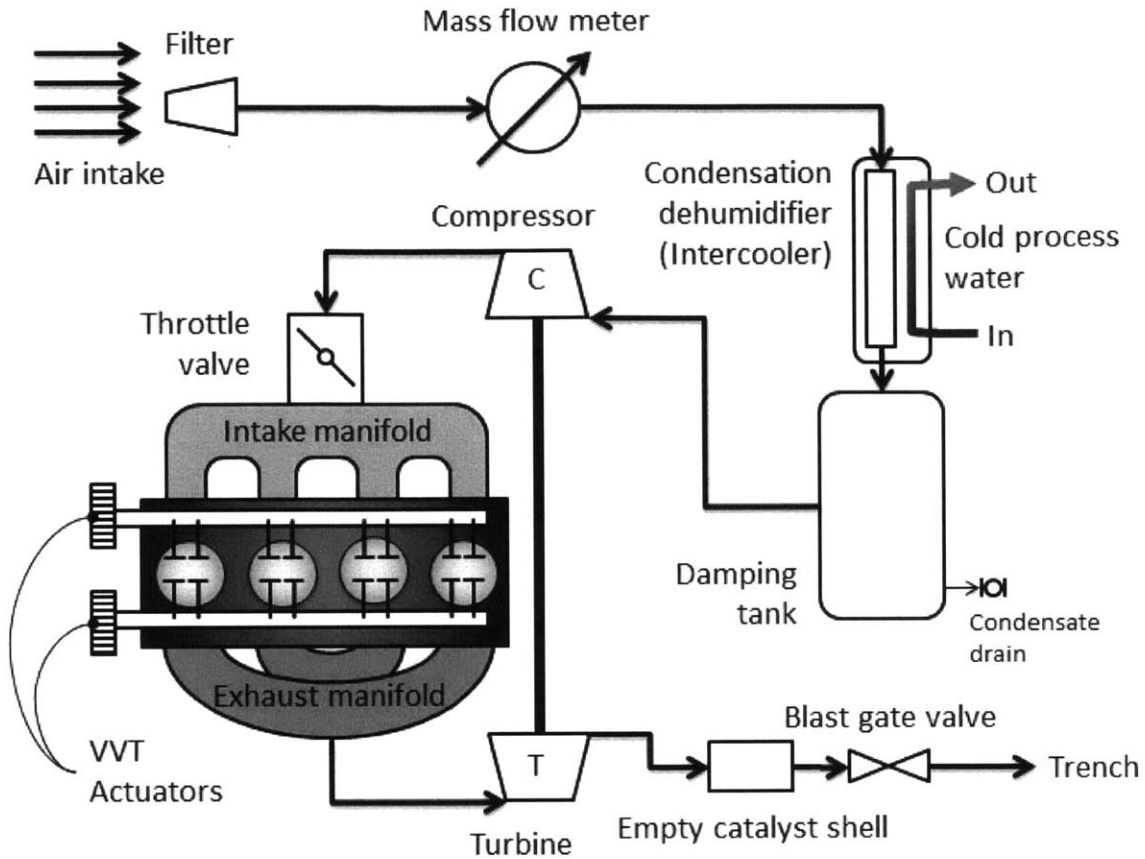
Figure A-3: Intake and exhaust system schematic

excessive hunting.

Figure A-3 shows a schematic of the engine intake and exhaust system.

Fuel system

The working pressure of the direct injection fuel system is 3-15 MPa [435-2176 psig]. The engine is equipped with one production issue multi-hole solenoid-controlled injector per cylinder. The production engine is equipped with cam-driven precision tri-lobe pump. Other researchers have shown that obtaining stable outlet fuel pressure from such pumps under unstable operation RPM such as cold-start is challenging.[6]. That pump was removed from the engine to simplify fuel purge procedures and reduce control requirements. An alternate design using high pressure N_2 gas in a hydraulic accumulator to pressurize fuel was used instead. Comparable systems are already
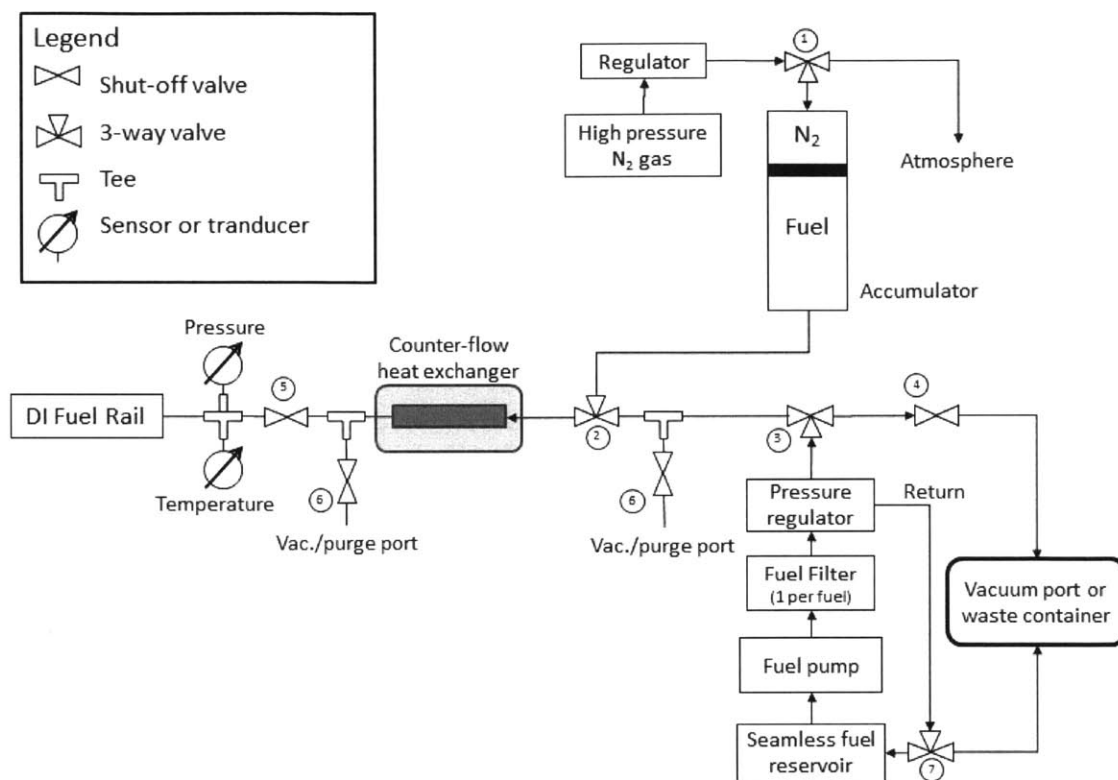
Figure A-4: Fuel system schematic

operating reliably on other engines in the Sloan Automotive Laboratory at MIT. The fuel pump port on the cylinder head was covered to prevent leaks of oil present at fuel pump drive lobe on the camshaft.

The high pressure cylinder is replenished by, and PFI fuel rail is supplied by a low-pressure fuel system comprising a pump, filter and various purge ports. All components were selected from aftermarket automotive part retailers for compatibility with ethanol. Separate filter elements were used for each fuel to minimize sources of cross-contamination between fuels. Figure A-4 shows a schematic view of the fuel systems. Fuel is cooled by a one-pass counter-flow heat exchanger before it reaches the engine.

The engine control computer sends fuel injector pulses to a Siemens injector driver. The Siemens injector driver converts the injector control pulse to a high peak current, low-hold current injection pulse necessary to actuate the injector. A high initial
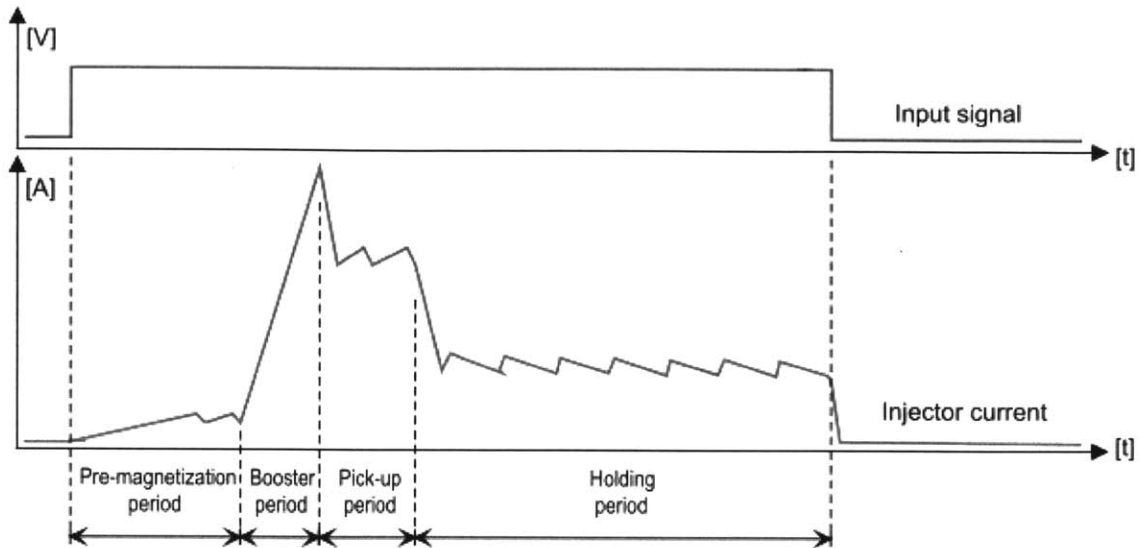
Figure A-5: DI peak and hold injector current profile

current is necessary for fast injector opening. Once the injector begins to open, the current decreases to a level necessary to hold it open. A schematic representation of the peak and hold current profile is shown in Figure A-5.

Industry sponsors supplied the current-time profile data necessary to achieve repeatable injection. These values are applicable only to this injector and injector driver combination at the request of the manufacturer who graciously provided the data are confidential. At very short injector pulse widths the injection period is dominated by the opening and closing transient. Due to the dynamics of the injector opening and closing processes short pulse widths produce higher variability in the mass of fuel injected per pulse. For this engine, injector and injector driver system the minimum pulse width that still injects a repeatable quantity of fuel is approximately 300-500μs. For shorter pulses than this, the injector is in the "ballistic range" where the injector needle is in constant motion during the injection. This does inject fuel but the quantity is less controlled and may contribute to cycle-to-cycle variability in mixture strength and combustion. Such variability is highly engine-specific and generally detrimental to cold-start engine behaviour.

Mechanical setup

The engine was coupled to a Froude Consine AG80 eddy current absorbing dynamometer by a driveshaft with compliant rubber coupling to damp torque engine-out fluctuations. The production starter motor and an external electric motor crank-start and motor the engine when it is not firing. Although the load cell on the dynamometer was capable of measuring the brake torque output of the engine, the measurement was not used.

Heating, cooling and oil

Two separate fluid temperature control systems were installed on the engine to permit operating temperatures of fuel, oil and engine coolant systems in a range between -20°C to 105 °C.

Low temperature operation Three chillers were utilized for low temperature operation. One for fuel, one for intake air (condensation dehumidification) and one for coolant and oil. The coolant and oil shared a chiller because the production engine has an internal oil cooler integrated to the oil and coolant circuits.

All experiments were performed with the engine inlet coolant at 20°C (+/- 2°C) unless otherwise noted. The engine inlet coolant temperature is subject to closed-loop control by the Icewagon DE2WC refrigeration system.

High temperature operation Fuel and intake air were not cooled during high temperature operation. For operation with heated coolant, an OMEGA CN-7823 PID controller governs an immersion heater in the coolant reservoir and a normally closed solenoid valve controlling city water supply to a counterflow heat exchanger. Engine coolant from the heated reservoir is pumped continuously through the engine whose production coolant thermostat was removed.

Control

The engine is controlled using 2 desktop computers executing code developed at MIT. The user controls a master computer and inputs engine operating parameters such as fuel injection timing, fuel injection pulse width(s), spark timing, spark dwell, intake cam timing and exhaust cam timing. The master computer controls a slave computer on which the engine control code is executed in an infinite loop. The slave computer has analog-to-digital and digital-to-analog capabilities to read sensors and issue control commands. The slave computer control code executes a schedule of engine events. The schedule is executed according to the engine crankshaft encoder position. The slave computer engine control schedule permits multiple fuel injections and accepts separate input for timing and duration of each of up to 3 injections per cycle. The default program issues identical fuel injection commands to each cylinder though in principle cylinder-specific trim could be integrated. All inputs can be changed in real time as desired. Separate hardware cut-off switches can interrupt fuel and spark signals before they reach the engine for safety purposes. A master kill-switch can terminate the operating loop.

A.1.2 Instrumentation and data acquisition

National Instruments hardware and LabView software is used to acquire data from the experimental data onto a desktop PC. Table A.3 summarizes the sensors and measurements recorded by LabView. Subsequent subsections describe the configuration and installation location of each sensor. Details of data collection frequency are available in Appendix A. Figure A-6 presents the location and type of signals monitored schematically.

Pressure

Intake   Intake pressure is measured approximately 5 cm upstream of the intake port.

Crankshaft position	BEI encoder, 360 °per rev.
Cylinder pressure	Kistler 6125A sensor, Kistler 5010b charge amplifier
Intake pressure (MAP)	Honeywell SA-001-BAC1DE sensor
Exhaust pressure	OMEGA PX209-030A5V sensor
Fuel pressure	OMEGA PX309-3KG5V pressure transducer
Air-fuel ratio	ETAS LA-4 Lambda Meter
Intake cam timing	OEM intake cam sensor
Exhaust cam timing	OEM intake cam sensor
Temperature	K-type thermocouples
Exhaust HC	Cambustion HFR-400 Fast FID
Exhaust composotion	Horiba MEXA-554JU and Horiba MEXA-584L

Table A.3: DAQ sensor details

Exhaust Exhaust pressure is measured approximately 8 cm downstream of the exhaust port.

Cylinder pressure In-cylinder pressure is measured with a Kistler 6125A pressure transducer mounted in the cylinder head with a flame arrester to minimize thermal shock. This model of piezoelectric pressure transducer is commonly used for engine research. Like many pressure transducers, this model of sensor and charge amplifier have an offset drift, therefore the sensor must be pegged to another sensor to obtain the absolute value of the cylinder pressure. In some cases the absolute pressure is not important, for instance the absolute pressure is not important for determining NIMEP since it is a contour integral over a cycle.

Pegging is done digitally on the data acquisition computer. The pegging routine is to equate cylinder pressure and intake manifold pressure when the piston is near BDC of the intake stroke. At BDC intake, the piston is not moving and it is sufficiently late in the intake stroke for pressure equilibration across the intake valve. A 10-point average of intake manifold pressure and cylinder pressure, centered around BDC, was used to reduce the susceptibility of this pegging routine to noise. The exhaust manifold pressure sensor agreed well with the cylinder pressure transducer near TDC of the exhaust stroke the cylinder pressure has equilibrated with the exhaust manifold, which indicates the pegging routine was successful.
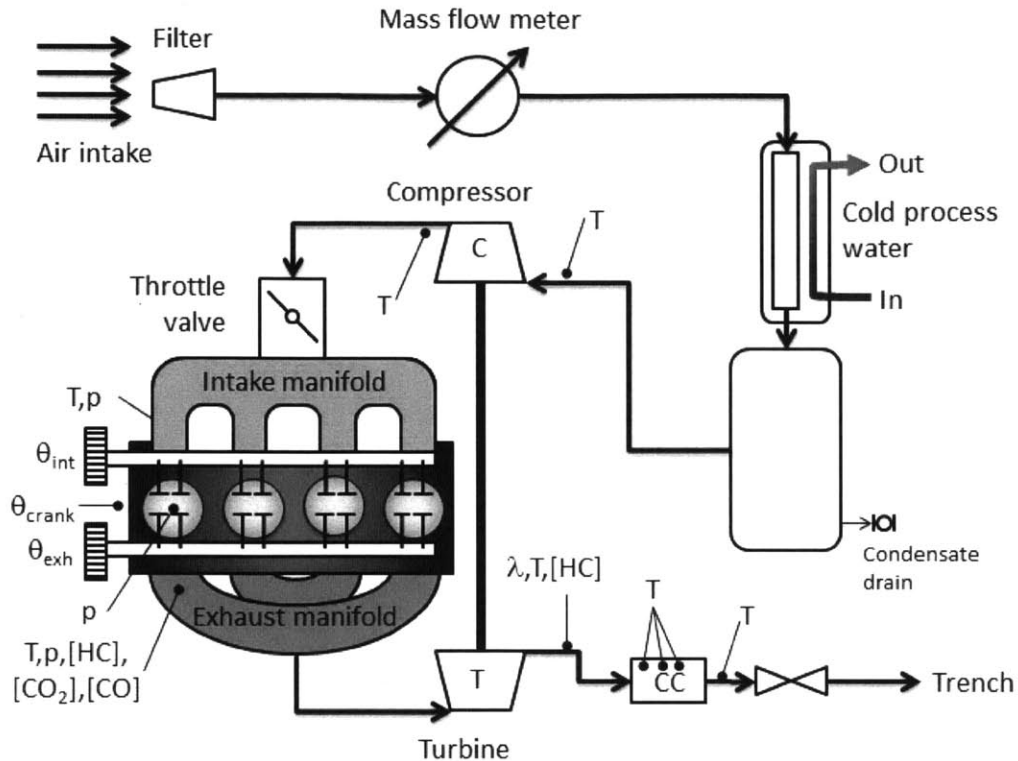
Figure A-6: This schematic shows the location and type of most sensors used in the experiment.

Fuel   Fuel pressure is measured approximately 15cm upstream of the fuel rail with an OMEGA PX309-3KG5V pressure transducer.

Flow

Air   Air flow rate is measured by a EPI Flow thermal air flow meter model number 8716-MPNH-SSS-133-AC115-AIR. It is installed in a straight, smooth length of hose between the filter and condensation dehumidifier to ensure measurements free of fluctuation.

A second, indirect measure of air flow can be calculated from fuel flow rate and air-fuel equivalence ratio (λ) is available but not used due to uncertainty regarding the quantity of fuel that ends up in the oil reservoir.

Fuel   Fuel flow is not measured directly. Fuel flow is calculated from engine cycle frequency and fuel-per-injection. Fuel-per-injection is based on an "end-to-end"

bench test correlation of fuel injector pulse width (issued by the slave computer) and fuel mass actually injected. The bench test correlation was conducted at numerous injection pressures and pulse widths. The injectors provide linear response between fuel mass and injector pulse width in the range of 0.5 ms to 3.0 ms. Below 0.5 ms there is some deviation from linear response but it is repeatable non-linearity down to approximately 0.25 ms. Above 3.0 ms was not tested since it is well beyond the cold-start fuel requirement. Fuel mass increases as square root of injection pressure so fuel mass is calculated from injector pulse width as follows:

$$m_{fuel,0} = a_0 + a_1 t + a_2 t^2 + ...$$

Where t is injector pulse width and a_i come from correlation at p_{ref}, then

$$m_{fuel,actual} = m_{fuel,0} \sqrt{\frac{p_{actual}}{p_{ref}}}$$

The influence of in-engine heating on injector behaviour, an effect which is absent in the benchtop correlation, is expected to be minimal. The effect of transient heating of fuel between injections is not expected to appreciably change the fuel flow rate. Several trials during the bench top pulse width correlation were used to assess the accuracy of the calibration method. Sources of uncertainty such as evaporation of fuel (and subsequent loss from the collection vessel), condensation of water from the ice bath were quantified and found to be less than 1% for the test protocol used.

The influence of in-cylinder pressure on the overall pressure differential across the injector is usually small except for operation with low fuel pressure (e.g. 30 bar) and injections late in the compression stroke. In those cases, the cylinder pressure near TDC may approach 5-8 bar, or 16-25% of the absolute fuel pressure. The impact of this error is small because the amount of fuel delivered near TDC is usually 30-40% of total fuel and a correction for cylinder pressure is applied to the fuel pressure correction.

Fuel pulse width correlations for different gasoline test fuels did not differ within the uncertainty of the correlation. A density correction for other fuels is used.

163

Exhaust composition

Hydrocarbons Exhaust gas hydrocarbon content is measured by a Cambustion HFR-400 fast-response flame ionization detector (FID) with a 10-90% response time of approximately 1 millisecond. The engine had two sample ports. One sample point is in the exhaust manifold runner of cylinder # 4, (nearest to the engine flywheel) approximately 8 cm downstream from the exhaust valve seat. The second sample point is 2.5 cm downstream from the turbine exit. Samples were drawn from the exhaust to the sample head through a heated transfer sample lines (TSL-H) with hole diameter of 0.026 inches. The TSL-H had a transient time of approximately 3 milliseconds. The fast-response FID instrument operating parameters were constant for all experiments. TSL-H temperature: 180°C, sampling head temperature (HSM): 350-375°C, CP VAC: 350 mmHg, ΔP FID: 100 mmHg. The instrument was calibrated before and after each experiment using two span gases with nominal propane (C_3H_8) concentrations of 1500 ppm_{C3} (4500 ppm_{C1}) and 2500 ppm_{C3} (7500 ppm_{C1}) balance nitrogen. The instrument was zeroed with nitrogen (N_2) gas. Any non-linear calibrations or span drift greater than 5% between the pre- and post-experiment calibration triggered FID data to be discarded.

FID Theory of operation This instrument uses a hydrogen flame to ionize hydrocarbon molecules from unburned or partially burned combustion products in the exhaust stream. The sample head contains an electrode at a considerable potential difference to the housing. This electrode attracts the ionized hydrocarbon fragments. The current resulting from ion impact with the electrode is proportional to the original concentration of carbon atoms in the exhaust. The current is measured by the FID base unit and converted to a voltage that is read by the data acquisition system.[62–64]

The FID has different sensitivity for different classes of hydrocarbons such as alkanes (paraffins), alkenes (olefins), aromatics and oxygenates. The sensitivity is related to the different ionization probability of each class of hydrocarbons in the hydrogen flame in the FID. An adjustment to the FID measurement is possible if the

164

exhaust gas composition, or species distribution is known.[65, 66]

The combustion of gasoline comprising only hydrocarbons produces exhaust gas species with nearly identical sensitivity. Following calibration with a suitable gas of the same sensitivity (e.g. propane) no correction is necessary.

However, fuels with significant oxygenate content produce exhaust gas with significant quantities of formaldehyde and acetaldehyde. The FID sensitivity to these oxygenates differs by approximately 25%. Kar and Cheng found that, over a variety of speeds and loads, FID readings of exhaust gases from engine operation with gasoline ethanol fuel blends could be corrected to beter than 90% accuracy if the ethanol volume fraction in the original fuel was known.[65, 66]

CO, CO_2 Other exhaust products including CO and CO_2 were measured by Non-Dispersive Infrared (NDIR) using a Horiba MEXA-554JU and Horiba MEXA-584L. The exhaust gas was dried with a condenser in ice-water and a calcium sulfate lab dessicant column to obtain measurements on a dry basis. Fuel equivalence ratio and stoichiometry are used to predict wet-basis measurements.

Equivalence ratio Air-fuel ratio or equivalence ratio is measured using an ETAS LA-4 wideband UEGO oxygen sensor. It is installed in a port approximately 10 cm downstream from the turbocharger turbine outlet flange in a configuration comparable to the production vehicle. In this installation it measures the engine-average equivalence ratio.

Temperature

Intake, exhaust, coolant and ambient temperature data is measured by Omega Inconel and Stainless steel sheathed K-type thermocouples. For liquid measurements, shield-grounded thermocouples are used. For air and exhaust measurements, small-diameter, exposed tip junctions are used. For the exhaust gas temperature measurement in the exhaust manifold runner nearest the engine, a custom aspirating radiation shield is constructed. Caton's results suggest that this thermocouple configuration yields a

165

temperature reading closer to the mass-average temperature than the time average or instantaneous equilibrium temperature. This is widely considered a more accurate way to obtain thermal enthalpy data for exhaust gas flow. [67] For the size and type of thermocouples on this engine that do not have radiation shields, exhaust temperatures above 700°C begin to introduce errors of 50°C or more and time lag on the order of 1-5 [s]. GT-POWER engine simulations can be used to estimate true gas temperatures from thermocouple readings.

Other

Valvetrain Intake and exhaust cam positions are measured using production Hall effect inductive intake cam position sensors. The sensors are installed in the rear of the engine at the opposite end of the engine from the VVT cam phasers. The sensors generate four voltage pulses per revolution of the cam when a metal feature machined into the camshaft rotates past the sensor. Two of the voltage pulses are long, two are short. The state of the engine (e.g. which stroke a given cylinder is undergoing) can be derived by comparing the timing of the rising and falling edges of these sensors and a known baseline pulsetrain from the manufacturer. These camshaft signals were digitally processed to determine the cam phaser position and inform control action on the slave control computer.

Crankshaft position An optical encoder is installed on the engine and coupled to the crankshaft. The encoder signal is aligned with the engine cycle phasing by use of an AVL-428 capacitive piston position sensor.

A.1.3 Experimental protocol

Regular engine preparation procedures are described in detail in Appendix B. At this point, the most important feature of engine preparation is that the engine is preheated before testing. The constant speed, constant load cold-idle tests measure the eventual steady state that an engine would achieve during cold start. The thermal transients that precede that steady-state are characterized separately.

A.2 Data post-processing

Raw data collected by LabView is post-processed using custom code in MathWorks MATLAB. This code performs several functions:

- Compute mean effective pressure and indicated efficiency from intake and cylinder pressure measurements.
- Compute cycle to cycle variability statistics (e.g. COV, LNV).
- Estimate heat release rate and mass fraction burn profile from cylinder pressure measurements.

  - Compute combustion phasing and duration from burn profile.
  - Fit a Wiebe logistic function to the burn profile.

- Estimate residual gas fraction and volumetric efficiency
- Calculate thermal enthalpy flow rate
- Calculate chemical enthalpy flow rate
- Estimate unburned hydrocarbon mass flow rate from concentration and exhaust mass flow rate.

The next section describes some of the data post-processing steps in greater detail.

A.2.1 RGF Estimation

Combustion dynamics depend on mixture composition, especially residual gas fraction defined in Equation A.1.

$$x_{residual} = \frac{n_{trapped}}{n_{total}} \text{ where } n_{total} = n_{fuel} + n_{air} + n_{trapped} \tag{A.1}$$

Where $x_{residual}$ is the residual gas fraction in [mol/mol], and n_i are molar quantities of subscripted species. The amount of fuel and air in cylinder can be readily determined from measurements of injector pulse width, equivalence ratio and air flow measurements. However, $n_{trapped}$ remains unknown due to cycle to cycle variability, back-flow and initial charge temperature uncertainty.

Fast in-cylinder composition measurements are difficult and sometimes unreliable so in order to characterize the composition in the combustion chamber, namely $n_{trapped}$, the residual gas fraction is estimated based on a model of Fox et al. This empirical model explicitly accounts for the back flow of exhaust gas into the cylinder during valve overlap, which is relevant here because of the engine's variable valve timing.[68] Fox and Cheng's model correlates reasonably with GT-POWER engine simulations of this engine.

A.2.2 Combustion heat release analysis

Pressure data from the combustion chamber is the primary source of information on combustion and heat release. Numerous techniques have been developed, of which Rassweiler-Withrow is arguably the most famous and most common. It is the subject of the first part of this section.

Rassweiler-Withrow

In their landmark paper, Rassweiler and Withrow correlated optical data on engine combustion flame progress to measured cylinder pressure data using plaster molds of apparent zones of burned and unburned mixtures at different instances during combustion. The basic algorithm them decomposes changes in combustion chamber pressure as the result of either piston motion or compression due to flame propagation and chemical heat release. [69] The Rassweiler-Withrow algorithm is simple and reliable which explains why it is popular and widely used. However fails for data from very late combustion, which is typical for cold-start.

For conventional combustion timing, combustion occurs near TDC, between the end of the compression stroke and beginning of the expansion stroke. In other words, for conventional combustion timing, when combustion ends, a polytropic expansion process begins that lasts until the exhaust valve opens (EVO). A heat release analysis algorithm identifies the end of combustion by the beginning of isentropic expansion. The algorithm regresses the expansion data to obtain polytropic exponent for the

expansion process, which is used to compute the mass fraction burn profile. The data for the left PV-diagram in Figure A-7, is collected with normal combustion timing. The expansion process after combustion is linear (in log-log scale) and Rassweiler-Withrow heat release analysis would succeed. The right plot in Figure A-7, shows a PV diagram for late combustion. To summarize Figure A-7, for late combustion there
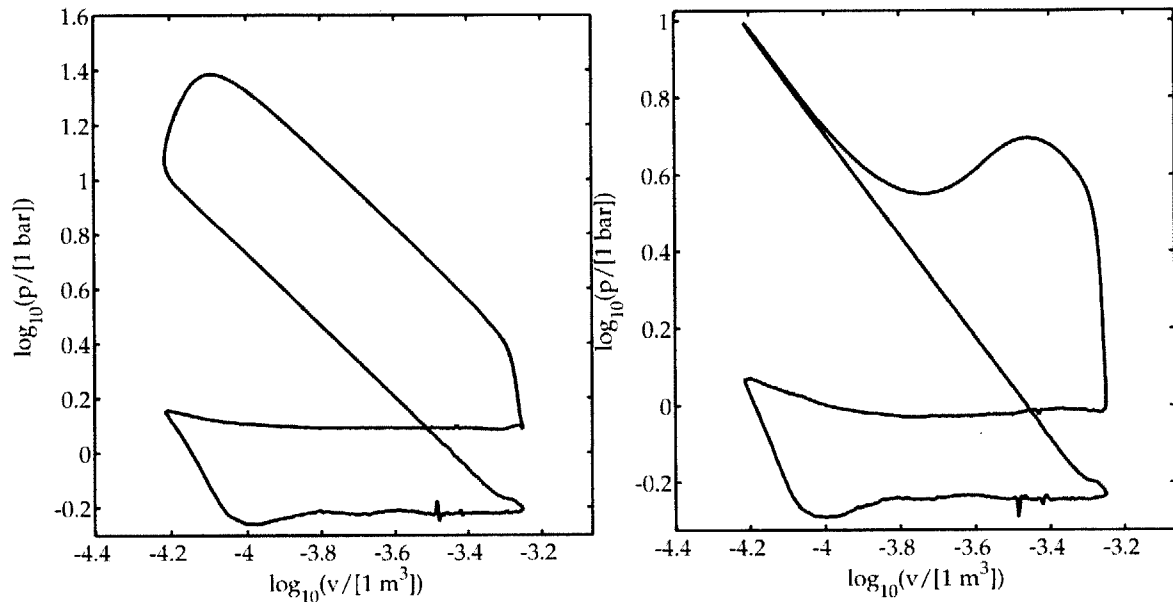
Figure A-7: For early combustion timing (left), compression and expansion processes, which are polytropic but nearly isentropic, appear linear in log-log scale (polytropic with $n \sim \gamma$). For late combustion timing (right), the nearly isentropic compression process is still present but combustion starts well into the expansion stroke. For combustion timing (right), early expansion stroke basically back tracks along compression stroke until combustion starts. Actual expansion pressure is slightly lower than compression pressure due to heat transfer and leakage losses. The combustion process is active up to and perhaps after EVO. Compared to the early ignition case (left), it is more difficult to say if combustion ends before blowdown, which begins at EVO.

is little or maybe no isentropic expansion after combustion. Lacking a definitive end-of-combustion point, conventional Rassweiler-Withrow heat release analysis fails. A new heat release analysis method based on the First Law of thermodynamics handles these cases, which is described in the second part of this section.

First Law method

The model is based on the First Law of thermodynamics with some assumptions. The objective was a tool to provide a CA50 surrogate to compare combustion response to engine operating parameters. For example, high residual gas fraction causes combustion phasing (e.g. CA50) to be retarded. For a control volume of the combustion chamber, the first law equation is:

$$\frac{dU}{dt} = \frac{dQ_{hr}}{dt} - \frac{dQ_{conv}}{dt} - \dot{W} + \sum_i \dot{m}_i h_i \tag{A.2}$$

Where U is the internal energy of the gas, Q_{hr} is chemical heat release due to combustion, Q_{conv} is convective heat transfer from the gas to the combustion chamber walls, $\dot{W}$ is the work transfer from the combustion chamber gas to the piston, m_i is the mass of gas in the combustion chamber and h_i is the enthalpy of combustion chamber gas. For an ideal gas with constant properties, $U = m \cdot c_v \cdot T = \frac{PV}{\gamma-1}$, and for a piston-cylinder system $\dot{W} = p\frac{dV}{dt}$, where γ is the specific heat ratio of the gas, p is the pressure of gas in the combustion chamber, V is the volume of the combustion chamber. These simplifications and a substitution of engine crank angle (CA, or θ) for time yield the following expression for net heat release $Q_{net} = Q_{hr} - Q_{conv}$:

$$\frac{dQ_{net}}{d\theta} = \frac{\gamma}{\gamma-1} p\frac{dV}{d\theta} + \frac{1}{\gamma-1} V\frac{dp}{d\theta} \tag{A.3}$$

The model:

- Assumes ideal gas law, which is an excellent assumption for all temperatures and pressures in the engine.

- Assumes control mass, which is an excellent assumption between IVC and EVO.

- Assumes constant gas properties (constant c_v, γ, etc.) - Properties during combustion are not constant. The changes in temperature and composition during combustion are substantial. However, since the mixture has an air to fuel mixture of approximately 14.6:1 on a mass basis, and air is mostly nitrogen, it is a reasonable assumption. Meaningful correction, such as adding variable

170

properties and iterating would be computationally intense.

- Neglects crevice and blow-by effects
- Predicts net heat transfer, offering no information on chemical heat release individually.

. Even with these assumptions, the model performs well. Total energy release is usually around 80% of the input fuel energy based on lower heating value. The remaining ~20% of fuel input energy may be accounted in four ways:

1. Fuel lost to the oil sump via wall films, or

2. Energy lost due to blowby gases, or

3. Energy accounting in this method is wrong due to constant properties assumption, or

4. Combustion inefficiency due to partially oxidized or unburned fuel.

Despite this energy loss, the model performs its intended function to give a reasonable measure of combustion phasing for even very late combustion. Figure A-8 compares heat release predictions for conventional Rassweiler-Withrow heat release analysis and the First Law method described here. Therefore the First Law combustion heat release analysis provides a reasonable proxy for conventional measure of combustion phasing and burn duration. The First Law method provides an additional useful empirical finding that CA50 is strongly correlated with the timing of maximum heat release rate (CA of maximum $\dot{Q}_{net}$). Figure A-9 shows that this correlation is quite reasonable for a wide array of engine operating conditions including late ignition, rich air-fuel ratio ($\Phi \geq 1$), lean air-fuel ratio ($\Phi \leq 1$), and high residual gas fraction. This was unexpected because visual inspection and numerical analysis of conventional fuel mass burn curves show that the early stages of combustion (e.g. 0-10% fuel mass burned) is slow for the low-temperature, low-load, late conditions of cold-start. This empirical finding is useful because the timing of maximum rate of heat release can be used to estimate combustion phasing (i.e. CA50) even in very late combustion cases cases where combustion continues during and after EVO. EVO invalidates the control mass assumption, and changes to cylinder pressure during the exhaust process

171
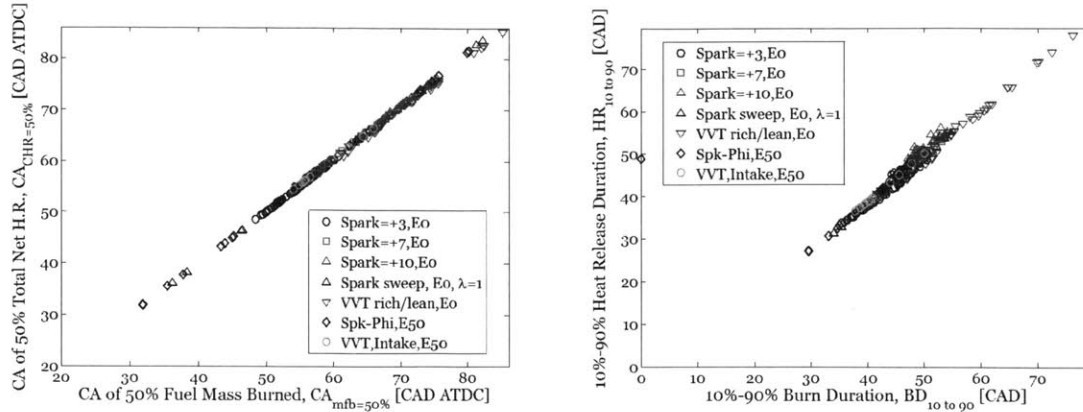
Figure A-8: This plot contains data for operating points where combustion is early enough that both conventional Rassweiler-Withrow and First Law-based analyses are available. The right plots shows data for the 50% fuel mass fraction burn angle (CA50) from conventional Rassweiler-Withrow combustion heat release analysis (horizontal axis) agree well with CA50 data from this First Law method (vertical axis). The left plot shows data for the 10% to 90% fuel mass fraction burn duration (BD_{10-90}) from conventional Rassweiler-Withrow combustion heat release analysis (horizontal axis) agree with data from the First Law method (vertical axis) as well.

preclude calculation of a complete burn curve. Even for extremely late combustion, a full burn curve can be extrapolated from the early heat release data and CA50 estimate from maximum heat release rate.

A.3 Engine test preparation

This section describes the typical preparation procedure for setting up an engine test.

1. Activate the engine exhaust trench evacuation fan and plant cooling water supply pumps.

2. Activate test cell electrical supply.

3. Verify operation of test cell hazardous gas monitor with permanent marker.

4. Open plant cooling water manifold for test stand.

5. Activate engine coolant and oil chiller, set to desired temperature and begin cold-soak. Or activate the engine coolant heater and coolant pump.

6. Check engine oil for proper level and visual and olfactory evidence of dilution or contamination.
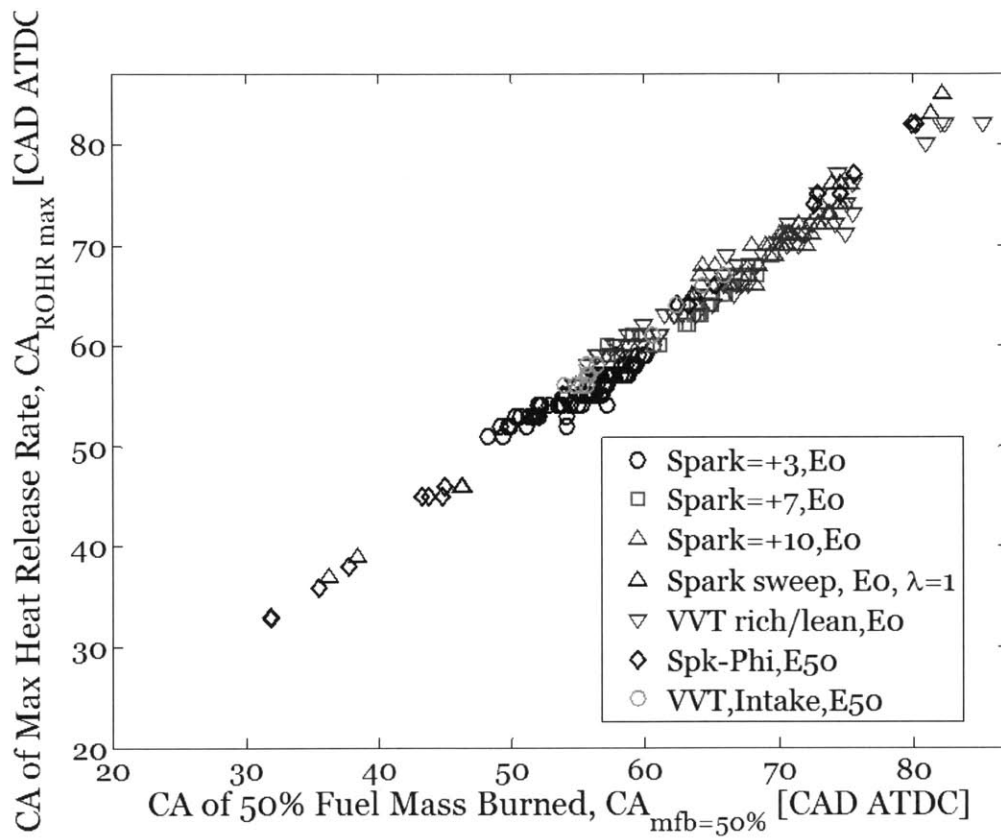
Figure A-9: This plot contains data for operating points where combustion is early enough that both conventional Rassweiler-Withrow and First Law-based analyses are available. The crank angle timing of maximum heat release rate (vertical axis) correlates well with CA50 from Rassweiler-Withrow (shown) and from First Law combustion heat release analysis methods.
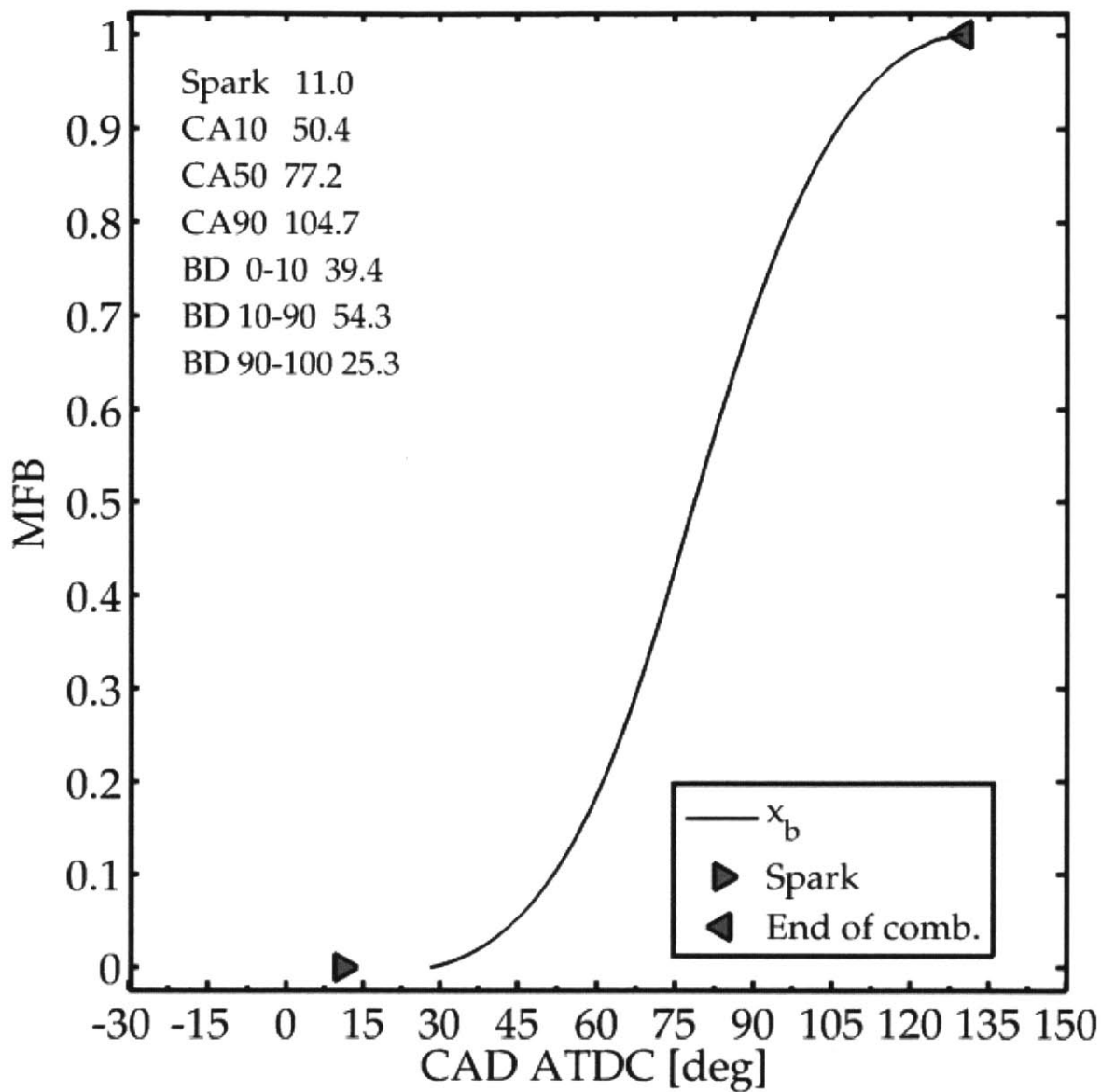
Figure A-10: This fuel mass fraction burn curve is based on a Rassweiler-Withrow combustion heat release analysis. A duration of 39.4 [CAD] elapses from ignition (spark) at +11 [CAD ATDC] until the first 10% fuel mass fraction has burned (approximately 50 [CAD ATDC]), the middle 80% of fuel mass (10% to 90%) takes 54.3 [CAD] to burn, and the final 10% of fuel takes 25.3 [CAD] to burn. The conclusion is that the early stage of combustion is slow.

7. Turn on master power switch.

8. Turn on engine instruments and battery charger.

9. Power on the data acquisition system.

10. Verify appropriate zero readings, no noise or drift.

11. Power on the emissions measurement equipment and line heaters and calibrate according to the manufacturer's instructions. For the FID, allow at least 45 minutes pre-heat.

12. Re-fill the fuel system. Evacuate and purge with N2 between fuels if necessary. Update the fuel H/C, O/C and fuel H_2O content settings for emissions measurement devices.

13. Pressurize the fuel supply cylinder with N2. Verify fuel system pressure.

14. Record ambient temperature and humidity.

15. Take pre-test emissions system calibration readings.

16. Set fuel injection switch to disable.

17. Set ignition switch to enable.

18. Program the DI injector driver with appropriate current profile for given fuel pressure.

19. Set the pressure transducer charge amplifier to 'operate' mode.

20. Turn on the dynamometer controller. Set RPM control, manual set point of 1200 [rpm].

21. Set the motor controller target speed to 1180 [rpm] (i.e. lower than dynamometer set point above)

22. Set throttle to wide-open.

23. Briefly crank the engine starter motor to confirm the engine is free to rotate.

24. Enable the electric engine drive motor.

25. Crank the engine's starter motor using key. Release engine starter above 250 rpm.

26. Allow the engine to stabilize at 1180 [rpm].

27. Engage the dynamometer clutch and let speed stabilize at 1180 [rpm].

28. Verify the WOT motoring pressure signal is correct and free of noise.

29. Start the master computer control code for moderate load.

30. Start the slave computer control program and check for operation by varying valve timing.

31. Switch the emissions routing valves from air/vent to sample engine exhaust.

32. Set fuel injection switch to enable.

A.4   Experiment Protocol

This section describes the experimental protocol.

After the engine is prepared and emissions systems are calibrated, the engine exhaust is pre-heated by running for 10-15 minutes with GIMEP equal to 3.0 [bar] and ignition timing of 10 [CAD ATDC]. This test point is a baseline. The fuel mass, manifold pressure, equivalence ratio and cycle-to-cycle variability of this test point are compared between days to ensure the engine is operating repeatably. The most common cause for drift from this baseline is contamination of spark plug or injector with fuel deposits. The countermeasure for these sources of drift is described in the next section.

The engine is then stopped to install the FID sample probes. Then the engine is restarted at the nominal engine set point for cold-idle is an engine speed of 1200 [rpm], NIMEP equal to 2.0 [bar].

After every hour of operation the engine is shut down to perform a calibration of the FID to measure drift, sensitivity and ensure the sample lines have not clogged with particulate matter. During this period the other emissions equipment are re-calibrated, then left to breathe ambient air.

During the experiment proper, the parameter of interest is varied, while MAP, fuel and ignition timing are used to compensate and keep the engine at the cold-idle operating point, which is described in the next section.

A.5   Cold-idle operating point specification

This section describes the reference cold-idle engine operating point. It is based on recommendations and consensus from industrial research sponsors for a representative cold-idle point.

Table A.4: Cold-idle operating point specification

Engine parameter	Value	Units
Engine Speed	1200	rpm
NIMEP	2	bar
Spark	Varied	CAD ATDC$_{compr.}$
Fuel/Air Equiv. Ratio (Φ)	1	
Dilution External EGR	0	%
Coolant/Oil Temperature	20	°C
Fuel Inj. Timing	Production intent	CAD ATDC$_{gasex.}$
Fuel Inj. Pressure	5.0	MPa
Ambient pressure	100	kPa
Intake Air Temperature	20	°C
Intake Air Vapor Pressure	1	kPa
Exhaust Back Pressure	0.5	kPa

When triggered by the user, the data acquisition system records the experimental data according to the parameters in the next section.

A.6   Data collection frequency

Table A.5 describes the standard type, frequency and amount of data collection. After engine data collection has concluded, the test setup is deactivated according to procedure in the following section.

A.7   Shutdown procedure

1. Set fuel injection switch to disable.

2. Set the throttle to WOT.

3. Disable the drive motor.

Table A.5: Typical data collection quantity and frequency

Signal	Collection Frequency	Amount collected
Cylinder pressure, intake manifold pressure, exhaust manifold pressure, FFID (2 ch.)	1/[CA]	100 consecutive cycles
Ignition, start of injection, camshaft position	1/[CA]	10 consecutive cycles
Engine speed, equivalence ratio, NDIR emissions, air flow meter, oil pressure, fuel pressure	1/[cycle]	5 consecutive cycles
Temperatures (13 ch.)	1/[cycle]	5 cycles
Injector pulse width	100 [kHz]	3.0 [s]
Transient temperatures	1 [Hz]	User set

4. Disable the dynamometer clutch.

5. Turn off the dynamometer controller.

6. Disable the engine starter motor and remove the key.

7. Slowly vent the fuel system N2 pressure.

8. Remove the FID sample probes. Record post-test calibration then sample ambient air for 30 minutes. Verify zero reading.

9. Switch the emissions to sample engine ambient air for 30 minutes. Verify zero reading.

10. Turn off other engine systems in reverse order of activation.

The preceding parts of this chapter cover normal engine experiments. The less frequent engine and experimental are described in the next section.

A.8 Other engine procedures

This section describes regular but infrequent maintenance activities and experiments. They are included for completeness and for reference of future intrepid engine researchers.

A.8.1 Transient tests

Some tests characterize the transient thermal response of the exhaust system or waste-gate as a turbine bypass. For these experiments, the engine preparation is similar to above without the pre-heat at the 3.0 [bar] GIMEP baseline point. The DAQ is also configured to take periodic temperature measurements at fixed, user-specified time intervals.

A.8.2 Oil change

Impingement of fuel and combustion gases onto the cold cylinder wall during cold-start can cause the oil to accumulate significant quantities of fuel and water. Over a period of time this dilutes the oil. In an ordinary engine, operation at high coolant and oil temperatures causes the fuel and water dissolved in the oil to evaporate in the crankcase, whereupon it is transported via the positive crankcase valve (PCV) system to the intake and combustion chamber where the fuel vapour can burn and water vapour can be exhausted.

Since this research engine is run for extended period of time in a cold start configuration, the oil could experience severe dilution. Oil that is significantly diluted by fuel could become a disproportionate source of hydrocarbons when they desorb in the expansion stroke.

To minimize the influence of oil-sourced hydrocarbons the oil and filter were changed at regular intervals and the fuel content of the oil was qualitatively monitored by smell. At each oil change the engine was drained, flushed with virgin motor oil, motored for a period of time, and flushed and filled again to ensure oil in all parts of the oil circuit and heat exchangers was replaced.

Oil dilution appeared to be most severe with ethanol and blends containing ethanol than with neat gasoline. This was not quantified, but oil drained after ethanol experiments was a light grey-brown colour and had qualitatively very low viscosity. Oil drained after gasoline experiments was dark brown or black and had higher viscosity. For constant load, the lower heating value of ethanol causes greater fuel mass to be

injected and consequently a greater mass of fuel to accumulate in the oil. The dilution was not quantified. It was verified through a fractional boiling experiment that grey used oil from ethanol experiments turned black when boiled to just above 100°C which would evaporate the suspended ethanol (T_b=78°C) and water (T_b=100°C. Severely agitating a sample of used oil from gasoline experiments with approximately 5-10 % by volume ethanol and 5-10 % by volume water and produced a mixture that was superficially similar to used oil from ethanol experiments. It is possible that the greater apparent degree of dilution with ethanol was remarked based only on the difference in used oil colour. There is no useful conclusion for production vehicles since a short period of operation at higher oil temperatures could remove the contamination.

A.8.3 Spark plug change

During cold start experiments, the spark plugs are prone to fouling due to low temperatures and rich mixtures. Dirty spark plugs increase cycle-to-cycle variability and increase the probability of partial-burn misfire. The spark plugs were removed, cleaned with hydrocarbon solvent, and replaced at regular intervals. No special measures were taken to ensure the spark plug electrodes were indexed to the same angular position each time. The degree of fouling was not the same for all plugs, suggesting some inter-cylinder mixture differences.

A.8.4 Injector deposits

As with the spark plugs, the direct injection fuel injectors were prone to deposit formation. Such deposits could alter the plume shape and direction or block injector holes entirely. To minimize the potential impact of fuel injector deposits on engine operation, the fuel injectors were removed and cleaned at regular intervals.

A.8.5 High-load/lean operation

As a further countermeasure the engine was run at high load (GIMEP=6.5-7.5[bar]) and moderately lean air-fuel equivalence ratios (λ=1.15) to facilitate the oxidation

of injector deposits, spark plug deposits and combustion chamber surface deposits. This procedure was limited by the power dissipation limit of the dynamometer, and the lack of controls over the turbocharger. After this high-load/lean operation, the exhaust system had noticeably less particulate accumulation and required frequency of spark plug and injector cleaning decreased.

A.8.6 Back-pressure regulation

To prevent damage and premature catalyst ageing during prolonged operation in a simulated cold-start configuration, the catalyst brick was removed. The exhaust system was modified with an empty catalytic converter housing, and a blast gate valve to simulate the back-pressure imposed by and actual catalyst. Following recommendations from industry sponsors, the exhaust back pressure was set so that an average exhaust pressure of 1.05 [bar] was achieved during engine operation at MBT spark timing for a load of NIMEP=2.0 [bar] and 1200 [rpm].

A.8.7 Injector calibration

The DI fuel rail and injectors were calibrated in a custom bench-top rig to simulate engine-block mounting but permit collection of injected fuel. The collection vessel had a tight-fitting seal around the injector, and was cooled in an ice-water bath to facilitate condensation (minimize lost fuel vapours). This calibration established a correlation of fuel mass injection as a function of pulse width at different fuel pressures.

This page intentionally left blank

APPENDIX B

TEST FUEL PROPERTIES

haltermannsolutions

fueling the world, one solution at a time.

Telephone: (800) 969-2542

Product Information

FAX: (281) 457-1469

Johann Haltermann Ltd.

PRODUCT: **EPA TIER II EEE FEDERAL REGISTER** Batch No.: AJ0221LT10

PRODUCT CODE: **HF0437** Tank No.: 105

Date: 10/3/2012

TEST	METHOD	UNITS	HALTERMANN Specs			RESULTS
			MIN	TARGET	MAX	
Distillation - IBP	ASTM D86	°F	75		95	87
5%		°F				110
10%		°F	120		135	126
20%		°F				149
30%		°F				175
40%		°F				204
50%		°F	200		230	223
60%		°F				234
70%		°F				244
80%		°F				263
90%		°F	305		325	319
95%		°F				342
Distillation - EP		°F			415	411
Recovery		vol %		Report		96.9
Residue		vol %		Report		1.1
Loss		vol %		Report		2.0
Gravity	ASTM D4052	°API	58.7		61.2	59.2
Density	ASTM D4052	kg/l	0.734		0.744	0.742
Reid Vapor Pressure	ASTM D5191	psi	8.7		9.2	9.2
Carbon	ASTM D3343	wt fraction		Report		0.8646
Carbon	ASTM E191	wt fraction		Report		0.8631
Hydrogen	ASTM E191	wt fraction		Report		0.1339
Hydrogen/Carbon ratio	ASTM E191	mole/mole		Report		1.847
Stoichiometric Air/Fuel Ratio				Report		14.580
Oxygen	ASTM D4815	wt %			0.05	None Detected
Sulfur	ASTM D5453	wt %	0.0025		0.0035	0.0031
Lead	ASTM D3237	g/gal			0.01	None Detected
Phosphorous	ASTM D3231	g/gal			0.005	None Detected
Silicon	ASTM 5184	mg/kg			4	<1
Composition, aromatics	ASTM D1319	vol %			35	28
Composition, olefins	ASTM D1319	vol %			10	1
Composition, saturates	ASTM D1319	vol %		Report		71
Particulate matter	ASTM D5452	mg/l			1	0.6
Oxidation Stability	ASTM D525	minutes	240			1000+
Copper Corrosion	ASTM D130				1	1a
Gum content, washed	ASTM D381	mg/100mls			5	<0.5
Fuel Economy Numerator/C Density	ASTM E191		2401		2441	2426
C Factor	ASTM E191			Report		0.9991
Research Octane Number	ASTM D2699		96.0			96.5
Motor Octane Number	ASTM D2700			Report		88.6
Sensitivity			7.5			7.9
Net Heating Value, btu/lb	ASTM D3338	btu/lb		Report		18492
Net Heating Value, btu/lb	ASTM D240	btu/lb		Report		18475
Color	VISUAL			Report		Undyed

184

BIBLIOGRAPHY

[1] John B. Heywood. *Internal combustion engine fundamentals*. McGraw-Hill, 1988.

[2] General Motors. General motors powertrain media viewing gallery. http://media.gm.com/media/us/en/gm/photos.detail.html/content/Pages/galleries/us/en/Powe January 2013.

[3] Eran Sher. *Handbook of air pollution from internal combustion engines: pollutant formation and control*. Academic Press, Boston, 1998.

[4] Ronald M. Heck, Robert J. Farrauto, and Suresh T. Gulati. *Catalytic Air Pollution Control: Commercial Technology*. John Wiley & Sons, February 2009.

[5] W. Anderson, J. Yang, D. D. Brehob, J. K. Vallance, and R. M. Whiteaker. Understanding the thermodynamics of direct injection spark ignition (DISI) combustion systems: An analytical and experimental investigation. Technical Report 962018, SAE International, Warrendale, PA, October 1996.

[6] Fuquan Zhao. *Technologies for Near-Zero-Emission Gasoline-Powered Vehicles*. SAE International, illustrated edition edition, October 2006.

[7] Jianwen Li, Ronald D. Matthews, Rudolf H. Stanglmaier, Charles E. Roberts, and Richard W. Anderson. Further experiments on the effects of in-cylinder wall wetting on HC emissions from direct injection gasoline engines. Technical Report 1999-01-3661, SAE International, Warrendale, PA, October 1999.

[8] Dongkun Lee. *Effects of secondary air injection during cold start of SI engines*. Thesis, Massachusetts Institute of Technology, 2010. Thesis (Ph. D.)–Massachusetts Institute of Technology, Dept. of Mechanical Engineering, 2010.

[9] Wai K. Cheng, Douglas Hamrin, John B. Heywood, Simone Hochgreb, Kyoung-doug Min, and Michael Norris. An overview of hydrocarbon emissions mechanisms in spark-ignition engines. Technical Report 932708, SAE International, Warrendale, PA, October 1993.

185

[10] KUO-CHUN WU and SIMONE HOCHGREB. The roles of chemistry and diffusion on hydrocarbon post-flame oxidation. *Combustion Science and Technology*, 130(1-6):365–398, 1997.

[11] Michael G. Norris, Wolf Bauer, and Simone Hochgreb. Oxidation of hydrocarbons from lubricant oil layers in spark-ignition engines. *Symposium (International) on Combustion*, 26(2):2645–2652, 1996.

[12] Michael G. Norris and Simone Hochgreb. Extent of oxidation of hydrocarbons desorbing from the lubricant oil layer in spark-ignition engines. Technical Report 960069, SAE International, Warrendale, PA, February 1996.

[13] Kuo-Chun Wu, Simone Hochgreb, and Michael G. Norris. Chemical kinetic modeling of exhaust hydrocarbon oxidation. *Combustion and Flame*, 100(12):193–201, January 1995.

[14] James A. Eng. The effect of spark retard on engine-out hydrocarbon emissions. Technical Report 2005-01-3867, SAE International, Warrendale, PA, October 2005.

[15] Richard Stone. *Introduction to Internal Combustion Engines*. Society of Automotive Engineers, 1999.

[16] Charles Fayette Taylor. *The Internal Combustion Engine in Theory and Practice: Combustion, Fuels, Materials, Design*. MIT Press, 1985.

[17] P.G. Hill and D. Zhang. The effects of swirl and tumble on combustion in spark-ignition engines. *Progress in Energy and Combustion Science*, 20(5):373–429, 1994.

[18] Sihun Lee, Kun Tong, Bryan D. Quay, James V. Zello, and Domenic A. Santavicca. Effects of swirl and tumble on mixture preparation during cold start of a gasoline direct-injection engine. Technical Report 2000-01-1900, SAE International, Warrendale, PA, June 2000.

[19] Dongkun Lee and John B. Heywood. Effects of charge motion control during cold start of SI engines. Technical Report 2006-01-3399, SAE International, Warrendale, PA, October 2006.

[20] Craig Wildman and Wai K. Cheng. The effects of charge motion and laminar flame speed on late robust combustion in a spark-ignition engine. Technical Report 2010-01-0350, SAE International, Warrendale, PA, April 2010.

[21] Gustavo Beira Colli, Danilo Castejon, Alvaro Salvetti, and Orlando Volpato. Heated injector cold start system for flex-fuel motorcycles. Technical Report 2010-36-0156, SAE International, Warrendale, PA, October 2010.

[22] Daniel Kabasin, Kevin Hoyer, Joseph Kazour, Rudolf Lamers, and Tobias Hurter. Heated injectors for ethanol cold starts. Technical Report 2009-01-0615, SAE International, Warrendale, PA, April 2009.

[23] Daniel Francis Kabasin, Youssef Joseph, William Fedor, Scott Geiger, and Tobias Hurter. Emission reduction with heated injectors. Technical Report 2010-01-1265, SAE International, Warrendale, PA, April 2010.

[24] Timothy D. Spegar, David Burke, and Lucille Lavan. Delphi's heated injector technology: The efficient solution for fast ethanol cold starts and reduced emissions. Technical Report 2012-01-0418, SAE International, Warrendale, PA, April 2012.

[25] L. Pettersson and K. Sjstrm. Onboard hydrogen generation by methanol decomposition for the cold start of neat methanol engines. *International Journal of Hydrogen Energy*, 16(10):671–676, 1991.

[26] Justin Fulton, Frank Lynch, and Bryan Willson. Hydrogen for cold starting and catalyst heating in a methanol vehicle. Technical Report 951956, SAE International, Warrendale, PA, August 1995.

[27] Grant Lumsden and Harry C. Watson. HAJI operation in a hydrogen-only mode for emission control at cold start. Technical Report 950412, SAE International, Warrendale, PA, February 1995.

[28] Martin J. Heimrich and Craig C. Andrews. On-board hydrogen generation for rapid catalyst light-off. Technical Report 2000-01-1841, SAE International, Warrendale, PA, June 2000.

[29] Rainer Wurms. Innovative technologies in current and future TFSI engines from audi. In *20th aachen colloquium automobile and engine technology*, volume 2011, 2011.

[30] Takuya Ikoma, Shizuo Abe, Yukihiro Sonoda, Hisao Suzuki, Yuichi Suzuki, and Masatoshi Basaki. Development of v-6 3.5-liter engine adopting new direct injection system. Technical Report 2006-01-1259, SAE International, Warrendale, PA, April 2006.

[31] Kevin R Lang. *Reducing cold start hydrocarbon emissions from port fuel injected spark ignition engines with improved management of hardware & controls.* Thesis, 2006. Thesis (Ph. D.)–Massachusetts Institute of Technology, Dept. of Mechanical Engineering, 2006.

[32] Kevin R. Lang and Wai K. Cheng. A novel strategy for fast catalyst light-off without the use of an air pump. Technical Report 2007-01-0044, SAE International, Warrendale, PA, January 2007.

187

[33] Brian E. Hallgren and John B. Heywood. Effects of substantial spark retard on SI engine combustion and hydrocarbon emissions. Technical Report 2003-01-3237, SAE International, Warrendale, PA, October 2003.

[34] T. Ma, N. Collings, and T. Hands. Exhaust gas ignition (EGI) - a new concept for rapid light-off of automotive exhaust catalyst. Technical Report 920400, SAE International, Warrendale, PA, February 1992.

[35] Fu-Quan Zhao, Ming-Chia Lai, and David L. Harrington. A review of mixture preparation and combustion control strategies for spark-ignited direct-injection gasoline engines. Technical Report 970627, SAE International, Warrendale, PA, February 1997.

[36] Mark Borland and Fuquan Zhao. Application of secondary air injection for simultaneously reducing converter-in emissions and improving catalyst light-off performance. Technical Report 2002-01-2803, SAE International, Warrendale, PA, October 2002.

[37] S. Russ, G. Lavoie, and W. Dai. SI engine operation with retarded ignition: Part 1 - cyclic variations. Technical Report 1999-01-3506, SAE International, Warrendale, PA, October 1999.

[38] S. Russ, M. Thiel, and G. Lavoie. SI engine operation with retarded ignition: Part 2 -HC emissions and oxidation. Technical Report 1999-01-3507, SAE International, Warrendale, PA, October 1999.

[39] Edward W. Kaiser, Waiter O. Siegl, Frederick H. Trinker, David F. Cotton, Wai K. Cheng, and Kristine Drobot. Effect of engine operating parameters on hydrocarbon oxidation in the exhaust port and runner of a spark-ignited engine. Technical Report 950159, SAE International, Warrendale, PA, February 1995.

[40] K. MIN and W. K. CHENG. Oxidation of the piston crevice hydrocarbon during the expansion process in a spark ignition engine. *Combustion Science and Technology*, 106(4-6):307–326, 1995.

[41] Karl Kollmann, Jrg Abthoff, Wolfgang Zahn, Hubert Bischof, and Jochen Ghre. Secondary air injection with a new developed electrical blower for reduced exhaust emissions. Technical Report 940472, SAE International, Warrendale, PA, March 1994.

[42] Dongkun Lee and John B. Heywood. Effects of secondary air injection during cold start of SI engines. Technical Report 2010-01-2124, SAE International, Warrendale, PA, October 2010.

[43] S. Mitsuishi, K. Mori, K. Nishizawa, and S. Yamamoto. Emission reduction technologies for turbocharged engines. Technical Report 1999-01-3629, SAE International, Warrendale, PA, October 1999.

[44] D. White. On the road to zero emissions. *Chemical engineer*, (615-16):34–41, 1996.

[45] Toru Kidokoro, Koichi Hoshi, Keizo Hiraku, Koichi Satoya, Takashi Watanabe, Takahiko Fujiwara, and Hideki Suzuki. Development of PZEV exhaust emission control system. Technical Report 2003-01-0817, SAE International, Warrendale, PA, March 2003.

[46] Kimiyoshi Nishizawa, Sukenori Momoshima, Masaki Koga, and Hirofumi Tsuchida. Development of new technologies targeting zero emissions for gasoline engines. Technical Report 2000-01-0890, SAE International, Warrendale, PA, March 2000.

[47] Kenneth Kar, Stephen Roberts, Richard Stone, Martin Oldfield, and Boyd French. Instantaneous exhaust temperature measurements using thermocouple compensation techniques. Technical Report 2004-01-1418, SAE International, Warrendale, PA, March 2004.

[48] Karthik Ramanathan and Chander Shekhar Sharma. Kinetic parameters estimation for three way catalyst modeling. *Industrial & Engineering Chemistry Research*, 50(17):9960–9979, September 2011.

[49] G.C. Koltsakis, P.A. Konstantinidis, and A.M. Stamatelos. Development and application range of mathematical models for 3-way catalytic converters. *Applied Catalysis B: Environmental*, 12(23):161–191, June 1997.

[50] D. Chatterjee, O. Deutschmann, and J. Warnatz. Detailed surface reaction mechanism in a three-way catalyst. *Faraday Discuss.*, 119:371384, 2001.

[51] Takafumi Yamauchi, Shuichi Kubo, and Satoshi Yamazaki. Detailed surface reaction model for three-way catalyst and NOx storage reduction catalyst. Technical Report 2005-01-1112, SAE International, Warrendale, PA, April 2005.

[52] R.E. Hayes, L.S. Mukadi, M. Votsmeier, and J. Gieshoff. Three-way catalytic converter modelling with detailed kinetics and washcoat diffusion. *Topics in Catalysis*, 30/31:411–415, July 2004.

[53] J. Kallenbach, P. Flrchinger, and A. Heibel. Modeling of automotive aftertreatment catalysts. Technical Report 1999-01-3043, SAE International, Warrendale, PA, December 1999.

[54] Petr Koc, Milan Kubcek, and Milo Marek. Modeling of three-way-catalyst monolith converters with microkinetics and diffusion in the washcoat. *Industrial & Engineering Chemistry Research*, 43(16):4503–4510, August 2004.

[55] E. Robert Becker, Richard Watson, Mickey Brayer, Claus Vogt, and Mikio Makino. Prediction of catalytic performance during light-off phase with different wall thickness, cell density and cell shape. Technical Report 2001-01-0930, SAE International, Warrendale, PA, March 2001.

189

[56] Grigorios C. Koltsakis and Dimitrios N. Tsinoglou. Thermal response of close-coupled catalysts during light-off. Technical Report 2003-01-1876, SAE International, Warrendale, PA, May 2003.

[57] S.H. Chan and D.L. Hoang. Heat transfer and chemical reactions in exhaust system of a cold-start engine. *International Journal of Heat and Mass Transfer*, 42(22):4165–4183, November 1999.

[58] S. H. Chan and D. L. Hoang. Modeling of catalytic conversion of CO/HC in gasoline exhaust at engine cold-start. Technical Report 1999-01-0452, SAE International, Warrendale, PA, March 1999.

[59] G. N. Pontikakis, G. S. Konstantas, and A. M. Stamatelos. Three-way catalytic converter modeling as a modern engineering design tool. *Journal of Engineering for Gas Turbines and Power(Transactions of the ASME)*, 126(4):906923, 2004.

[60] G. C. KOLTSAKIS, I. P. KANDYLAS, and A. M. STAMAOS. Three-way catalytic converter modeling and applications. *Chemical Engineering Communications*, 164(1):153–189, 1998.

[61] J. C. W. Kuo, C. R. Morgan, and H. G. Lassen. Mathematical modeling of CO and HC catalytic converter systems. SAE Technical Paper 710289, SAE International, Warrendale, PA, February 1971.

[62] M. Peckham and N. Collings. Study of engine wall layer hydrocarbons with a fast-response FID. Technical Report 922237, SAE International, Warrendale, PA, October 1992.

[63] M. Peckham and N. Collings. Investigation into crevice out-gassing of an operating SI engine with a fast-FID. Technical Report 932642, SAE International, Warrendale, PA, October 1993.

[64] M. Peckham and N. Collings. In-cylinder HC measurements with a piston-mounted FID. Technical Report 932643, SAE International, Warrendale, PA, October 1993.

[65] Kenneth Kar and Wai Cheng. Using mass spectrometry to detect ethanol and acetaldehyde emissions from a direct injection spark ignition engine operating on Ethanol/Gasoline blends. Technical Report 2011-01-1159, SAE International, Warrendale, PA, April 2011.

[66] Kenneth Kar and Wai K Cheng. Speciated engine-out organic gas emissions from a PFI-SI engine operating on Ethanol/Gasoline mixtures. Technical Report 2009-01-2673, SAE International, Warrendale, PA, November 2009.

[67] J. A. Caton. Comparisons of thermocouple, time-averaged and mass-averaged exhaust gas temperatures for a spark-ignited engine. Technical Report 820050, SAE International, Warrendale, PA, February 1982.

[68] Jonathan W. Fox, Wai K. Cheng, and John B. Heywood. A model for predicting residual gas fraction in spark-ignition engines. Technical Report 931025, SAE International, Warrendale, PA, March 1993.

[69] Gerald M. Rassweiler and Lloyd Withrow. Motion pictures of engine flames correlated with pressure cards. SAE Technical Paper 380139, SAE International, Warrendale, PA, January 1938.